THE CHEAM SLIDE:

A STUDY OF THE INTERRELATIONSHIP

OF ROCK AVALANCHES AND SEISMICITY

by

CURT MARCEL NAUMANN

B.A.Sc., The University of British Columbia

A THESIS SUBMITTED IN PARTIAL FULFILLMENT

OF THE REQUIREMENTS FOR THE DEGREE OF

MASTER OF APPLIED SCIENCE

in

THE FACULTY OF GRADUATE STUDIES

The Department of Geological Sciences
(Geological Engineering Programme)

We accept this thesis as conforming
to the required standard

THE UNIVERSITY OF BRITISH COLUMBIA

July, 1990
© Curt Marcel Naumann, 1990

In presenting this thesis in partial fulfilment of the requirements for an advanced degree at the University of British Columbia, I agree that the Library shall make it freely available for reference and study. I further agree that permission for extensive copying of this thesis for scholarly purposes may be granted by the head of my department or by his or her representatives. It is understood that copying or publication of this thesis for financial gain shall not be allowed without my written permission.

Department of _GEOLOGICAL SCIENCES_

The University of British Columbia
Vancouver, Canada

Date _JULY 19, 1990_

ABSTRACT

It is being increasingly realized that there exists an interrelationship between seismicity and rock slope failures. Possible chronological clustering of rock avalanches in the Fraser River corridor was investigated to determine if a common seismic trigger existed. It was determined that the events occurred throughout the Holocene indicating that either these slides were not seismically triggered or that seismic triggers were chronologically unrelated. Cascadia Subduction Zone earthquakes are believed to have occurred throughout the Holocene (Adams, 1989; Atwater, 1987; Hull, 1987). The ages of the earthquakes were compared to the ages of rock avalanches in the Fraser River corridor, but no distinct correlation could be made.

The lack of distinct correlation between large rock avalanches in Fraser Corridor and paleoseismicity, and the absence of event clustering, indicated either seismicity was not a factor, or that these rock avalanches may not have been susceptible to seismic triggering. A stability study of Cheam Slide was performed to investigate the susceptibility of large rock avalanches to earthquake triggering. The results suggested that the seismic susceptibility of a slope is closely linked to the displacement the slope must undergo for failure to take place. A large critical displacement may render the slope relatively insensitive to seismic triggering, while a low critical displacement may result in high seismic susceptibility.

A comparison was made between the effects of seismic and pore pressure related triggering. The results indicated that a high critical displacement slope, which is close to failure, may be more likely to fail by high pore pressures than by seismic loading. Low critical displacement slopes which are stable enough to surviving hydrodynamic loading may, because of their susceptibility to seismic triggering, pose the greatest hazard.

TABLE OF CONTENTS

CHAPTER 4. INTERRELATIONSHIP OF EARTHQUAKES AND ROCK AVALANCHES

CHAPTER 5. INTRODUCTION TO STABILITY ANALYSIS

CHAPTER 6. MODELLING PARAMETERS

CHAPTER 7. COMPUTER MODELLING PROCEDURE

LIST OF TABLES

LIST OF FIGURES

ACKNOWLEDGEMENTS

CHAPTER 1

INTRODUCTION

1.1 Purpose and Scope

The eastern Fraser Lowland is experiencing unprecedented development pressure

in response to the rapid expansion of metropolitan Vancouver. This is manifest in

increases to both habitation and utilization of the valley corridor for the movement of

people and commodities. The land reserve policy of the provincial government limits

residential and recreational zoning of agricultural lands, hence the lower slopes of

adjacent mountains are increasingly utilized. Linear facilities, although concentrated

on the valley floor, are slowly encroaching on lower slopes as well. These facilities

include two transcontinental railway lines, trunk oil and natural gas pipe lines, major

power grids, the Trans Canada Highway and other major provincial highways, and a

fibre optics telecommunications line.

Despite the importance of the eastern Fraser Lowland for agricultural

productivity, habitation and a strategic corridor, virtually no regard has been given to

geological hazards and attendant risks affecting the area. Recent experience indicates

that rock avalanche hazards should be considered among the highest risks of all geological hazards.

Large tension cracks were recently found in the slopes of Mount Breakenridge, located on the eastern edge of Harrison Lake. It was recognized that if the slope failed catastrophically it could cause a wave hazard to Harrison Hot Springs. All building permits were frozen in the community while a geotechnical investigation was performed.

The British Columbia Hydro and Power Authority (Hydro) Wahleach Power Plant was temporarily closed in 1989 due to a rupture in the steel lining of the power tunnel. It was determined that the southeast slope of Fraser Valley in which the tunnel was located showed evidence of small but continuing deformation. On the basis of an extensive investigation, Hydro is proceeding with re-location of the tunnel and is temporarily operating the existing plant after making tunnel repairs. The slope is being carefully monitored.

Two small earthquakes of Richter local magnitude (M_L) 3.2 and 3.1 occurred immediately prior to the January, 1965 Hope Slide and are suspected of being the trigger (Mathews and McTaggart, 1978; Wetmiller and Evans, 1989). The initiation of landslides during earthquakes has been well documented (Keefer, 1984). The Lower Mainland is a seismically active area and the consequences of a large earthquake on the stability of the Fraser Valley slopes has not yet been considered.

More than thirty landslides having volumes of up to 500 million cubic metres have been identified in, or adjacent to, the Fraser River corridor (Savigny, 1990a).

Fraser River has been blocked by landslide dams as recently as about 1200 radiocarbon years before present (years BP) (Ryder *et al.*, 1990). Clearly, there is a need for improved understanding of the significance of landslide hazards in the Fraser River corridor, particularly in response to a major earthquake.

This thesis is an enquiry into the possible interrelationship between earthquakes and rock avalanches in the Fraser River corridor. Two approaches are taken. First, the chronology of known rock avalanches is determined and the likelihood of an earthquake trigger is considered from the standpoints of the clustering of events and the correlation with paleoseismicity established by others. Second, the relative significance of pore pressure related and seismic triggers is evaluated through detailed investigation and stability modelling of Cheam Slide. Cheam Slide is believed to be the largest of several landslides to have occured in the Fraser River corridor. It is also situated closest to the Wahleach Power Plant and so its investigation represents a logical and timely starting point.

1.2 Cheam Slide Location

Cheam Slide is located on the southeast (left) side of Fraser River, 15 km east of Chilliwack, British Columbia. It is near the eastern extent of Fraser Lowland, and some 125 km east of the City of Vancouver (Fig. 1.1).

1.3 Previous Work

Little research had been done about Cheam Slide at the beginning of this study. The conspicuous hummocky landform on the floor of Fraser Valley had been known for decades and had long been suspected of being a rock avalanche deposit. A B.A.Sc. thesis by Smith (1971) described the landform as a colluvial deposit, but no source area was defined.

Golder Associates Ltd. (1984), in a report to the Regional District of Fraser-Cheam briefly mentioned a "massive ancient landslide" but the report was vague on the source zone and extent of the debris.

Thurber Consultants Ltd. (1984a) described some of the materials encountered in the vicinity of the Popkum Interchange as colluvium from Cheam Slide. Although the debris covered a large area, the report expressed uncertainty regarding the source area and the exact nature of the slide event. Thurber Consultants Ltd. (1984b) concluded that the Popkum Quarry area was not subject to hazards from deep or shallow failures of soil or bedrock, and furthermore, there were no slope stability hazards to residential dwellings located roughly 200 m north of the quarry.

As late as April, 1987, an informal meeting and site visit by more than ten knowledgeable consultants and research scientists reached agreement that the available evidence was inconclusive as to whether or not the landform was a slide deposit and where, exactly, the source area was (K.W. Savigny, 1989, personal communication).
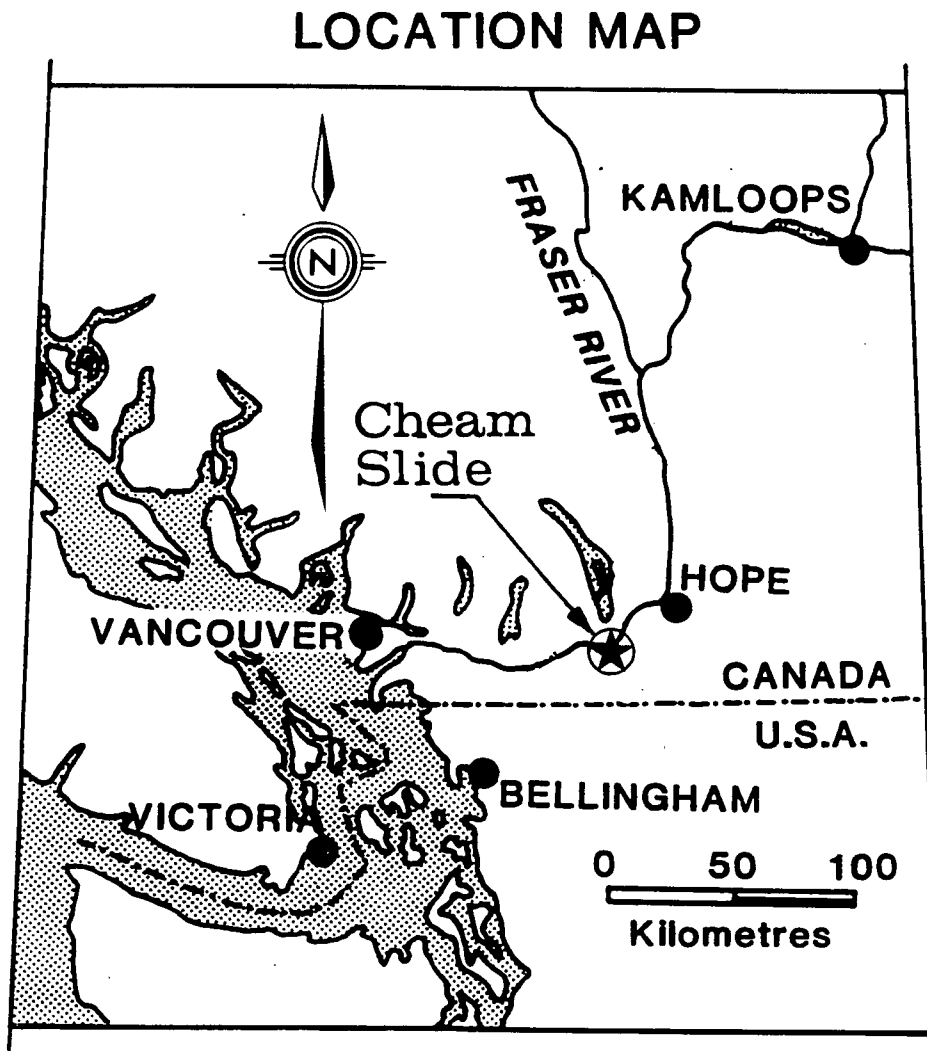
LOCATION MAP

Figure 1.1. Location map of Cheam Slide.

CHAPTER 2

GEOLOGIC SETTING

2.1 Physiographic Setting

Cheam Slide is located in the southwestern part of the Cascade Mountains of British Columbia. The local mountains are rugged with an average relief of 1650 m. Slopes rise steeply from the Fraser River floodplain, which has an elevation of 20 to 40 m in this location.

Slope drainage in the slide area is directly into Fraser River with the drainage pattern controlled by bedrock structures in the steep mountain slopes. Debris flows occur occasionally in the steeper streams as do snow avalanches from the upper slopes of the mountain.

Evidence of glaciation includes over steepened slopes, aretes, cirques, and hanging valleys adjacent to Fraser Valley. Cheam Slide debris overlies what is believed to be a distal glacial outwash deposit (R. Gerath, 1990, personal communication).

Much of the virgin forest in the Cheam Slide area has been clearcut. The newer cuts have a dense secondary growth of brush whereas the older cuts have a healthy

crop of new forest. Where virgin forest survives, the flora is typical of the coastal area. The trees types are Douglas fir (*Pseudotsuga*), Hemlock (*Tsuga*) and cedar (*Thuja*). Balsam (*Abies*) is common at higher altitudes. Above 1600 m elevation forest gives way to alpine meadow and above 1750 m vegetation becomes sparse.

2.2 Climate

2.2.1 Precipitation

The climate of Fraser Lowland is classified as inshore marine. The District of Cheam is located at the east end of Fraser Lowland, about 125 km inland of Strait of Georgia. Because of the effects of the Coast Mountains to the north and the Cascade Mountains to the south, the rainfall in the eastern Fraser Lowland is heavier than the western Fraser Lowland.

The average annual rainfall in the District of Cheam is about 1650 mm as compared to the Vancouver International Airport which has an average of about 1050 mm (British Columbia Department of Agriculture, 1916-1976). About 75% of the annual precipitation falls from October to March inclusive, with November often being the wettest month. The mean annual 24 hour extreme rainfall for the District of Cheam is about 65 mm (Environment Canada, 1951-1980). Rainfall in excess of 140 mm over a 24 hour period has been recorded.

2.2.2 Temperature

Fraser Lowland has one of the mildest climates in Canada. The mean daily maximum temperature for the District of Cheam is about $12.5^{\circ}C$ (Environment Canada, 1951-1980). The mean daily temperature is $10^{\circ}C$ and the mean daily minimum temperature is $5^{\circ}C$. The number of days below $0^{\circ}C$ is 80.

2.2.3 Paleoclimate

Using pollen frequencies, Mathewes and Heusser (1980) estimated the mean July temperature and mean annual precipitation trends in southwestern British Columbia during the Holocene. It was found that the paleotemperature was $14^{\circ}C$ at about 12 000 years BP. The temperature increased dramatically between 10 000 and 10 400 years BP to slightly above $16^{\circ}C$. The maximum temperatures clustered between 10 000 and approximately 7500 years BP, then steadily decreased until 6000 years BP. There was little temperature change from 6000 years BP to present. Precipitation was high between 12 000 and 10 400 years BP dropping to minimum Holocene values between 10 000 and 7500 years BP Precipitation rose to present levels at about 6500 years BP.

2.3 Bedrock Geology

2.3.1 Rock Units

The Cascade Mountain system in northwestern Washington and southern British Columbia consists of a central, north to northwest trending, gneissic and granitic core.

The core is flanked on either side by belts of sedimentary and volcanic rocks which have locally been subjected to low-grade regional metamorphism. Cheam Slide is located at the northern end of the western belt of these sedimentary and volcanic rocks. The core in this region consists of the intrusive granodioritic Chilliwack and Mount Barr batholiths, and Custer Gneiss. The Oligocene Chilliwack Batholith lies to the southeast of the Cheam Slide. Directly to the east-northeast of the slide is the younger Miocene Mount Barr Batholith. To the north, across Fraser Valley, the mountain core continues in the form of predominately intrusive granitic rocks until it merges with the Coast Mountains. Figure 2.1 shows the bedrock geology in the Cheam Slide area (Monger, 1989).

The Chilliwack Group and Cultus Formation are the two major lithological units present in the slide area (Monger, 1966). The older Devonian to Permian Chilliwack Group consists of fine to coarse grained volcanic arenites, argillites, cherty or argillaceous limestone, and local conglomerates and tuffs. Stratigraphically above, and lying unconformably over the Chilliwack Group, is the Upper Triassic and Lower Jurassic Cultus Formation. It is comprised of fine to medium grained volcanic arenites, argillites and slates. Both units are complexly folded and faulted in the region but retain their stratigraphic integrity.

2.3.2 Structure and Tectonics

The Cheam Slide area has undergone two major phases of deformation (Monger 1966 and 1989). The first phase of deformation occurred in mid-Cretaceous time.

This deformation produced northeast trending folds indicating principal compressive stresses in the northwest-southeast direction. As deformation continued, the northeast trending folds were overturned to the northwest. Southeast dipping thrust faults represent the limiting condition of this deformation phase. The thrusting resulted in the truncation of the lower limbs of recumbent anticlinal folds in some areas.

The second phase of deformation was superimposed onto the structures of the first phase. The principal stress direction during this phase of deformation was northeast-southwest. This phase of deformation is believed to be responsible for the northeast dip of the beds at low to moderate angles, for the production of large open folds, and for reverse faults with northeast dipping fault planes (Monger, 1966). The style of minor structures formed during this phase suggest that they are a result of brittle deformation in contrast to the plastic deformation of the phase one folds. The different deformation styles suggests a time difference between phases.

The second phase of deformation took place prior to intrusion of the Oligocene Chilliwack Batholith. Unorientated biotite and cordierite porphyroblasts, in thermally metamorphosed rocks close to the contact, grow across minor structures from the second phase of deformation offering a mininum age of phase two deformation (Monger, 1966).

2.4 Surficial Geology

2.4.1 Surficial Materials

Surficial materials in the Cheam Slide area are dominantly river sediments and slope deposits. Their areal distributions are shown in Figure 2.2 (Armstrong, 1980) and a schematic cross-section is shown in Figure 2.3. Lying above the Cheam Slide debris are the Salish Sediments. These are, most extensively, deposits of marl and peat remaining from the draining of Lake Cheam, and less extensively; lowland peat, organic silt loam, and silty loam deposits.

Directly beneath the slide debris lie channel and overbank deposits, silty loam, silt, loam, silty clay and minor organic sediments of Fraser River Sediments. These deposits are up to 4 m thick and are underlain by extensive modern Fraser River and/or older flood plain and deltaic (?) sand and gravel up to 60+ m thick.

The southeast end of the slide debris is overlain by slope deposits of landslide rubble, gravel and minor sand <10+ m thick. These deposits can also be found at the foot of the slopes to the northeast and southwest of the Cheam Slide debris.

Aside from the distal glacial outwash deposit beneath the slide debris, glacial sediments are not seen in the immediate slide area. Their closest occurrence is on the northwest slope of Fraser Valley about 700 m to the southwest (Armstrong, 1980).

2.4.2 Geomorphic Development

2.4.2.1 Glacial

The last glaciation commenced in southwestern British Columbia between 23 000 and 26 000 years BP and terminated about 11 000 years BP (Armstrong, 1981). Termed the Fraser Glaciation, this corresponds to the end of the Wisconsin Glaciation. The Fraser Glaciation reached its climax during the Vashon Stade about 15 000 years BP. At this time the Vashon ice was more than 1800 m thick in Fraser Lowland, the land was isostatically depressed by at least 300 m and sea level was eustatically lowered by about 100 m.

Vashon ice withdrew rapidly and, by about 13 000 years BP, most of the central and western Fraser Lowland was invaded by the sea resulting in a submergence of the land by more than 200 m. This was followed by rapid emergence of the land of at least 150 m by about 12 000 years ago.

Sumas ice began to advance approximately 12 000 years ago and, during the subsequent 500 years, there was another submergence of more than 100 m. Following the Sumas ice advance, the land again emerged and the sea level was within 15 m of present.

During the time between the retreat of Vashon ice and the beginning of complete deglaciation, piedmont glaciers terminated in the sea. By about 10 500 years BP, Fraser Lowland and most of the surrounding mountains were free of glacier ice.

2.4.2.2 Fraser River

No evidence exists in Fraser Lowland of a pre-Vashon Fraser River and the pre-Vashon history of Fraser River is largely unknown (Armstrong, 1981). Pebble lithology of gravel bars between Hope and Chilliwack indicate a high percentage of quartzite pebbles, originating from the Caribou Mountains which lie several hundred kilometres north of Hope. No pre-Vashon gravel deposits of high quartzite content have been found in Fraser Lowland, thus, it is probable that Fraser River did not flow in Fraser Lowlands until after Fraser Glaciation.

2.5 Mass movements

2.5.1 Landslide Inventory

Many mass movements in Fraser Valley have been documented. Piteau and Associates (1977) completed a survey of mass movements from Hope to Lytton along the CP Rail right-of-way. Evidence of about 75 postglacial or interglacial landslides was reported, some of which were very large and caused major river diversions. Some slopes, geologically speaking, were considered in an active state of failure.

Savigny (1990b) completed an inventory of landslides in a larger corridor extending between 20 and 30 km on each side of the Fraser and Coquihalla valleys. The inventory was carried out using 1:50 000 scale, panchromatic aerial photographs. Large landslides (at least 1×10^6 m^3) were outlined directly on the air photographs and the data later transferred to a 1:250 000 scale base map. Figure 2.4 shows the inventory along with linear features as seen on the air photographs.

More than thirty large, deep-seated landslides ranging in size from at least 1 x 10^6 m^3 to more than 500 x 10^6 m^3 were identified. In several cases, landslides predated, or occurred during, Late Wisconsinan (Fraser) Glaciation. The classification of these landslides was difficult to assign because the original morphology was modified by glacial erosion. Of those that were classified, the majority were rock slumps, one was a slow earth flow comprised of ultramafic clasts, and four were major rock avalanches. Three of these rock avalanches, the Katz, Lake-of-the-Woods, and Cheam slides, are in Fraser Corridor (Fig. 2.4).

Preliminary investigations of the Katz and Lake-of-the-Woods slides have been completed by Thurber Consultants Ltd. (1988a and 1988b). The results were released to the University of British Columbia by Dr. Peter Cave, Director of Planning, Regional District of Fraser-Cheam. Because of the similarity of the Lake-of-the-Woods and Katz slides to Cheam Slide, summaries of these investigations are presented in the following subsections, together with new chronological data obtained as part of this study.

2.5.2 Katz Slide

2.5.2.1 General

Katz Slide is located on the northwest (right) side of Fraser Valley, 13 km southwest of Hope and 16 km northeast of Wahleach (Fig. 2.4). The elevation of the top of the slide scar is about 800 m and base level elevation is 100 m. Much work

remains to be done to clarify the nature of the rock mass deformations in Katz Slide. The following is a preliminary interpretation of the available data.

Bedrock comprising the slopes in the slide area is part of the Spuzzum Pluton which locally consists of quartz diorite, interbedded with bands of dark micaceous schist (Monger, 1989; Thurber Consultants Ltd., 1988a). A regional fault, believed to be a northeast continuation of the Vedder Fault, trends northeast through the southeast summit area of the unnamed mountain on which Katz Slide occurred (Savigny, 1990b).

Vedder Fault is believed to form the backscarp of Katz Slide. The mountain appears to have spread laterally similar to the model proposed by Beck (1968) as illustrated in Figure 2.5. A large graben structure, which is approximately 120 m across and 35 to 45 m deep, applies the lateral load. The southeast flank of the unstable mass, which is also the headscarp of Katz Slide, appears to have moved southeast and translated downward. The nature and origin of the basal failure surface is not known. It is suspected of being deep exfoliation joints which dip southeast toward Fraser Valley (Fig. 2.5). The sides of the unstable mass and of Katz Slide are believed to be controlled by pervasive, steeply dipping, northwest-trending discontinuities which are visible on air photographs as lineaments (Fig. 2.4).

Airphoto analysis of the Katz Slide area indicates that two events have likely occurred and a third slide may be incipient. Each is believed to be a result of the lateral spreading model, but the pre-failure configurations of events one and two are not known.

The first event was the largest and it is believed to have dammed Fraser River. A small lake probably formed behind the dam, but was quickly infilled with sediment. The fluvial sediments prograded downstream covering all but the largest blocks on the surface of the landslide dam. At the time of the second event, shallow channels carrying the flow of Fraser River were located on the northwest (right) and southeast (left) side of the valley.

The second event was not as large as the first. It extended about half way across the valley, blocking the channel on the northwest side and diverting all flow into the channel on the southeast side of the valley. The slide debris from the second event covers an area of 1.1 km^2 and has a volume of about 15×10^6 m^3 (Thurber Consultants Ltd., 1988a).

Small rockslides and rockfalls have recently occurred from several locations on the oversteepened southeast slope of the unstable rock mass (Fig. 2.5). This evidence of rock mass deformations suggests that lateral spreading of the mountain is continuing. Hub extensometers have been installed across tension cracks and are currently being monitored.

2.5.2.2 Dating Procedure

The first slide event has not been dated. This may be possible by drilling upstream of the landslide dam to obtain dateable pollen, tephra, or organic material from the bottom of the aggraded river sequence or lacustrine deposits.

The date of the second event was obtained by taking cores of the deposits in the deepest section of the abandoned northwest channel. Figure 2.6 shows the sample location map and Figure 2.7 shows the core log and stratigraphic location of the dated sample (for a complete stratigraphic description see Appendix I). A hard sand stratum was found at the bottom of the section. This is overlain by a thin layer of organics which is overlain by a thick layer of fine sediments. The organics are interpreted as an indicator of the cessation of active flow and the commencement of vertical accretion in the channel. The uncalibrated ^{14}C date for the organic sample was determined to be 3260 ±70 years BP (Appendix II).

2.5.2.3 Mobility

The angle of inclination from the farthest extent of the slide debris to the top of the slide scarp is about 18.3°. The calculated F value is 0.33 (see inset Fig. 2.8 for definition). The mobility of the Katz Slide is shown in Figure 2.8 with of other Canadian Cordillera landslides and is seen to be slightly less mobile than predicted by Scheidegger's relationship (Scheidegger, 1973).

2.5.3 Lake-of-the-Woods Slide

2.5.3.1 General

Lake-of-the-Woods Slide (LOTW) is located 4 km north of Hope on the west (right) side of Fraser Valley (Fig. 2.4). The slide scar extends from an elevation of 500 to 800 m. The orientation of the failure planes, which are joint controlled, gives

the slide a distinctive wedge shape. The bedrock in the immediate slide area is quartz diorite which is part of the Spuzzum Pluton (Monger, 1989). The Hope Fault runs north-south directly beneath the slide scar. The slide volume has been estimated at 20×10^6 m^3 (Thurber, 1988b).

Lake-of-the-Woods (also known as Schkam Lake) was formed when the rock avalanche blocked a glaciofluvial channel. The surface of the slide debris appears very blocky but because of the ability of the debris to retain water, the interior of the deposit must either contain very fine material, or organics in the basin act as an impermeable liner.

2.5.3.2 Dating Procedure

An attempt was made to obtain wood samples entrained in the debris for ^{14}C dating. The shoreline was traversed and the lake bottom was investigated by SCUBA diving. No wood was found on the shoreline and a heavy sediment blanket covering the lake bottom prevented finding wood below the water line. As an alternative, it was decided that the age of the organic material directly overlying the pre-lake surface of the glaciofluvial channel, would provide a reasonable estimate of the age of the rock avalanche.

Piston sampling of the lake bottom sediments by SCUBA divers was attempted in the 12 m deep water but with limited success. Depth control accuracy of the sampling device was insufficient and the sampler was very difficult to operate

underwater. It was decided that the lake bottom sediments would have to be sampled from the surface.

To support the sampling rods, 15 m of casing was fabricated. Two Zodiacs were lashed together and securely anchored above the sampling site. The casing was dropped between them to the lake bottom. The sampler was lowered into the casing and core samples obtained from the basal 2.0 m of the lake bottom sediments. A location map and typical core log are shown in Figures 2.9 and 2.10, respectively. Mazama ash (6845 ±50 years BP; Bacon, 1983) was found 25 cm above the mineral bottom, providing a minimum age of the lake.

Two samples of gyttja (soft organic ooze) from the lake sediments were ^{14}C dated. To minimize the smearing of dates, the samples were limited to the bottom 2 cm of each of the two cores. The samples were dated at 8260 ±70 and 8430 ±60 years BP (Appendix II). From this information the slide is considered to have occurred approximately 8500 years BP, using the older date as a minimum and considering that the actual dates represent an average of 2 cm of organic material.

2.5.3.3 Mobility

The angle of inclination from the farthest extent of the slide debris to the top of the slide scarp is about 19.8°. The calculated F value is 0.36 (see inset Fig. 2.8). The mobility of Lake-of-the-Woods Slide is shown in Figure 2.8 with other Canadian Cordillera landslides and is seen to be slightly less mobile than predicted by Scheidegger's relationship (Scheidegger, 1973).

2.5.4 Debris flows and Rockfalls

Debris torrents are common from the steep mountain stream channels in the area. These debris torrents are small in comparison to rock slides and thus the risk is very localized but is still of concern. There are also extensive rockfalls in the area (Golder Associates Ltd., 1984). The highways at the bottom of the valley slopes between Cheam Slide and Hope are usually closed at least once a year by rockfalls and debris slides despite extensive geotechnical work done to control such events (Silver Creek resident, 1989, personal communication).

2.6 Seismicity

The coastal area of British Columbia has long been recognised as seismically active. Recent major historical events include two Vancouver Island earthquakes; 1918 - M_L 7 and 1946 - M_L 7.3, and a 1872 M_L 7.4 earthquake in Northwestern Washington. The location of these earthquakes are shown in Figure 2.11 along with many smaller documented events (Milne et al., 1978).
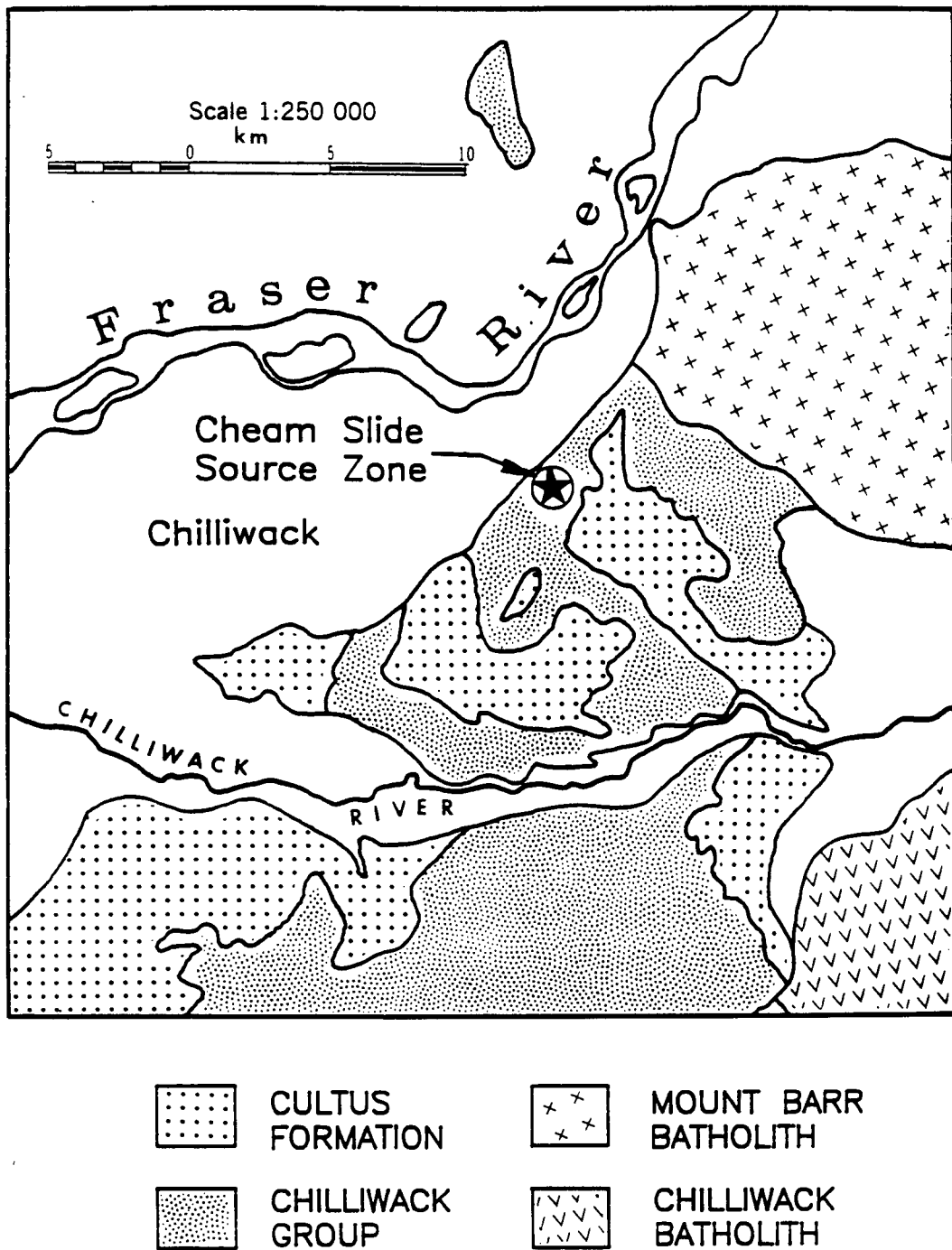
Figure 2.1. Bedrock geology of the Cheam Slide area (after Monger, 1989).
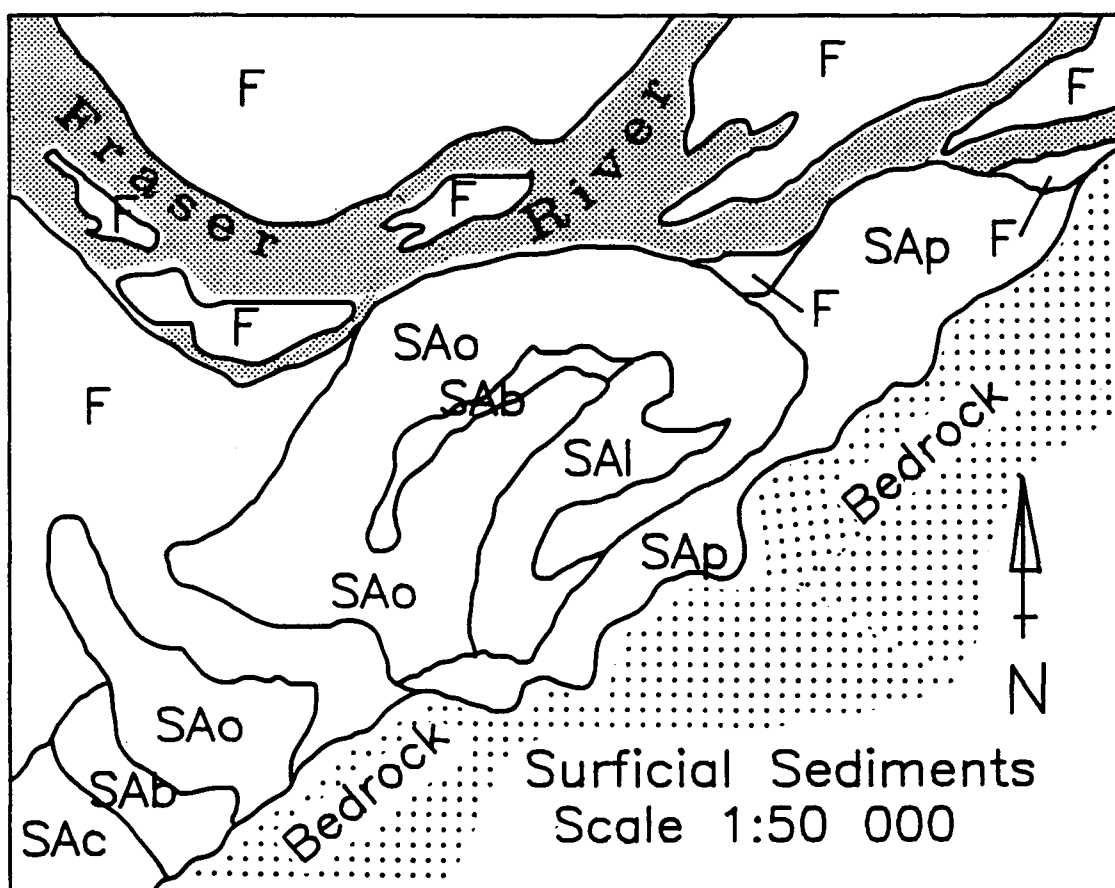
Figure 2.2. Surficial Geology of the Cheam Slide area (after Armstrong, 1980).
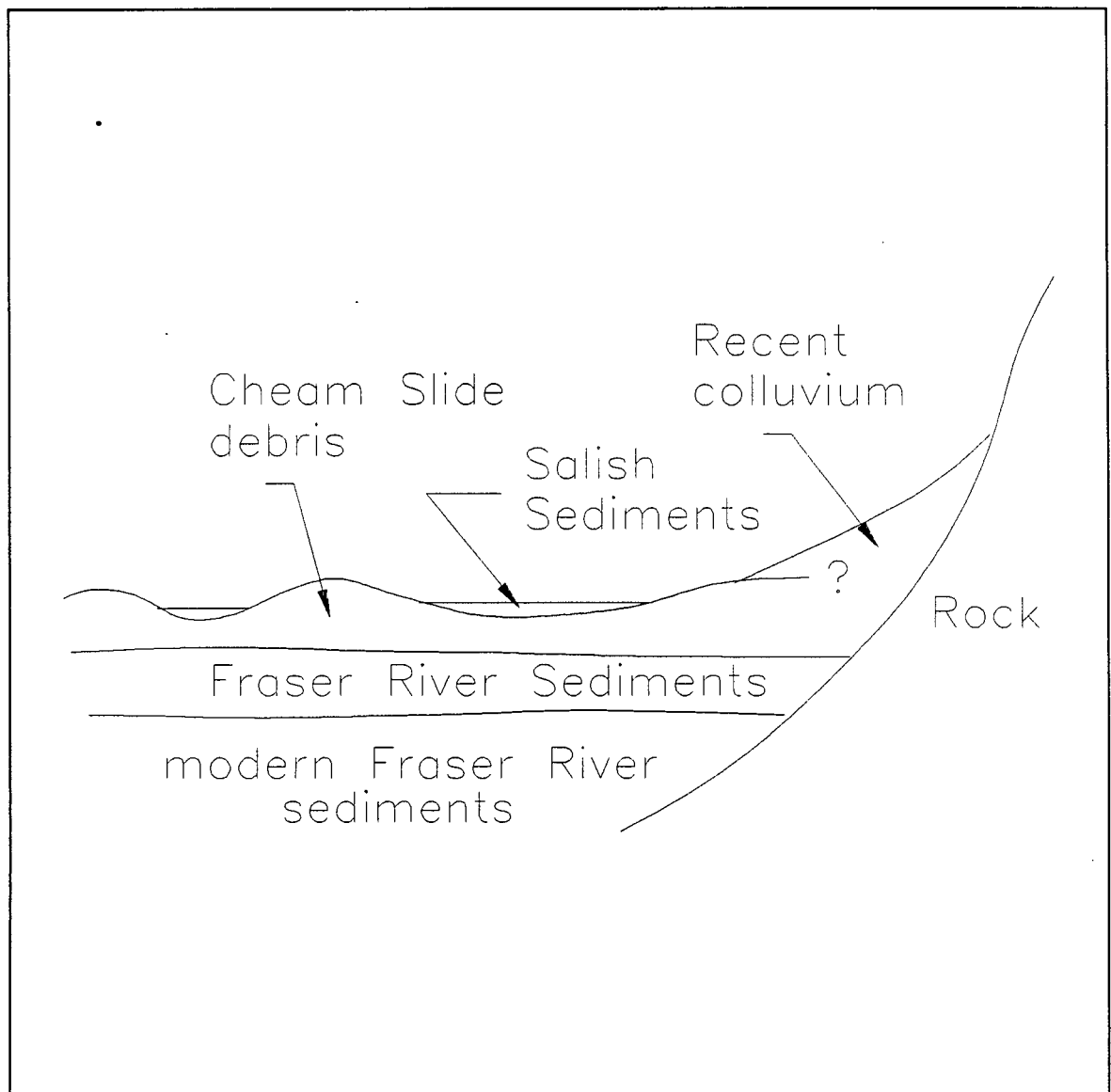
Figure 2.3. Schematic cross-section showing the vertical distribution of surficial materials above and beneath the Cheam Slide debris.
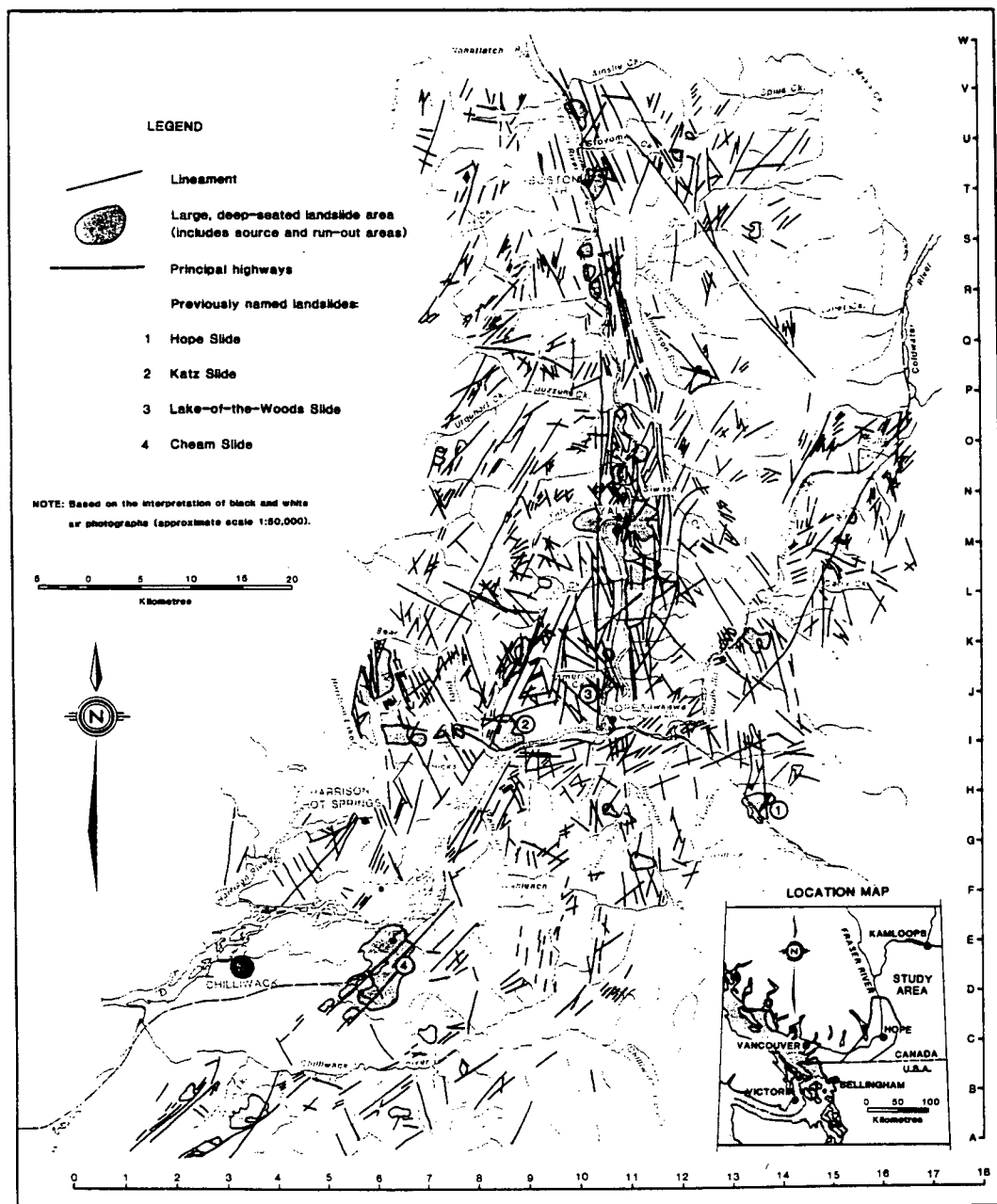
Figure 2.4. Inventory of mass movements and lineaments, Fraser Corridor area (after Savigny, 1990b).
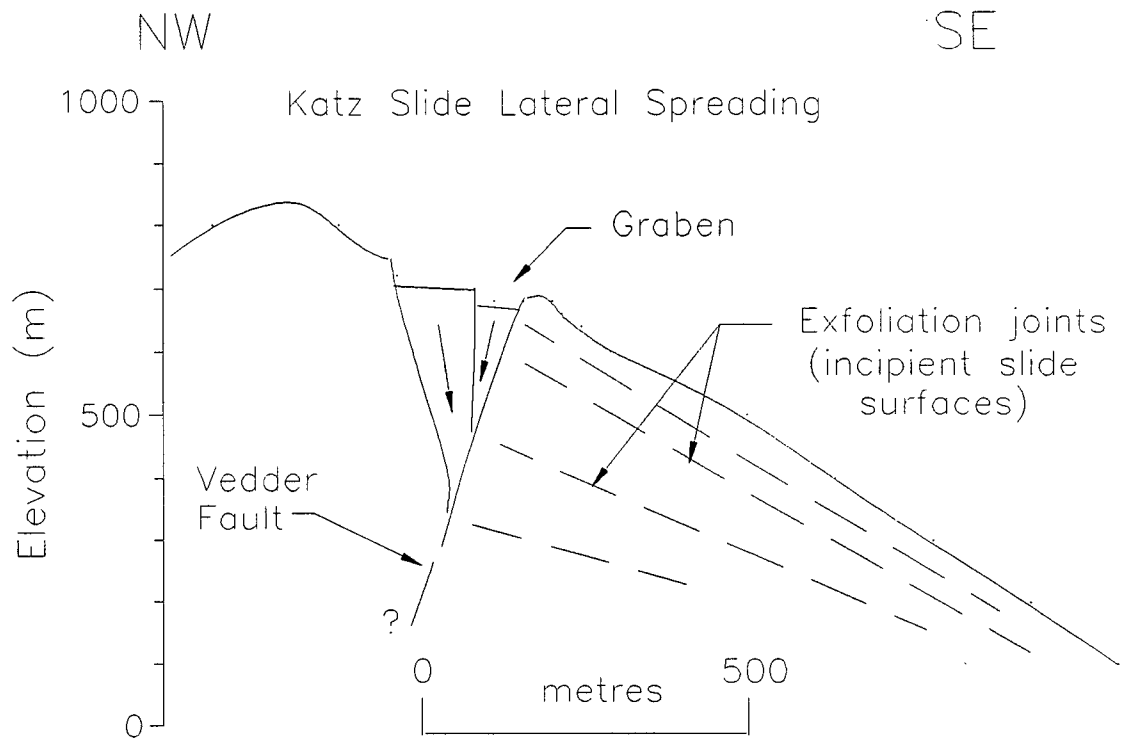
Figure 2.5. Lateral spreading believed to be occurring at the summit of Katz Slide (after Savigny, 1990b).
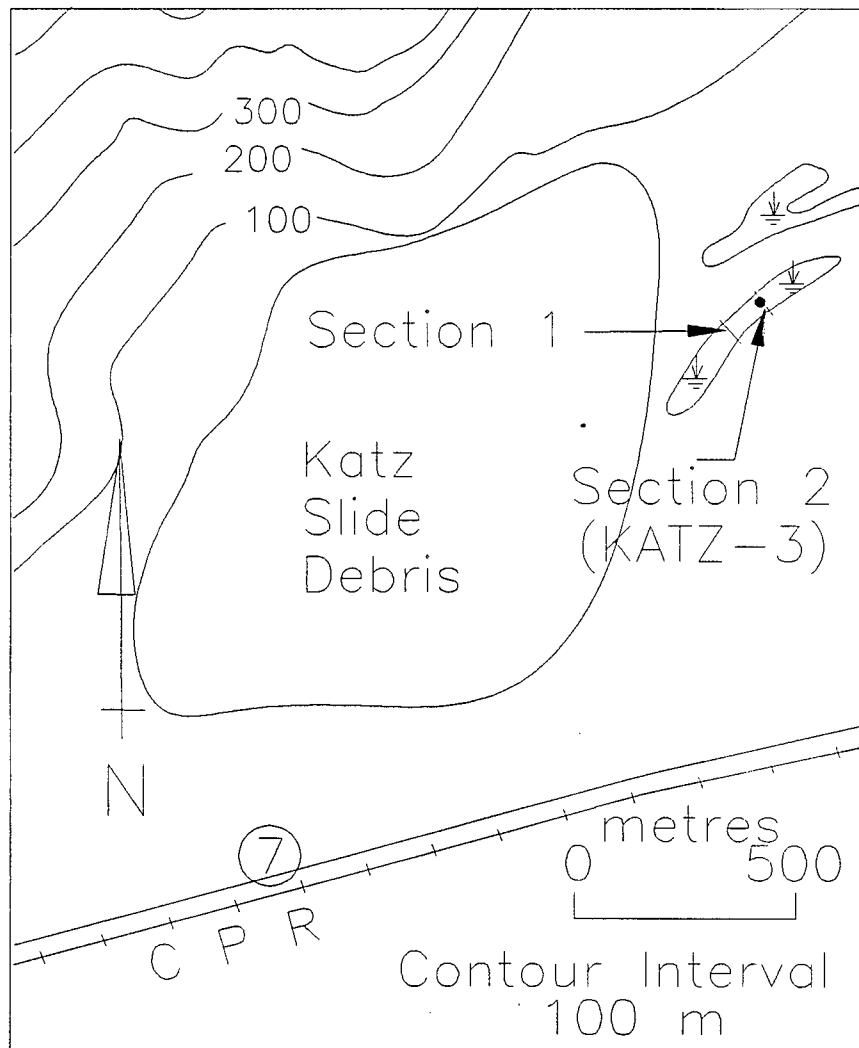
Figure 2.6. Location map showing Katz Slide paleochannel Sections 1 and 2, and piston core KATZ-3.

Katz Slide — Paleochannel Cutoff
Section 2 (KATZ–3)

LEGEND

5 Organic mat
4 Black organics
3 Silt, interbedded with silty sand and sand
2 Silt, interbedded with silty clay and clay
1 Sand

^{14}C 3260 $\pm$70 B.P.

10X VERTICAL EXAGGERATION
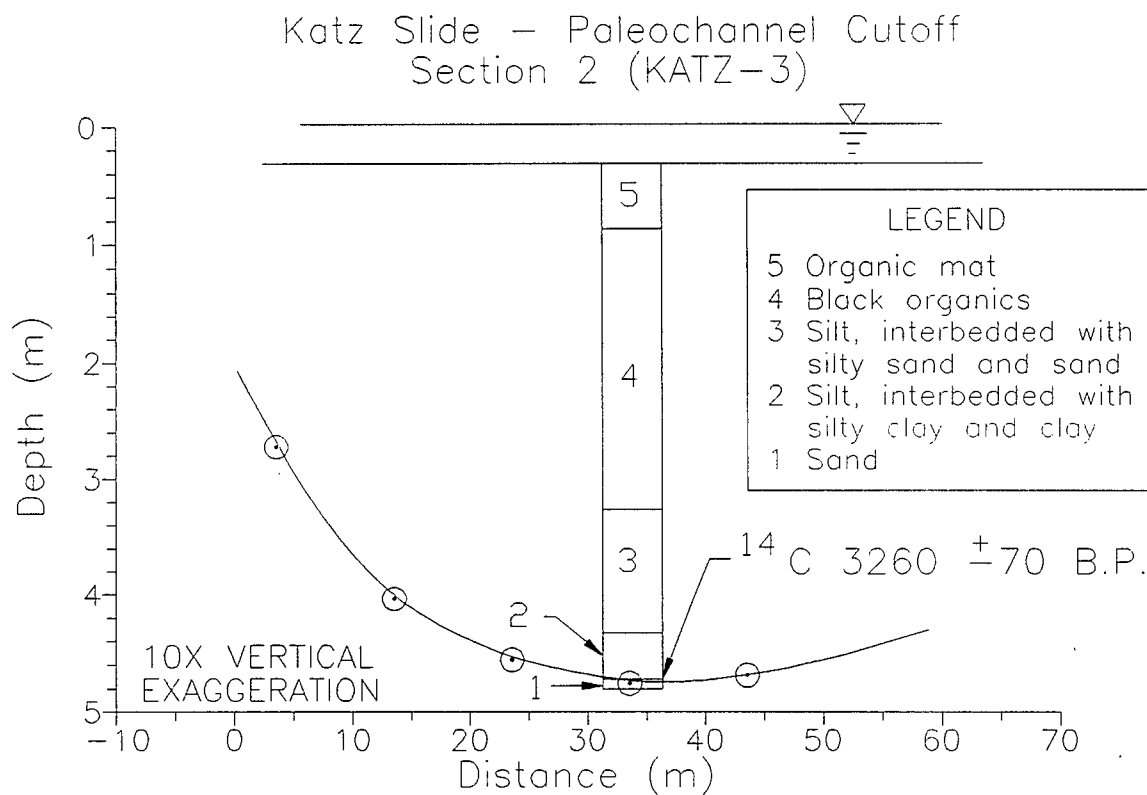
Figure 2.7. Section 2 of the Katz Slide paleochannel showing location of ^{14}C sample (see Fig. 2.6 for Section 2 location and Appendix I for a complete stratigraphic description).
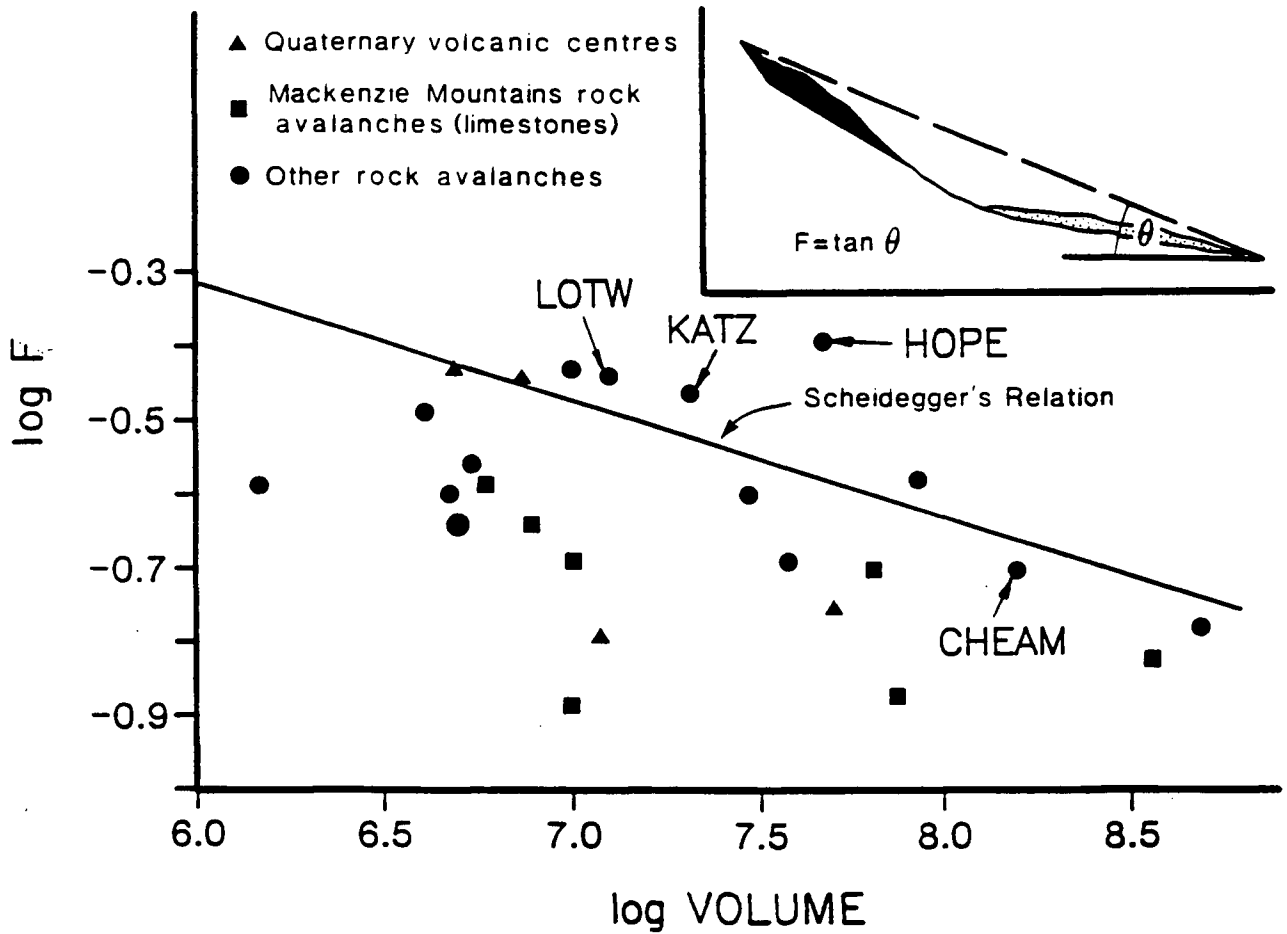
Figure 2.8. Mobility of the Katz, Lake-of-the-Woods, Hope, and Cheam slides along with other documented rock avalanches in the Canadian Cordillera and Scheidegger's relation (modified from Evans *et al.*, 1989).
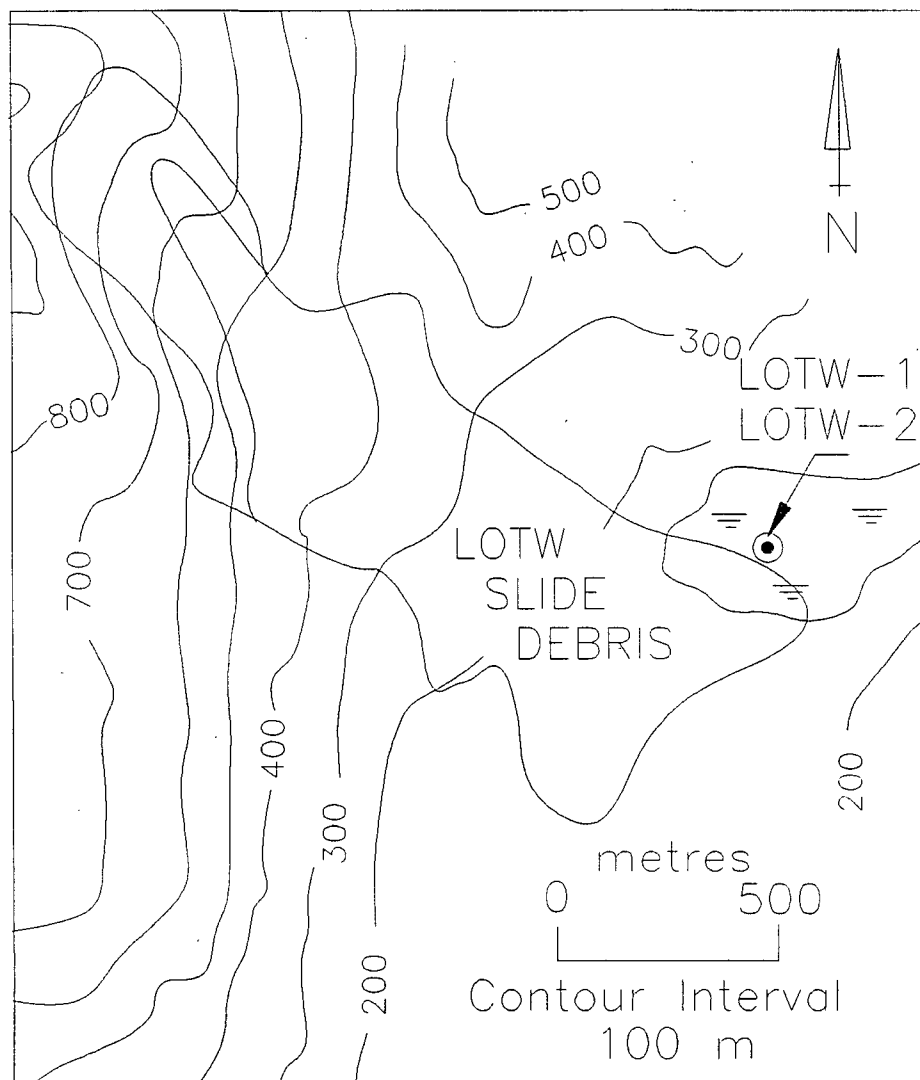
Figure 2.9. Location map showing Lake-of-the-Woods (LOTW) Slide piston cores LOTW-1 and LOTW-2.

Lake−of−the−Woods

0 m   Lake Bottom

4

2.4 m Core top

LEGEND

4 No recovery
3 Gyttja
2 Mazama Ash (6850 B.P.)

3

1 ^{14}C 8260 $\pm$70 B.P.
   ^{14}C 8430 $\pm$60 B.P.

2 ──── 4.19 m

3 ──── 1

4.44 m Mineral bottom
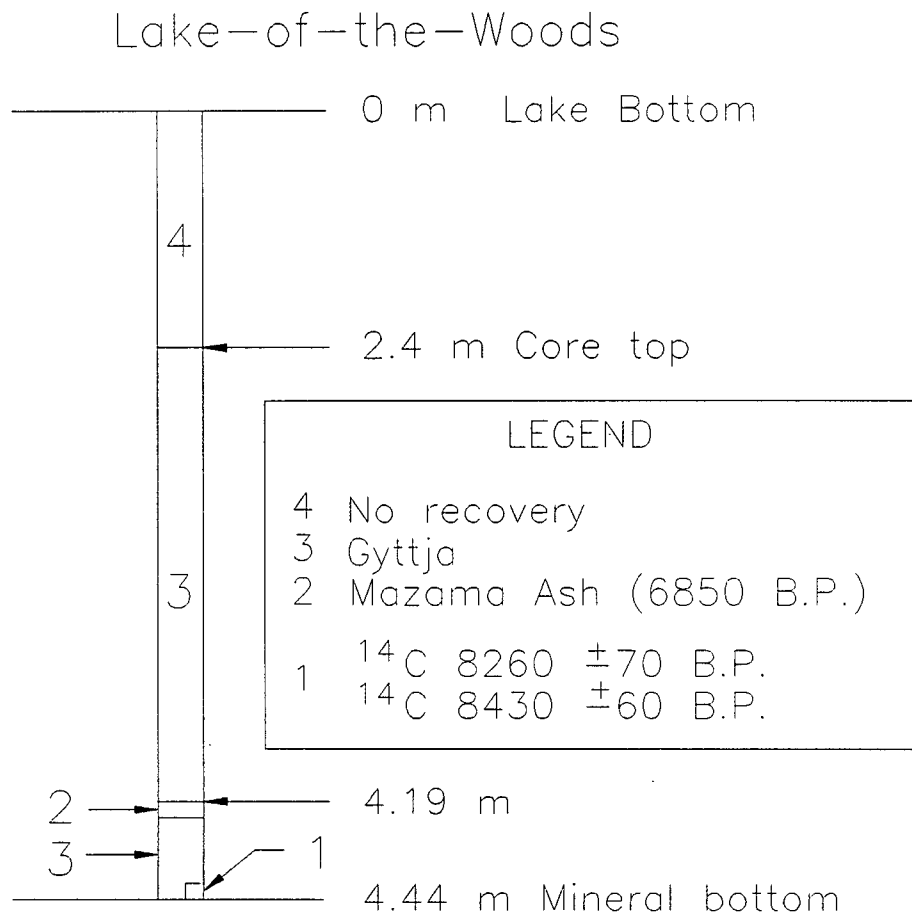
Diagram not to scale

Figure 2.10. Representative section of piston cores LOTW-1 and LOTW-2 taken from the lake bottom sediments at Lake-of-the-Woods showing sample locations for ^{14}C dates (see Fig. 2.9 for coring location).
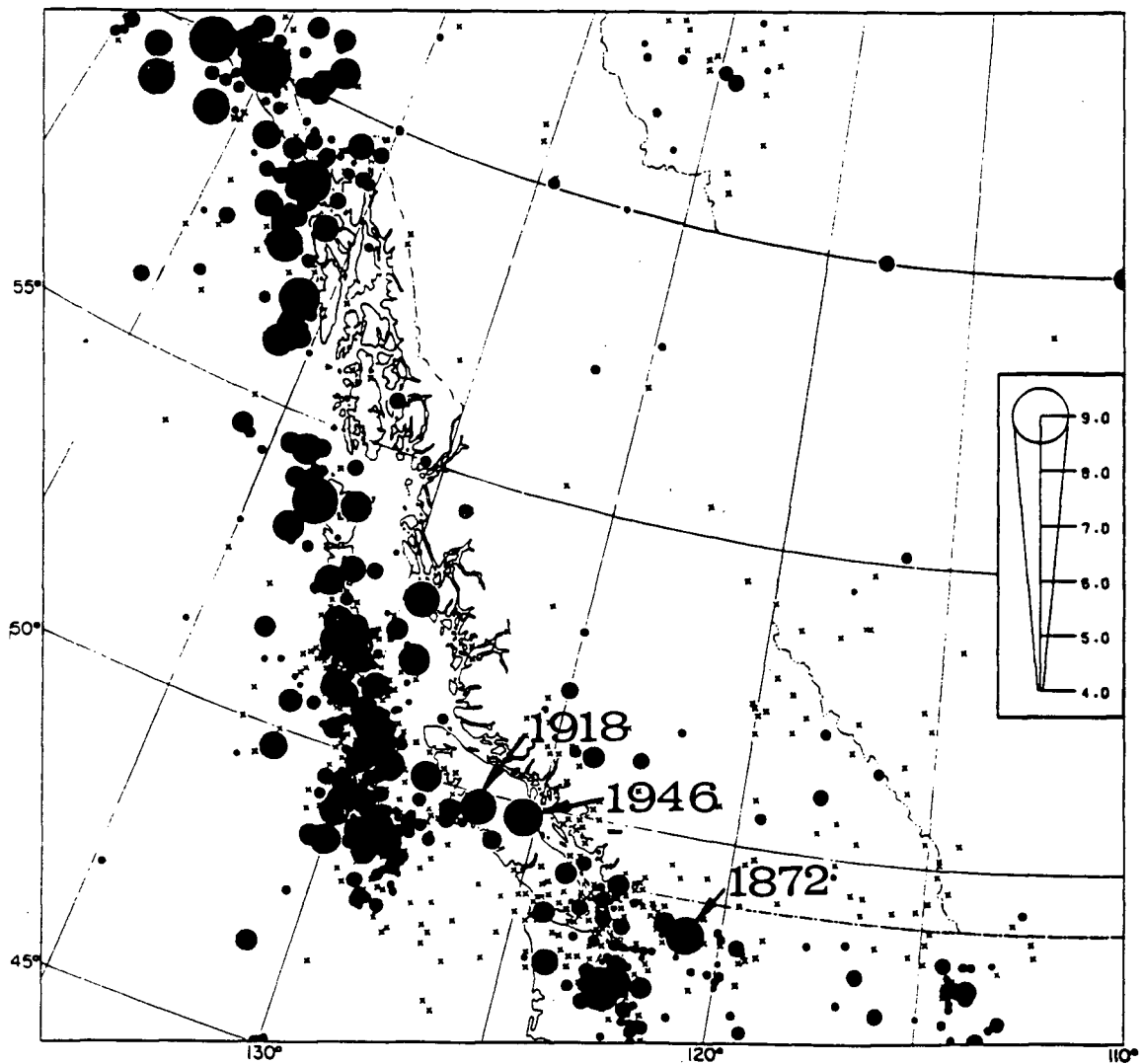
Figure 2.11. Western Canada regional distribution of earthquakes with magnitude greater than or equal to 3. The circle diameters are proportional to the earthquake magnitude and earthquakes of magnitude less than 4 are marked by "X" (from Milne *et al.*, 1978).

CHAPTER 3

CHEAM SLIDE DESCRIPTION

3.1 General

Cheam Slide was first suspected to have occurred because a hummocky landform on the valley floor was in sharp contrast to the surrounding, flat Fraser River floodplain. The hummocks were known to be aligned in subtle crescent shapes, concave toward adjacent mountain slopes. Lake Cheam was confined within the slide debris between hummocky ridges before being drained in 1945 for agricultural land use and subsequently mined for marl.

The source area of Cheam Slide is not obvious. Mountain cracking and related ravelling from the summit area of the unnamed mountain have obscured the configuration of the failure surface. Also the vegetative cover on the slope is similar to the surrounding slopes. Directly adjacent to the northeast edge of the slide scar a very large spur remains. Large grabens in this spur form conspicuous lineaments parallel to the slope trend. The slide debris, slide scar and spur are shown in Figure 3.1.

3.2 Colluvium Characteristics

3.2.1 Previous Study

Smith (1971) investigated the slide debris exposures along the Canadian National Railway (CNR) right-of-way as well as four other exposures. Three of these were located in borrow pits and one of which was located in a channel excavation. The location of the CNR track and the four locations (S1-S4) are shown in Figure 3.2.

Location S1 was a borrow pit with walls that exceeded 30 m in height. Small pockets of slide material were found by Smith (1971) along the top of the pit. A larger pocket had a stream deposit cut through it. Location S2 was another borrow pit. In this location the slide debris was intermittent and thin, ranging in thickness from 0 to 3.5 m. A hummock of slide material protruded through the organic lake bottom sediments at location S3. Location S4 was a gravel pit that resulted from the discovery of a gravel deposit when the Cheam Lake drainage ditch was dug. The slide debris in this area was described as having a thickness of 1 to 10 m.

The CNR right-of-way cuts along the edge of the debris deposit. Smith (1971) found that along the cut slope, the slide debris had an undulating base ranging in elevation from 25 to 45 m. The slide thickness was variable between 0 and 14 m.

As part of the field work for this study, a traverse of the slide debris area was made. All the exposures described by Smith (1971) were visited but were found to be heavily overgrown and provided no exposure. One small exposure, however, was found at the end of the pit at location S1 where a small amount of material had recently

been removed. This provided a small exposure of a sand dike, believed to be a flow structure resulting from the liquefaction of the sand by rapid loading towards the northwest.

3.2.2 CNR Gravel Pit

3.2.2.1 Stratigraphy

The CNR gravel pit is located at the northeast extent of the slide debris (Fig. 3.2). The pit is currently being mined for aggregate and the fresh cut slopes offer excellent exposure of the slide debris and surrounding units.

The base of slide debris was surveyed using a transit and level, and slope profiles and stratigraphic sections were measured at 12 locations. A plan view of the locations (P1-P12) is shown in Figure 3.3 along with the base of the slide debris and the top of the pit. South and east views of the pit walls are shown in Figures 3.4, 3.5 and 3.6 (see Appendix I for complete stratigraphic descriptions).

The slide debris is underlain by extensive fluvial deposits. These range from a thick gravel at the bottom of the section to a sand-silt-clay sequence near the top. The slide debris is broken into two units, one blue-grey in colour and the other tan. The tan coloured material lies closest to the ground surface and thus the colouring is believed to be the result of weathering. This is discussed further in Sections 3.2.3, 3.2.4 and 3.2.5. The top of the slide debris is covered by a thin soil horizon.

The actual top of the slide debris was difficult to define. The ground surface in the pit area was stripped of vegetation before the pit went into operation and much of the surface material was disturbed (loader operator, 1989, personal communication).

3.2.2.2 Rapid Loading Structures

During the stratigraphic mapping of the CNR gravel pit evidence of rapid loading was discovered. At the north end of the eastern pit wall there are two dike structures and a thrust sheet structure (Fig. 3.6) and at the south pit wall there is a second, although somewhat more obscure, thrust structure (Fig. 3.4). Directly to the north of P3 (Fig. 3.3) the gravel underneath the silt and sand deposit shows plastic deformation indicating the intensity of the loading.

The dikes at the north end of the eastern pit wall appear to be the result of plastic behaviour in response to undrained loading and attendant liquefaction caused by the impact of the slide debris. The thrust structure overlying the dikes is believed to be the result of overrunning of a stalled debris front, indicating the margin of the slide debris. Its formation is believed to be contemporaneous with the dikes. The south pit thrust structure shows similar deformation style but lacks the association with flow structures. All structures found in the CNR gravel pit indicate a southeast direction of transport of the slide debris.

3.2.3 Grain Size Analysis

Grain size analyses were carried out on samples of colluvium. The typical grain size distribution curve, shown in Figure 3.7, indicates a well graded deposit. A similar distribution could be expected for a glacial till.

Armstrong (1981) shows that the closest glacial drift deposit is the Sumas drift, some of which is located on the northeast side of Sumas Valley about 12 km to the southwest of the slide deposit. Armstrong (1981) investigated the range of particle size distributions for the Sumas Drift, Fort Langley Formation and Capilano glaciomarine sediments. His results along with the grain size distribution of the slide material are shown in Figure 3.7. The slide debris is coarser than the other three deposits suggesting different genesis.

Further evidence of the distinctive origin of the deposit is provided by clast characteristics. A glacial till would have sub-rounded to rounded particles at this location, whereas the deposit is predominantly angular clasts. The larger blocks in the slide debris are derived from the Chilliwack Group which is the most dominate unit in the nearby valley slopes. This indicates a local source area, supporting a colluvial genesis.

An attempt was made to determine the difference between top, middle and bottom regions of the slide debris and possible differences between the tan and blue-grey colluvium. The grain size data is plotted in Figure 3.8. The figure shows the lack of correlation between grain size distribution, sample location and colour. The silt

percentage for all samples remains constant at about 10%, and the gravel to sand ratio varies randomly from about 30:70% to about 75:25%.

3.2.4 Atterberg Limits

Atterberg limits of the colluvium material were determined according to the testing procedures outlined in Lambe (1951). The results are presented in a plasticity chart shown in Figure 3.9. The results indicate that the <#40 mesh fraction of the colluvium is dominantly of ML classification (silt of low plasticity, Unified Soil Classification System) with some samples of CL classification (clay of low plasticity). Since more than 25% of the colluvium material is sand sizes, it is classified as SM (sand with ML fines) to SC (sand with CL fines). The results in Figure 3.9 also show the lack of correlation between the location, colour, and Atterberg limits of each sample.

3.2.5 Powder X-Ray Diffraction

Powder X-Ray diffraction (XRD) analysis was performed on the portion of the slide debris passing #200 mesh sieve. The XRD results show dominantly illite and chlorite minerals with minor feldspar, quartz and smectite (Appendix III).

There is a distinct difference between the XRD results for the tan and blue-grey colluvium. Both show chlorite peaks of approximately the same intensity but the illite peak is much higher for the tan colluvium indicating a higher illite content. The higher illite content would give the colluvium a tan colour. A comparison between the

mineralogy of the tan and blue-grey colluvium in thin section confirms this. It is suspected that the chemical weathering of the volcanic parent rock is producing smectite which is quickly altered to illite (Williams *et al.*, 1982). Lesser amounts of chlorite can be expected because parent Mg-Fe silicate minerals are uncommon in the parent rock (Klein and Hurlbut, 1985).

3.3 Dating Procedure

3.3.1 Tephra Chronology

Entrained within the flow structures in the CNR gravel pit (Fig. 3.6) are deposits of buff white tephra. The optical characteristics of the four most recent ashes in southern and middle British Columbia are given by Nasmith *et al.* (1967) and against this data, a petrographic study was performed on the tephra collected at Cheam Slide (Appendix IV). The tephra was successfully identified as Mount Mazama ash indicating the slide event must have occurred since about 6845 years BP.

3.3.2 Radio Carbon Dating

The first indication of the age of Cheam Slide was obtained by Dr. John Clague of the Geological Survey of Canada[1]. He obtained a date for wood taken from a log entrained in the slide debris. The log was taken from a fresh roadcut leading to a

---

[1]Geological Survey, Lab No. GSC-4004.

gravel pit in the debris area. The ^{14}C date (corrected) for the wood sample was 5010 ±70 years BP.

Two methods to confirm this date for Cheam Slide were attempted as part of this study. First, the soils underlying swamps in the slide debris area were sampled for dateable organics, and second, wood samples were taken from within and beneath the slide colluvium exposed in the CNR gravel pit. The sampling locations are shown in Figure 3.2.

Several piston cores were taken from the swamp area. The cores consisted of blue-grey sand grading upward to very fine silt. This was followed by a layer of marl, then organics at the top. The marl layer was not considered suitable for carbon dating. The organic material above the marl was contaminated by modern rootlets, hence no ^{14}C dating was attempted.

Two wood samples were taken from the CNR gravel pit. The first sample was taken from a large log entrained in the slide debris. The second sample was a rootlet taken from the contact immediately below the slide colluvium. The sample locations within the gravel pit are shown in Figure 3.4.

The log sample and rootlet gave uncorrected carbon dates of 4360 ±90 and 4690 ±80 years BP, respectively (Appendix II). The results correlate reasonably well with the ^{14}C date of 5010 ±70 years BP obtained by Dr. Clague.

3.4 Source Area

3.4.1 General

The slide debris must have originated from the valley slopes near Bridal Falls as indicated by the direction of the flow structures in the debris deposit and from the arcuate alignment of the hummocks in the overall landform.

The slopes in the Bridal Falls area were first investigated using air photographs. From the investigation it was evident that a large asymmetrical wedge depression was present directly above Bridal Falls. The intersection of the two lateral surfaces daylights about 400 m above the Fraser Valley floor from which Bridal Creek spills forming Bridal Falls. Figure 3.1 shows the source area.

3.4.2 Slide Geometry

An enlarged 1:50 000 topographic map was used in combination with a 1:5000 topographic map (B.C Ministry of Environment) to create a 1:5000 base map of the slide area. From the map, the orientations of the failure planes were determined to be as follows: the southwest plane trends 340° with a dip of 21° and the northeast plane trends 265° with a dip of 39°. The orientation of the backscarp could not be determined from the topographic map because it has been obscured by colluvium from the steep slopes above.

With the general orientation of the failure planes known, a field investigation was initiated to search for weak zones in the rocks surrounding the slide scar which could have controlled the failure planes.

3.4.3 Discontinuity Measurement

Discontinuities were measured at all major outcrops in the slide region in an attempt to correlate their orientations to the failure plane orientations. Joint measurements were recorded according to the DISCODAT method (Herget, 1977). This is an unbiased approach using a traverse line along which the location and orientation of all discontinuities are measured. This information was supplemented by representative orientations of what were judged in the field to be the dominant discontinuities. These orientations were compared with (but not included in) the discontinuity data to ensure that all orientations were statistically correct.

3.4.4 Southwest Failure Plane

3.4.4.1 Structural Control

No correlation between any joint orientations and the southwest failure plane was found. In anticipation that the failure plane may be fault or bedding controlled, the surface trace of the southwest failure plane was determined from the 1:5000 topographic map and projected into possible outcrop locations both higher and lower on the mountain. In the field, the map trace was first followed in the southwest direction (upslope from the slide scar) and at an elevation of 1160 m, approximately 500 m southwest of the slide scar, a thrust fault was identified in outcrop (Fig. 3.10).

The thrust fault occurs between an underlying medium grained volcanic arenite and an overlying cherty limestone. The fault zone is approximately 1 m thick and can

be seen clearly in two separate locations 150 m apart. The fault zone is comprised of three subzones. The upper and lower subzones consist of clay to sand-size gouge. The middle subzone is a 70 cm layer of very weak, highly fissile breccia.

The map trace was next followed in the northeast direction from the outcrop through the slide scar and to the daylight position on precipitous slopes at about 400 m elevation in hopes of finding the continuation of the thrust fault. The lack of outcrop due to colluvium accumulation and heavy tree cover precluded the identification of any possible thrust fault continuation.

Although the thrust fault was located in only two locations, it is believed that the fault is the zone of weakness that controlled the southwest failure plane. The thrust fault may have been a product of the second phase of deformation, but the orientation is skewed from what would be expected from the northeast-southwest direction of the second phase of deformation. Intrusions of the Mount Barr and Chilliwack batholiths may have tilted the orientation of the fault from its original position.

3.4.4.2 Fault Gouge Description

If the southwest failure plane was controlled by the thrust fault then it is the weakest component of the fault zone that dominates the stability of the slide. Typically the strength of the weakest component of a fault is governed by clay content. Thin clay zones can be seen within the lower subzone. These undulating slickensided zones are typically 5 to 10 mm in thickness and continuous.

3.4.4.3 Fault Gouge Atterberg Limits

The procedure for the determination of Atterberg limits as described by Lambe (1951) was slightly modified for the testing of the fault gouge. Limits are generally performed on the fraction of soil that passes through the #40 mesh sieve (0.42 mm). However if the sample contains clay, it should never have been dryer than approximately its plastic limit. The only method to extract the particles larger than #40 sieve would be to use a wet sieve procedure. This would require mixing the gouge into a slurry for the sieve analysis, followed by a drying of the sample to a water content appropriate for Atterberg limit testing without going dryer than the plastic limit. It was decided that the risk of altering the sample from excessive drying was too great and the extra effort of the procedure would not be worthwhile since there should be very few particles larger than #40 mesh in the sample[2].

Two Atterberg limits tests were performed on the clay gouge and the results are shown in Figure 3.11. The average values are a liquid limit (LL) of 31.2%, a plastic limit (PL) of 21.1% and a plastic index (PI) of 10.1%. From these values the clay gouge has a CL classification (clay of low plasticity).

3.4.4.4 Fault Gouge Powder X-Ray Diffraction

---

[2] This proved acceptable since a later wet sieve analysis revealed that only 12% of the particles were larger than #40 mesh.

Powder XRD testing was performed on the fines (<#200 mesh) of the clay gouge and the results indicate the clay minerals are dominantly illite and chlorite (Appendix III).

The presence of a swelling clay (smectite) is of great importance to the strength of the clay gouge. Swelling clays are often interstratified with other clays, the most common types being illite-smectite and chlorite-smectite. Also, illite rarely occurs without the presence of at least some smectite (Wilson, 1987). Both chlorite and illite are present in the clay gouge thus some smectite can be anticipated. A detailed investigation showed that the clay gouge was about 10 to 40% smectite (Appendix III).

3.4.4.5 Fault Gouge Grain Size Analysis

After oven drying, the fault gouge sample was broken down using a mortar and pedestal and a dry sieve analysis was performed. The percent passing the #200 mesh sieve was low even though the sieve stack had undergone 20 minutes of vigourous machine shaking. Upon careful examination it was determined that many particles larger than #200 mesh could easily be powdered between the fingers indicating the material was insufficiently broken. Further breaking of the material by mortar and pedestal was deemed inappropriate since some of the competent larger particles could be crushed in the process. For this reason a combination wet sieving and hydrometer method was chosen. The methods followed are those outlined in Lambe (1951).

The entire gouge sample was first blended into a slurry with a deflocculating agent and distilled water. This slurry was carefully washed through a #200 mesh sieve

and into a hydrometer tube for the hydrometer analysis. The >#200 material was dried and a sieve analysis performed. The results of the dry sieve and hydrometer analysis are shown in Figure 3.12. The results show a relatively well graded material with a clay content of 25%, a silt content of 36% and a sand content of 39%.

The activity of the gouge was determined to be 0.4 using the clay content (25%) and plastic limit (10%; Sec.3.4.4.3). This value is typical of a material with an illite clay. If smectite was present in significant amounts, the activity would be much higher. It is concluded that the gouge likely has less than 20% smectite, which further restricts the percentage obtained from the XRD results of Section 3.4.4.4.

3.4.5 Northeast Failure Plane

3.4.5.1 Structural Control

The results of the joint survey (Sec. 3.4.2) were compared with the orientation of the northwest failure plane. On the spur, at an elevation of about 850 m, an jointed outcrop was found (Fig. 3.10). One joint set in the outcrop was found to have a orientation similar to the failure plane orientation as determined from the topographic map. An equal area stereoplot of the joints at this location is shown in Figure 3.13 along with the failure plane orientation.

The orientations do not exactly correlate. The average joint dip 10° steeper than that of the failure plane and the strike shows a rotation of $+15^{\circ}$. It is suspected that the spur has undergone relaxation after the slide event in the down slope direction as well as in the direction of the slide scar. This would lead to both a steeper dip and

a rotation of the rock joints. The steeper dip may also indicate that the failure plane does not follow the joint set exactly but steps through it. There was insufficient outcrop in the field to confirm this possible stepped nature of the failure surface.

3.4.5.2 Joint Description

The outcrop is heavily jointed and rockfalls continue from higher locations. The spacings of the rock joints were determined from the DISCODAT data and are shown in Figure 3.14. The joints show a roughly lognormal distribution with a mean spacing of about 14 mm. It is possible that these closely spaced joints reflect a larger pervasive series of joints which may have controlled the failure plane structurally. However, the pervasive nature of the joints was impossible to determine because of limited outcrop. Also, the closely spaced jointing may have been the result of relaxation of the spur.

3.4.6 Backscarp

The orientation of the backscarp could not be taken directly from the 1:5000 topographic map because of extensive talus deposits. The orientation of a joint set that roughly corresponded to the strike of the backscarp was deemed representative. At an undisturbed location to the north of the slide scar, at approximately the same elevation of the slide scarp (Fig. 3.10), a joint set with an average dip of 85° and a dip direction of 295° was found (see Fig. 3.10 for location). Figure 3.15 shows the stereoplot. It was also decided that the orientation of the grabens in the slide remnant

may be representative of the backscarp orientation. The average strike of the grabens was determined to be about 190° which corresponded well with the undisturbed joint orientations. Because of the greater accuracy of the undisturbed joint orientations a dip of 85° and a dip direction of 295° was used to represent the backscarp orientation.

3.5 Slide Volume

3.5.1 Source Reconstruction Volume

The pre-slide topography was reconstructed by the extension of contours, using the 1:5000 topographic map, to fill in the depression which resulted from the slide. The obscure nature of the depression made this a difficult task and therefore the results may be of limited accuracy. The pre-slide and post-slide topography were digitized, from which a source volume of 150×10^6 m^3 was calculated. A comparison of the two surfaces is shown in Figures 3.16a and 3.16b. For comparison, the well known Hope Slide near Hope, British Columbia, has a volume of about 47×10^6 m^3 (Mathews and McTaggart, 1969).

3.5.2 Colluvium Volume

The volume of the slide colluvium was determined by Smith (1971) utilizing the average elevation of the undulating basal surface of the slide debris in conjunction with an average topography elevation and the areal extent of the slide debris. The slide debris volume was calculated to be 56×10^6 m^3.

3.5.3 Volume Discrepancy

Using the volume from Smith (1971), and assuming 15% bulking, the source volume should be about 49 x 10^6 m^3, which is less than one third the volume determined from the source zone reconstruction done in this study.

There are several possible explanations for this volume discrepancy. Fraser River, which takes a sharp turn just before the slide debris (Fig. 3.1), may have flowed at the bottom of the southeast slope when the slide occurred, thus, a large volume of the material may have filled the channel. No investigation was done by Smith (1971) to determine basal slide debris elevations in this area. Another possible explanation is that the landslide scar developed in response to more than one event. Colluvium from one or more earlier events could have been removed by glacial or fluvial processes. The slope remnant from such an event could then have failed much later creating the hummocky colluvium deposit that remains today. There is also an indication on air photographs that the areal extent of the slide debris may be at least twice as much as considered by Smith (1971).

To accurately determine the volume of the Cheam Slide debris, the vertical and areal extent of the slide debris in the valley floor must be determined. A lack of natural exposure and drill hole data precluded any confirmation of the extent of the colluvium deposit in this study.

3.6 Kinematics

3.6.1 Direction of movement

The direction of movement of a wedge failure is controlled by the line of intersection of the two lateral failure planes, thus, a line connecting the centre of gravity of the pre-slide volume with the centre of gravity of the slide debris should be parallel to the line of intersection.

Using air photographs a line was drawn between the centre of gravity of the Cheam Slide debris and the centre of gravity of the source zone[3] (Fig. 3.1). The direction of movement was determined to be 327°. Using the failure plane orientations determined from the 1:5000 topographic map (Sec. 3.4.2) the direction of the line of intersection was determined to be 327°. The correlation between movement directions gives confidence to the chosen orientations of the failure planes.

3.6.2 Slide Mobility

The angle of inclination from the farthest extent of the slide debris to the top of the slide scarp is about 11.2^O. The calculated F value is 0.2 (see inset, Figure 2.8). When plotted in Figure 2.8, along with other Canadian Cordillera landslides, the mobility of this slide is not particularly unique and is quite close to the mobility predicted by Scheidegger's relationship (Scheidegger, 1973).

---

[3] The surficial centre of the slide debris was taken as the centre of gravity because variations in the thickness of the debris are not known. The centre of gravity of the source zone was determined from source zone reconstruction.

Figure 3.1. Air photograph showing Cheam Slide debris, slide scar and spur. Also shown is the direction of motion of the centre of mass (B.C. Government air photograph BC78101 No. 070).
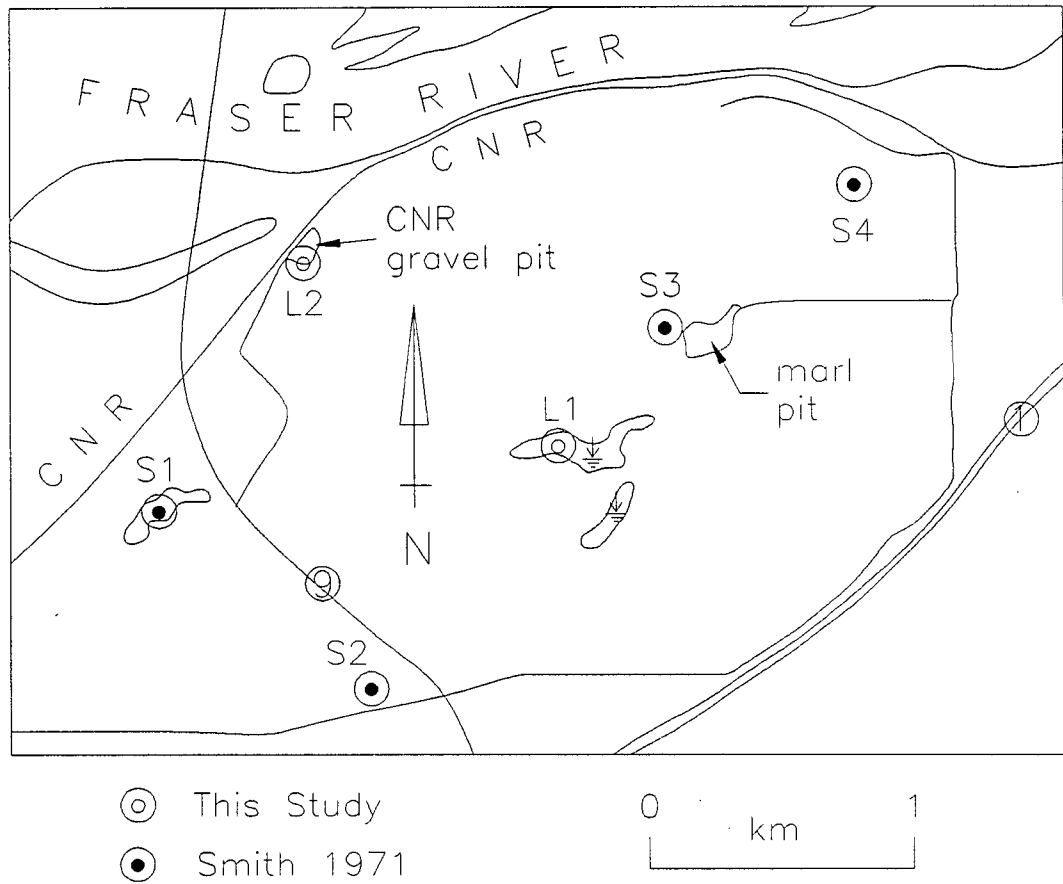
Figure 3.2. Location map of Cheam Slide debris showing CNR right of way, slide debris exposures S1 to S4, and the locations of ^{14}C sampling attempted as part of this study. L1 is the location of the swamp core sampling and L2 is the CNR Gravel Pit sampling location.
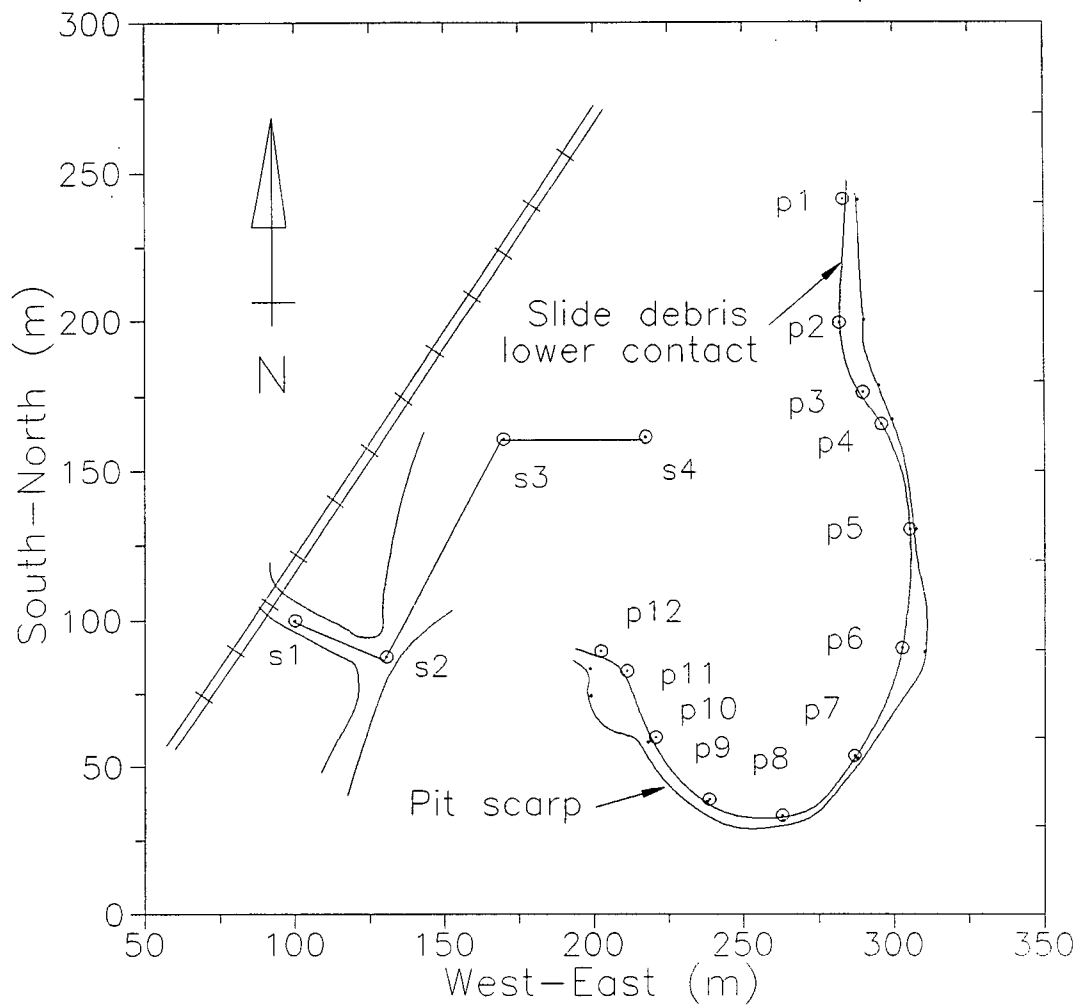
Figure 3.3 Plan view of CNR Gravel Pit showing the locations of survey stations corresponding to the lower slide debris contact (Fig. 3.4, 3.5, and 3.6 show corresponding vertical sections).
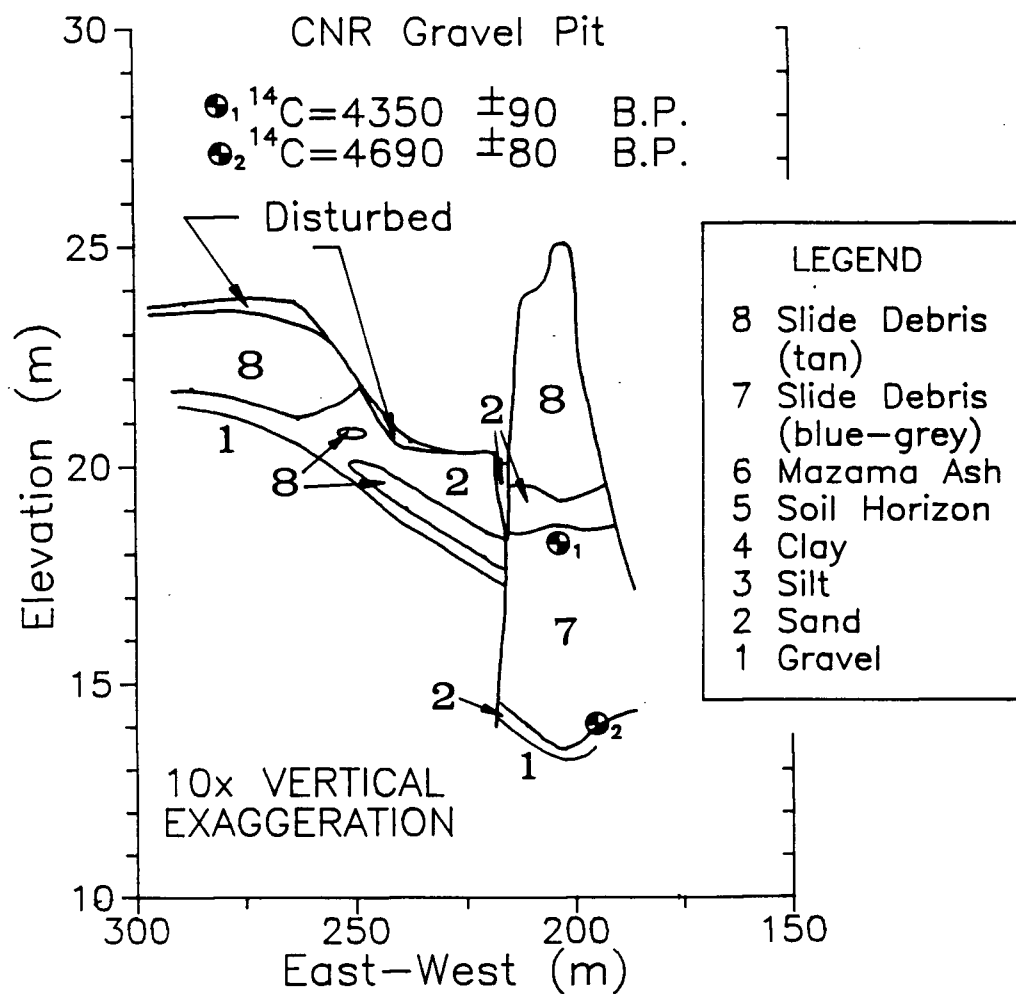
Figure 3.4. Vertical section (looking south) of the CNR Gravel Pit showing locations of samples taken for ^{14}C dating (see Appendix A for a complete stratigraphic description).
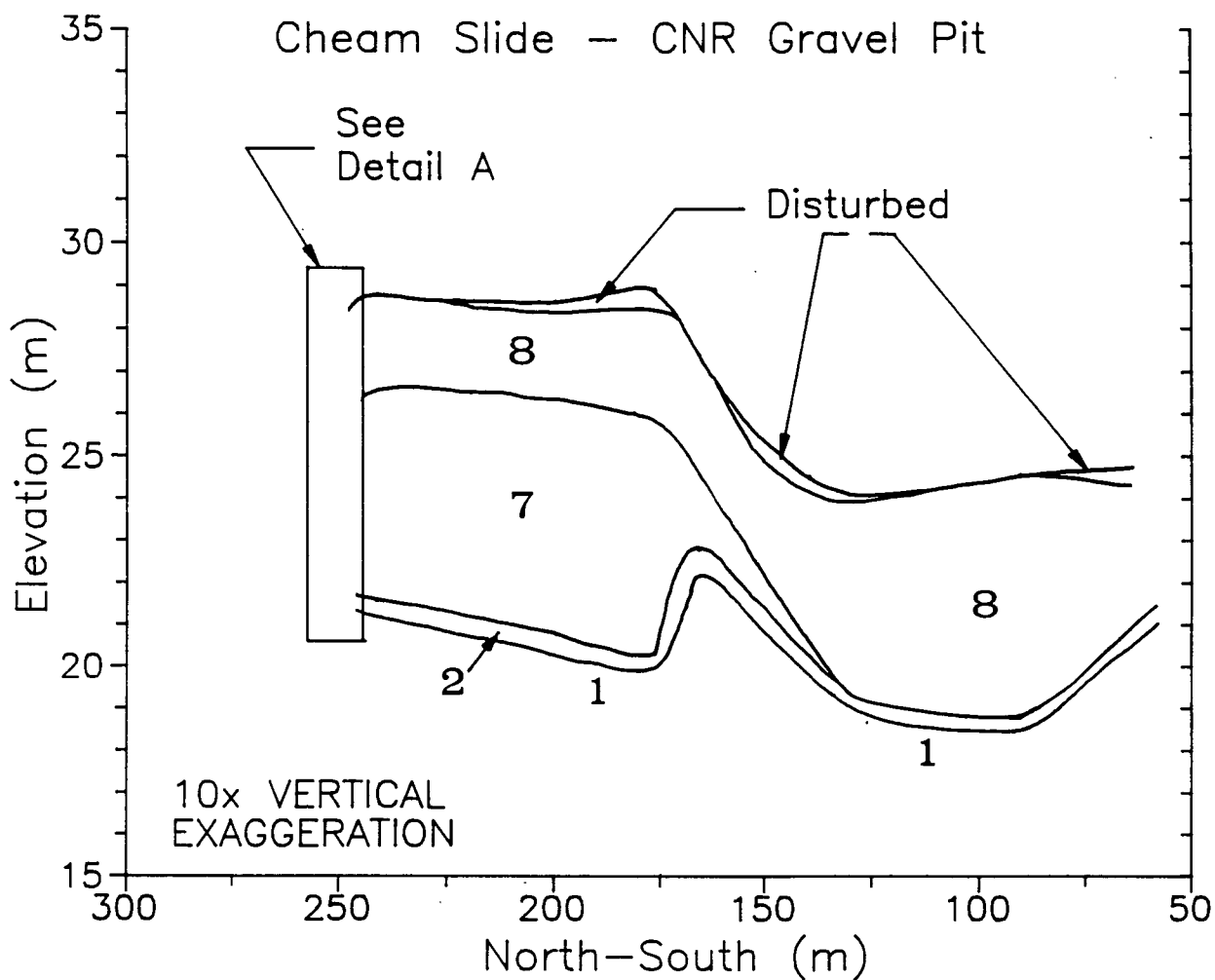
Figure 3.5. Vertical section (looking east) of the CNR Gravel Pit (see Fig. 3.4 for legend and Appendix A for a complete stratigraphic description).

DETAIL A

8

7

3

5

THRUST SHEET

FLOW
STRUCTURE

5

7

5

4

3

4

6

3

2

2

1

1

- - - Base of Section

metres

0   5

No Vertical Exaggeration
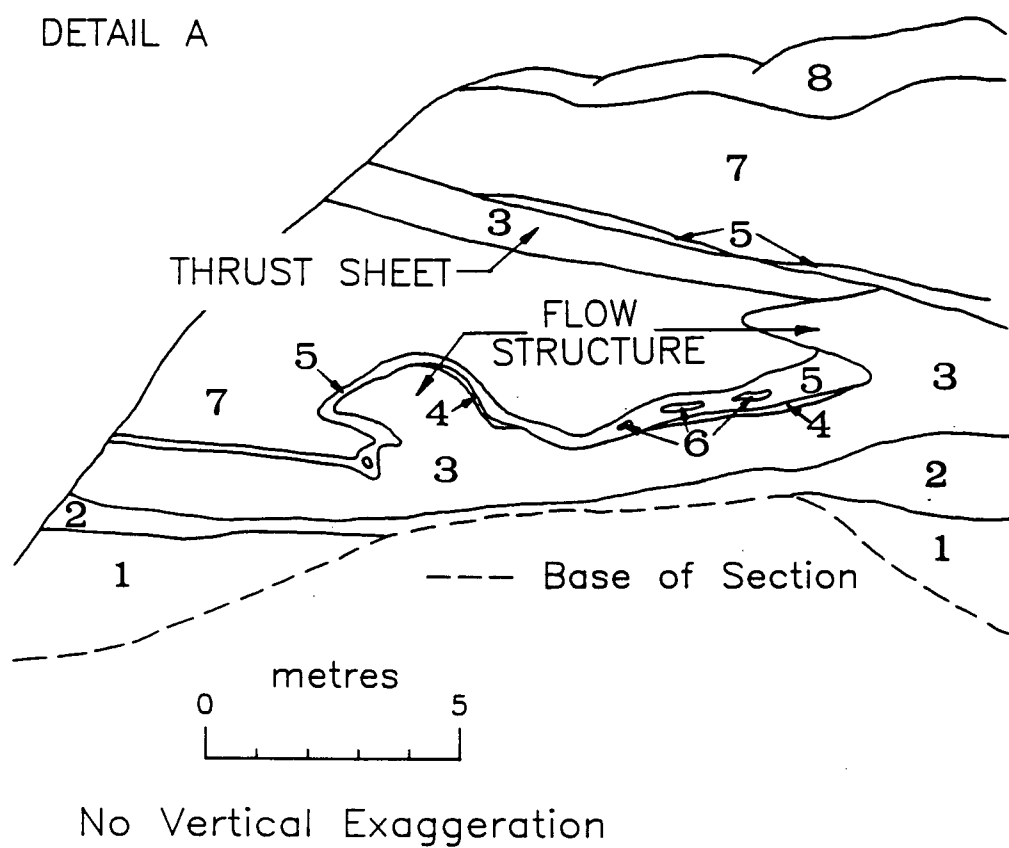
Figure 3.6. Detail A of Figure 3.5 showing dynamic loading structures (see Fig.

3.4 for legend and Appendix I for a complete stratigraphic description).
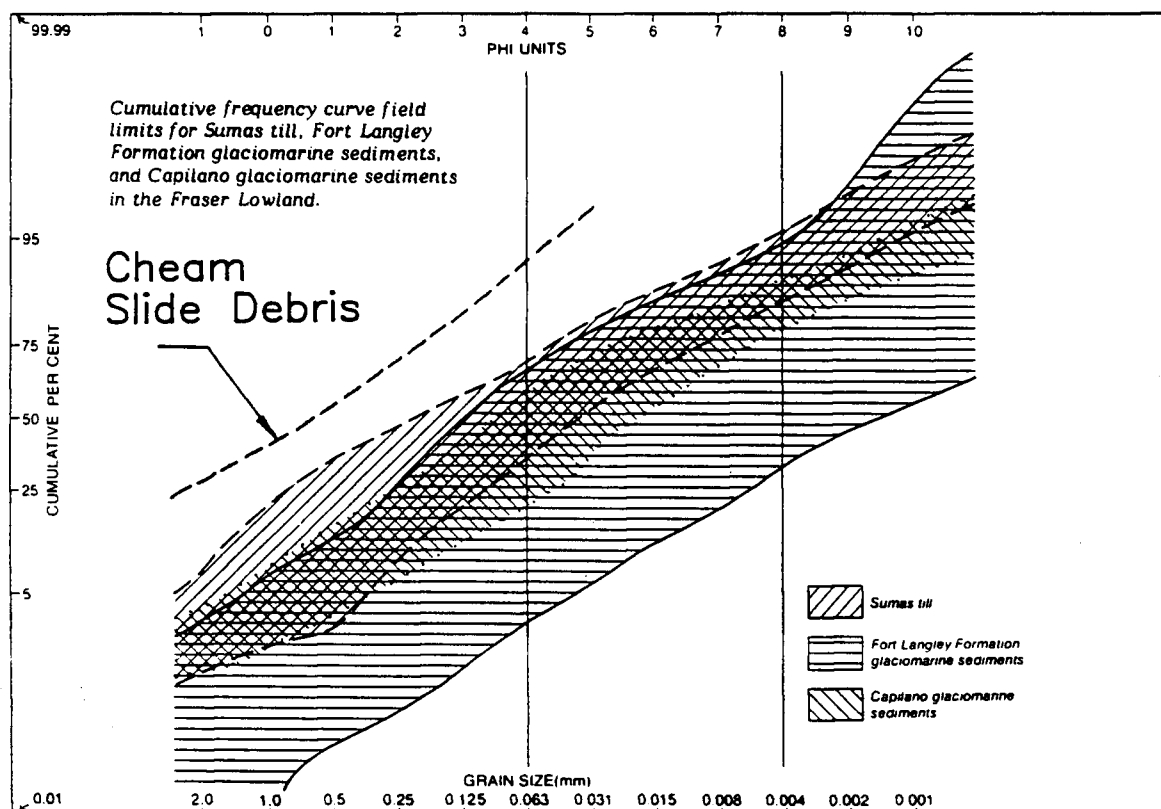
Figure 3.7. Grain size distribution of the Cheam Slide debris. For comparison, the grain size distribution of several other Fraser Lowland glacial deposits are shown (after Armstrong, 1981).
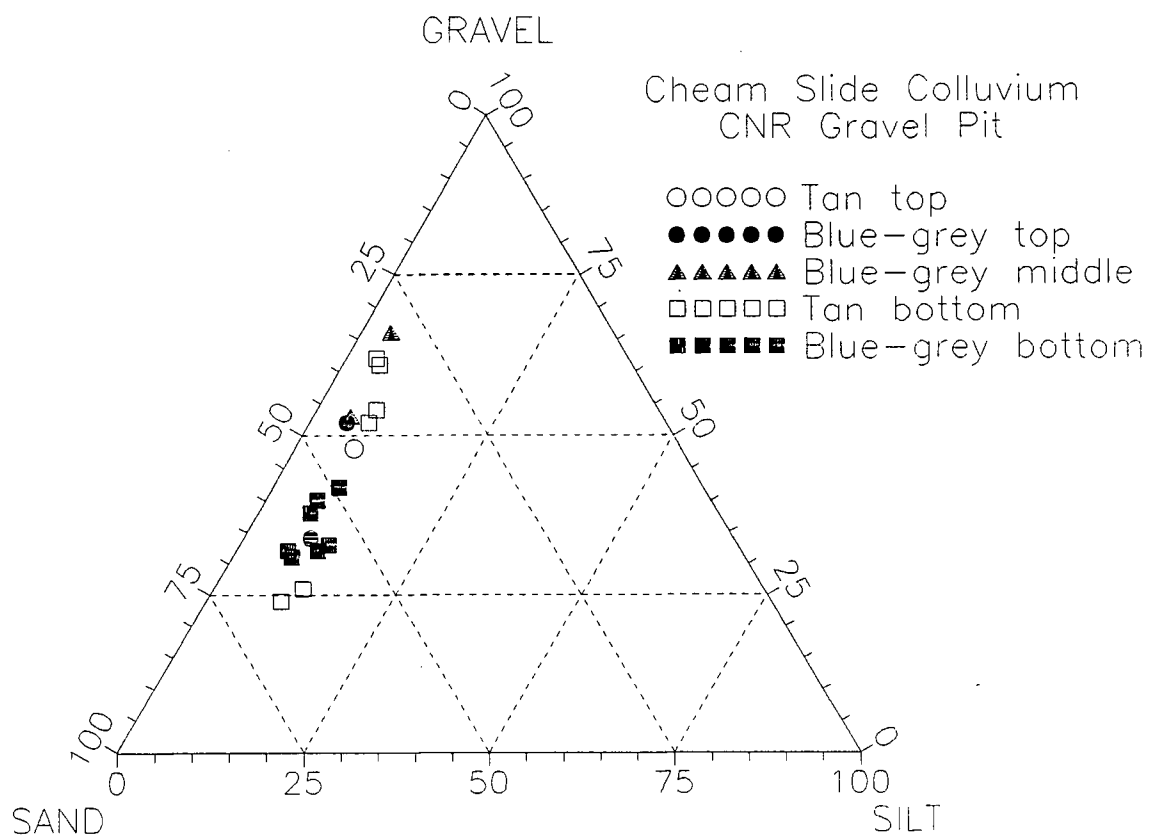
Figure 3.8. Gravel-sand-silt percentages of the Cheam Slide debris.
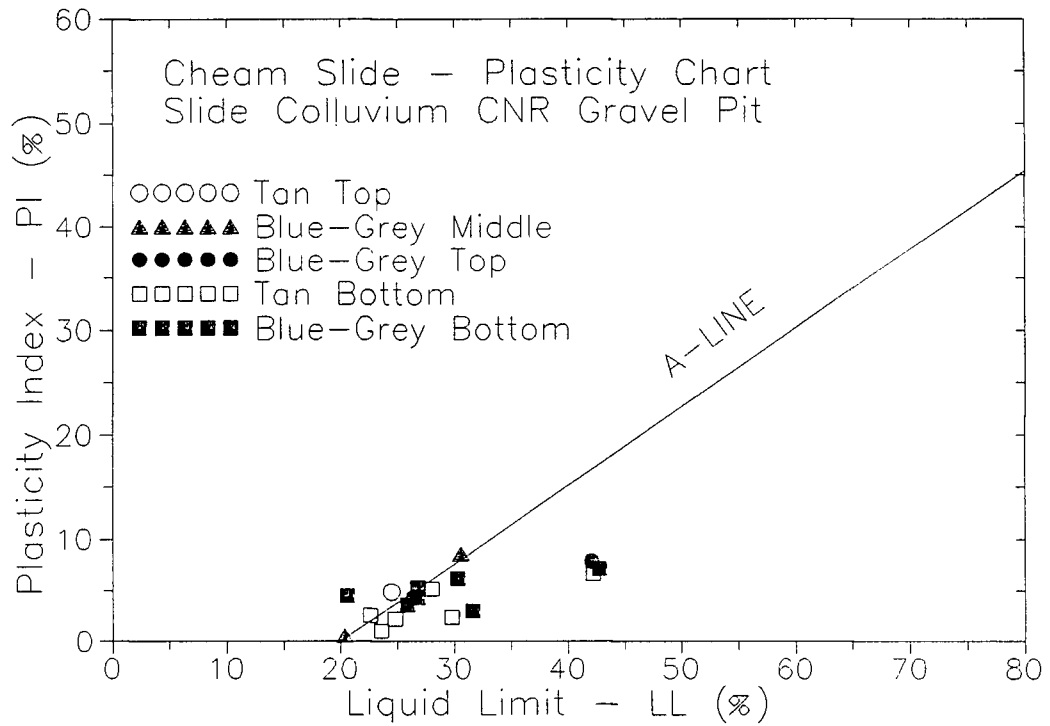
Figure 3.9. Plasticity chart of the <# 40 mesh fraction of the Cheam Slide debris. The fraction is dominantly CL-ML classification giving the total slide debris a classification of SM-SC.
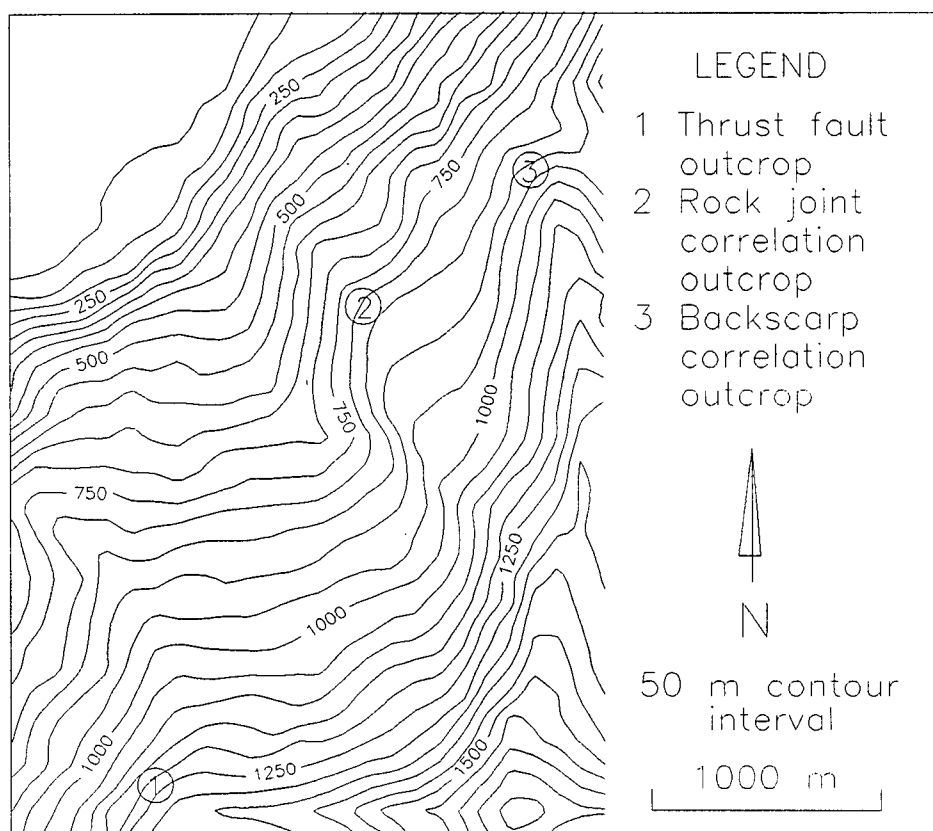
Figure 3.10. Location map of the thrust fault outcrop (1), the outcrop containing the joint set which was correlated to the orientation of the northeast failure plane (2), and the outcrop containing the joint set used to determine the orientation of the backscarp (3).
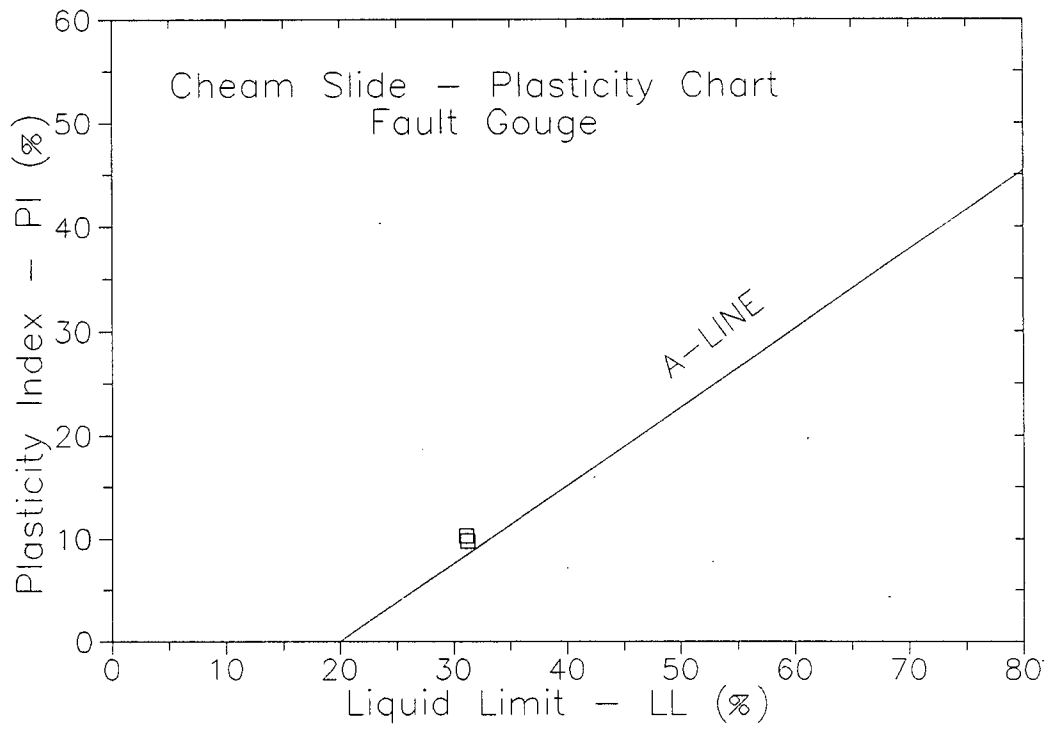
Figure 3.11. Plasticity chart of the thrust fault clay gouge.
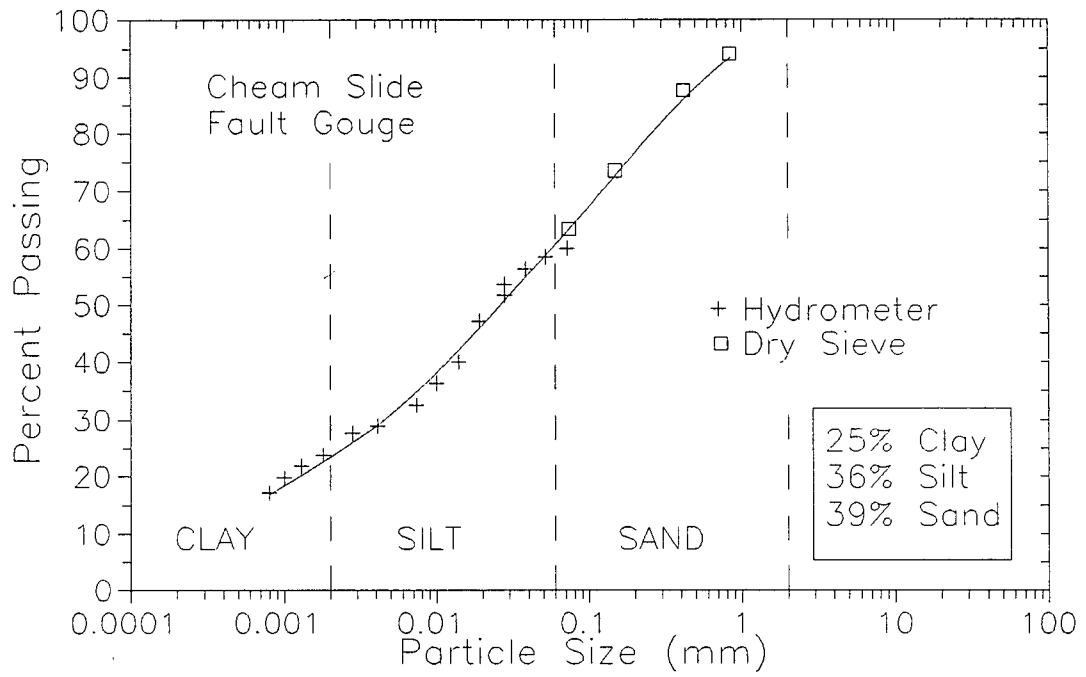
Figure 3.12. Combined hydrometer and dry sieve grainsize analysis of the thrust fault gouge.
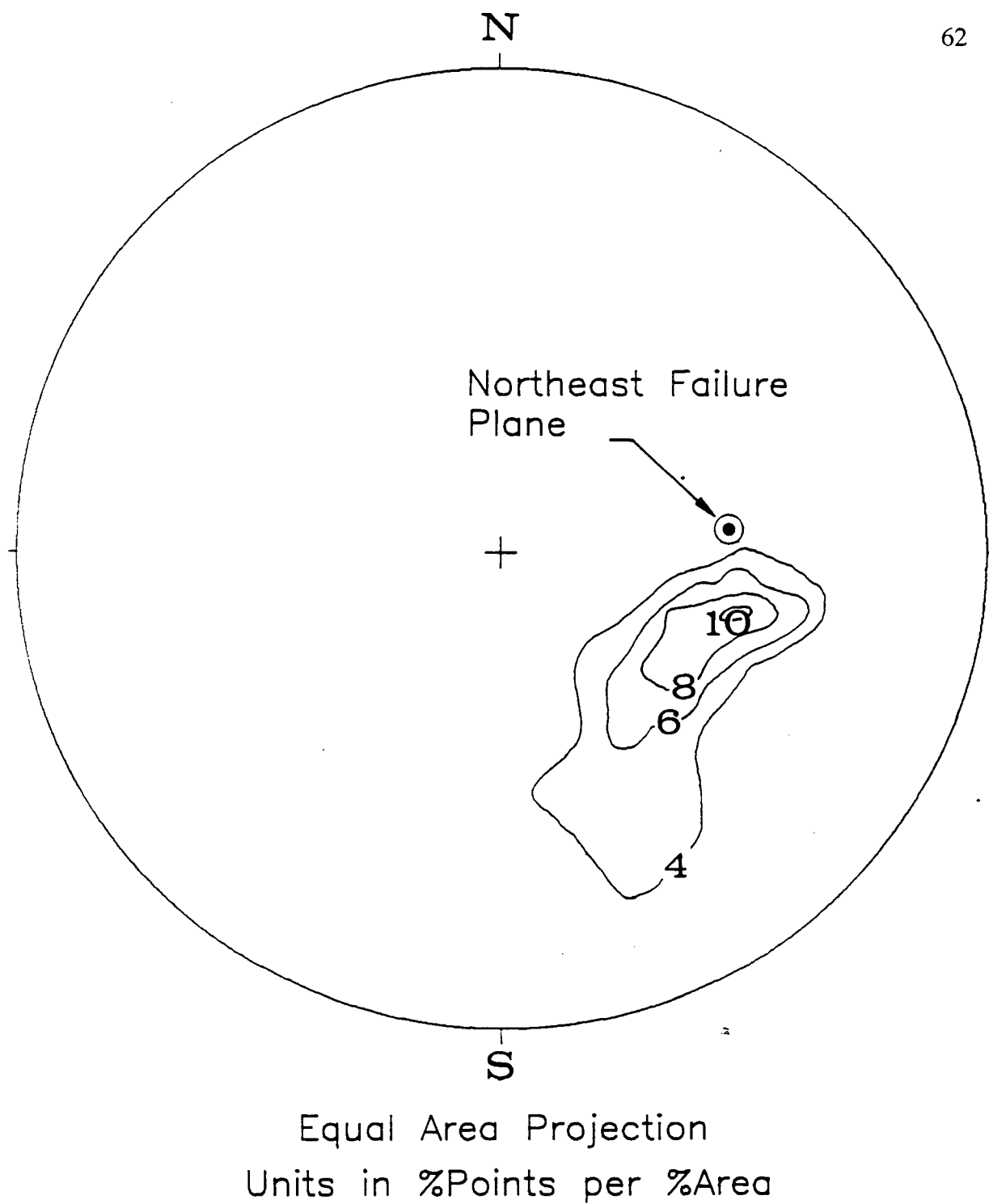
Figure 3.13. Equal area stereoplot showing the correlation of the joint set found in an outcrop on the spur (see Fig. 3.10 for location) and the northeast failure plane orientation as determined from the 1:5000 topographic map.
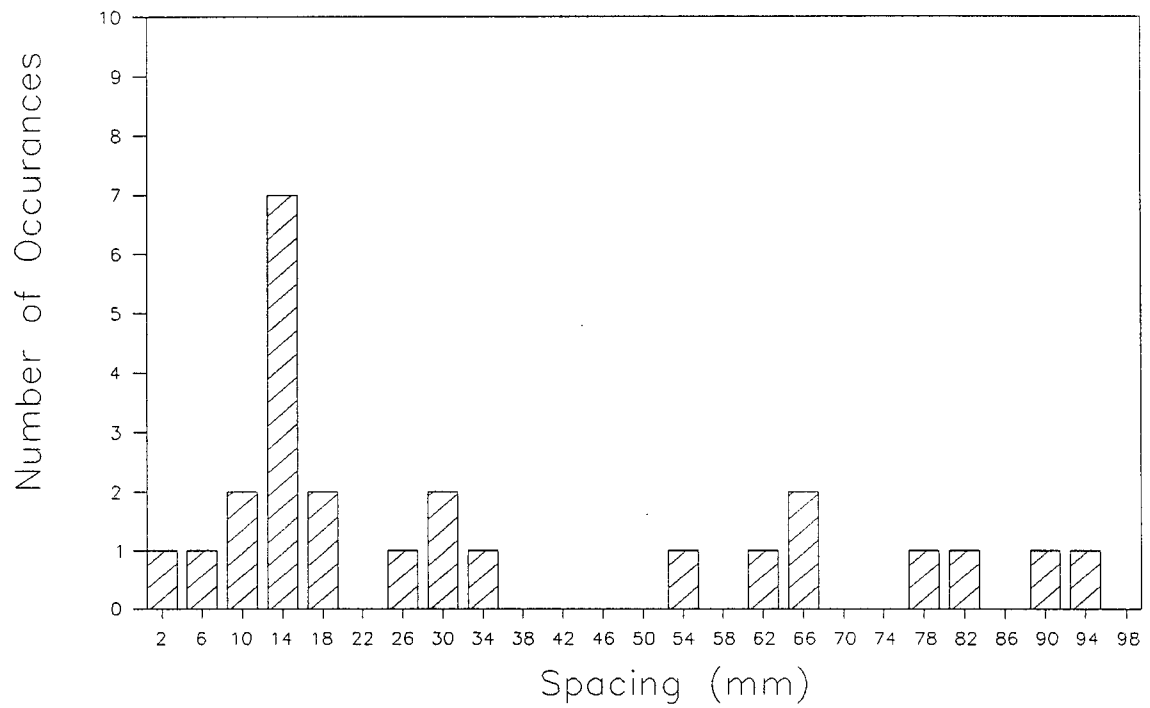
Figure 3.14. Histogram showing rock joint spacing in the spur outcrop (see Fig. 3.10 for location). The distribution is approximately lognormal and the mean spacing is about 14 mm.
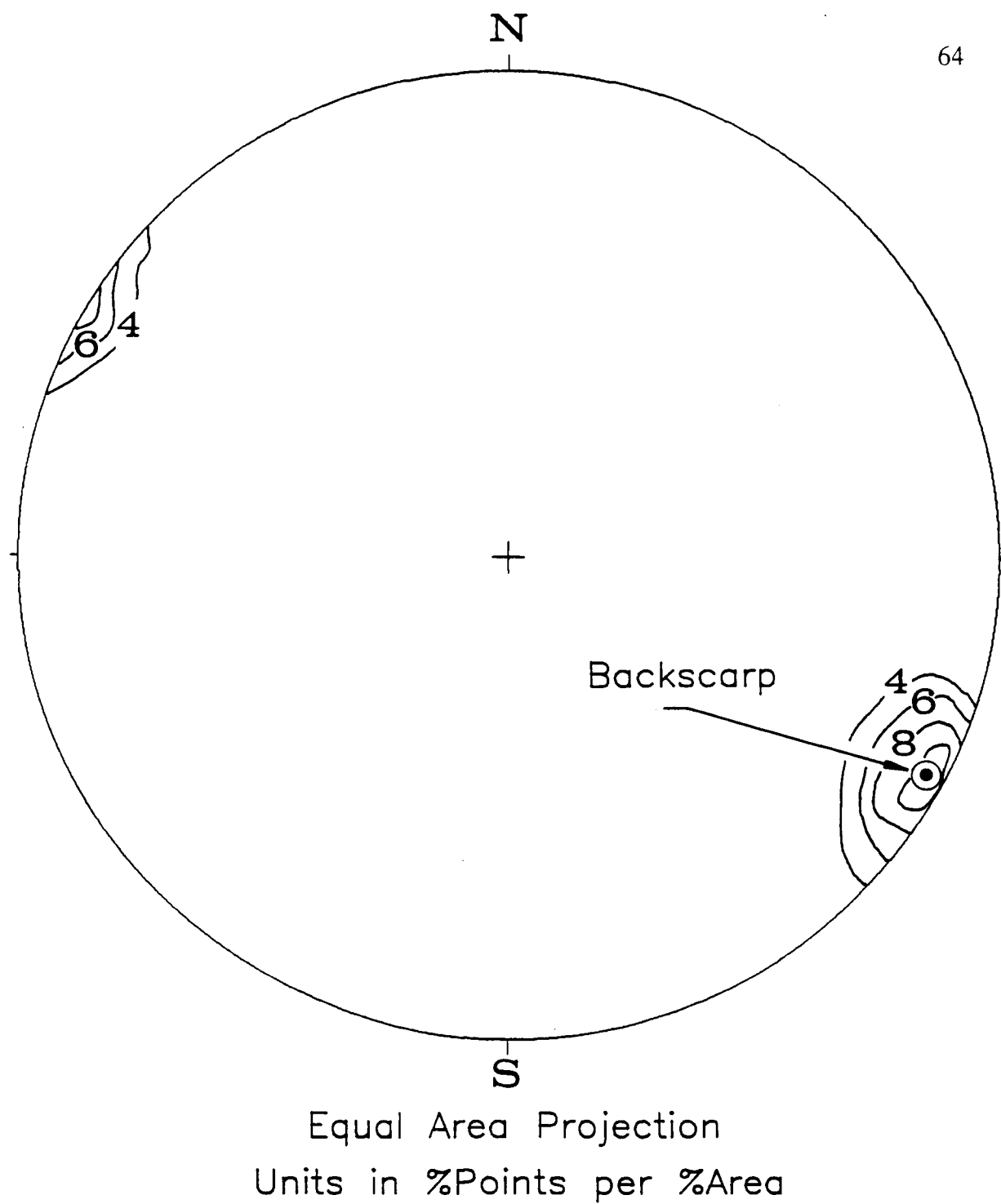
Figure 3.15. Equal area stereoplot showing the correlation of the undisturbed joint set (see Fig. 3.10 for location) and the chosen backscarp orientation.
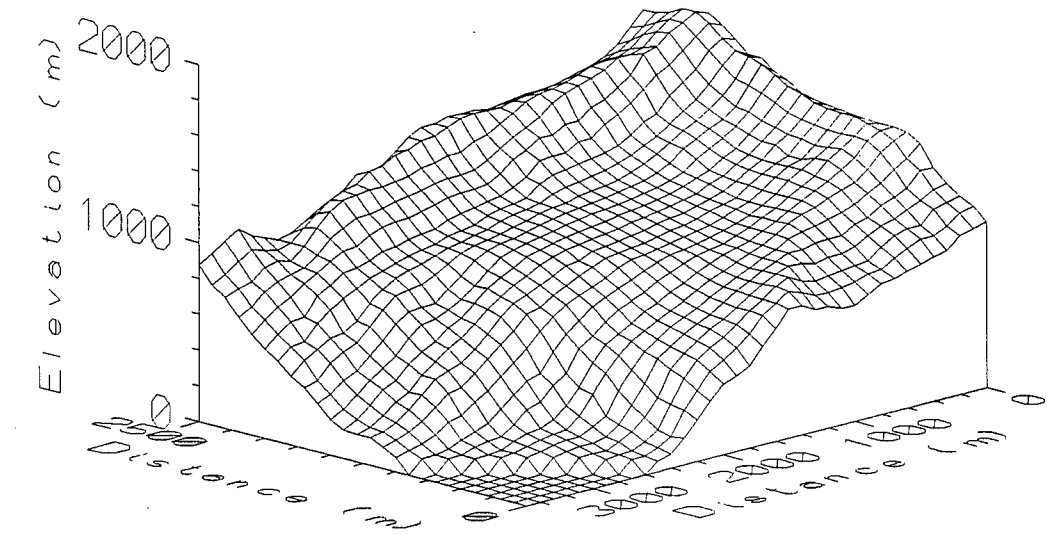
(a)
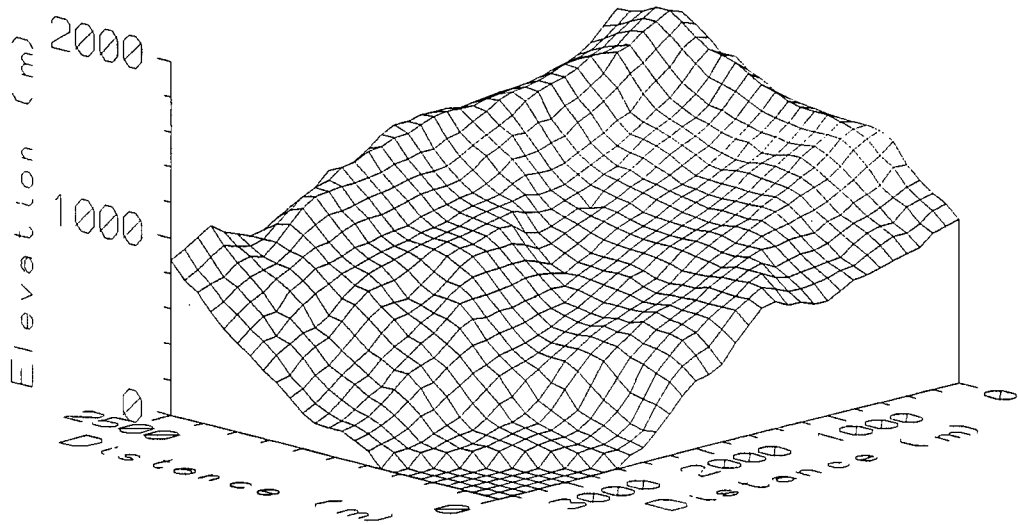
(b)

Figure 3.16. Pre-slide configuration (a) and Post-slide (b) configuration of Cheam Slide.

CHAPTER 4

INTERRELATIONSHIP OF EARTHQUAKES
AND ROCK AVALANCHES

4.1 Introduction

The random chronological occurrence of the Hope, Katz, Lake-of-the-Woods and

Cheam slides through the Holocene indicates that deglaciation and crustal rebound had

little or no influence on the failure initiation of the slides. Earthquakes are the

suspected trigger of the 1965 Hope Slide (Mathews and McTaggart, 1978; Wetmiller

and Evans, 1989). Large earthquake events have occurred through the Holocene and

these may have triggered landsliding (Heaton, 1990). To investigate the possibility of

seismic triggering a comparison between established paleoseismicity and the above

mentioned rock avalanche events was attempted.

Before the results are presented the tectonic setting of southwestern British

Columbia is reviewed in the next section to establish the framework for the recurrence

of large earthquake events.

4.2 Contemporary Tectonic Setting

The active tectonic setting of the southwest coast of Canada and the northwest coast of the United States is dominated by a subduction zone complex which is referred to as the Cascadia Subduction Zone (Fig. 4.1; Rogers, 1988). Most of the features of a subduction zone are present in the area and include: a Benioff zone of deeper earthquakes and seismicity in the overlying plate, an active chain of andesitic volcanoes, a zone of very low heat flux towards the ocean away from the volcanic line and a typical subduction zone gravity signature (Rogers, 1988).

From the magnetic anomalies preserved in the seafloor it has been determined that subduction has been active for at least 40 million years. The current vertical deformation and on going horizontal deformation indicate contemporary movement, as does the consistent level of seismicity in the offshore fracture zones with rate of plate and crust movement in the past few million years.

4.3 Megathrust Earthquake

The absence of large thrust earthquakes on the subduction zone interface in historic time is a matter of concern. Since the opening of the seismograph stations in Victoria, British Columbia and San Francisco, California in the early 1900's no thrust earthquakes either large or small have been detected. The first European settlers arrived in this area in the late 1700's. It is not likely that a large earthquake could have gone unnoticed in the last 200 years and certainly could not have escaped detection in the last 150 years.

The presence of seismicity in the overlying plate indicates that some stress is present as a result of subduction. The lack of thrust events on the subduction interface could mean that subduction is occurring by aseismic creep or else the subduction zone may be locked and rapidly accumulating strain. Deformations in the overlying plate suggest the latter is the correct assumption and this case could lead to a large scale thrust earthquake.

Rogers (1988) discussed the potential for a large megathrust earthquake. He compared the Cascadia Subduction Zone with other young lithosphere subduction zones and concluded that young lithosphere subduction zones are better able to cause megathrust earthquakes because of the greater positive buoyancy and steep rollback angle of the young oceanic crust. Through comparison to other young lithosphere subduction zones he predicted a rupture of the entire Cascade Subduction zone would cause an earthquake of moment magnitude (M_W) 9.3. Alternatively, if only the Juan de Fuca plate ruptured the result would be a M_W 9.1 earthquake (M_W 9.2 if the South Gorda was included). Maximum earthquake from the rupture of the Winona Plate would be M_W 8.2 and for the Explorer Plate the maximum would be a M_W 8.5 event.

The repeat time of a megathrust event in the Cascadia Subduction Zone cannot be based on observed seismicity. The repeat time can however be based on the characteristics of other young lithosphere subduction zone earthquakes (Rogers, 1988). Using an empirical relationship between age of subducting plate, rate of convergence and moment magnitude, the recurrence rate can be determined using a predicted slip

ratio of the amount of total possible to actual slip. Using this method, the predicted earthquake repeat times are variable. For a seismic slip to total slip ratio of 1.0-0.9 the repeat times range from about 70 years for rupture of the South Gorda Plate to about 650 years for the rupture of the entire Cascade Subduction Zone.

4.4 Chronological Earthquake and Rock Avalanche Comparison

4.4.1 Rock Avalanche Chronology

The chronology of four major rock avalanches near Fraser Corridor has been determined and the dates are as follows (all dates in years BP, unless otherwise noted):

```
Hope I ................9680 ±230 (1)
Hope II ..............1965 AD (1)

Katz ...................3260 ±70 (2)

Lake-of-the-Woods .....8260 ±70 (2)
                       8430 ±60 (2)

Cheam .................5010 ±70 (3)
                       4690 ±80 (2)
                       4350 ±70 (2)

(1) Mathews and McTaggart, 1978
(2) This study
(3) J. Clauge (Sample No. GSC-4004)
```

P. Williams (see Heaton, 1990) reported that three huge landslides fell into Lake Washington, just east of Seattle, about 1100 years ago ($\approx$983 years BP) and that two others occurred there about 1700 years ago ($\approx$1519 years BP). He suggested that the slides were triggered by great earthquakes on the Cascadia Subduction Zone.

4.4.2 Paleoseismicity

Adams (1989) predicted a correlation between megathrust earthquake events and turbidites in core samples from the Cascadia deep-sea channel. He found a total 13 turbidite deposits above a deposit of Mazama Ash dated at 6845 ±50 years BP (≈7660 sidereal[4] years). The deposits in all the tributaries over about 580 km of coastal margin occurred simultaneously indicating large scale events believed to have been megathrust earthquakes. The last five events were dated at 268, 617, 1046, 1903, and 2466 years BP. Also cited by Adams is a date by Griggs *et al.* (1969) of 4646 years BP which correlated to the eight turbidite of Adams.

Atwater (1987) studied buried lowland soils in the southwestern Washington area and discovered evidence of many decimetres of subsidence over an area of about 40 km long and wide. Carbon dating revealed events occurring at 268, 1385, 2368, 2770,and 3038 years BP. At a location in northwestern Washington, rapid subsidence took place at 894 years BP.

In a study of eight buried soils from South Fork Willapa River in southwestern Washington, Hull (1987) concluded that sudden burial occurred at 131, 1747, 2460, 2860, 3141, 3760, and 4290 years BP. Also cited is an undated event that occurred sometime between 131 and 1747 years BP. Hull (1987) further stated that the data indicated a regional burial at this site which is in agreement with a tectonic model that

---

[4] The period in which the sun apparently returns to the same position among the stars (Funk and Wagnalls Standard College Dictionary).

requires significant trench-normal subsidence during large earthquakes at Cascadia Subduction Zone.

4.4.3 Discussion

The chronology of the four rock avalanches is compared with established paleoseismicity in Figure 4.2. All three paleoseismicity studies agree that the last event occurred somewhere in the last 100 to 300 sidereal years. Adams (1989) and Hull (1987) both show events at about 1000 years BP. Adams (1989), Atwater (1987) and Hull (1987) date an event at about 2500 years BP. Atwater (1987) and Hull (1987) cite events at about 2800 and 3100 years BP.

The correlation of the rock avalanche chronology to the paleoseismicity is weak. The Hope I and the Lake-of-the-woods events occur before any established paleoseismicity, thus no correlation is possible. The large range of dates for Cheam Slide precludes any direct correlation between the time of slope failure and paleoseismicity except that there was likely a large seismic event during that time span of the Cheam Slide dates. There is weak correlation between the Katz Slide event and established paleoseismicity. Atwater (1987) and Hull (1987) cite event dates of 3038 and 3141 years BP, respectively which are close to the Katz Slide date of 3260 years BP. The slide events of 983 and 1519 years BP of Williams (see Adams, 1989) show weak correlation to the seismic events of Atwater.

Clearly, the correlation between paleoseismicity data and rock avalanches is weak. However, as work continues and more data is gathered, decisive evidence may

be found indicating that correlations do exist.
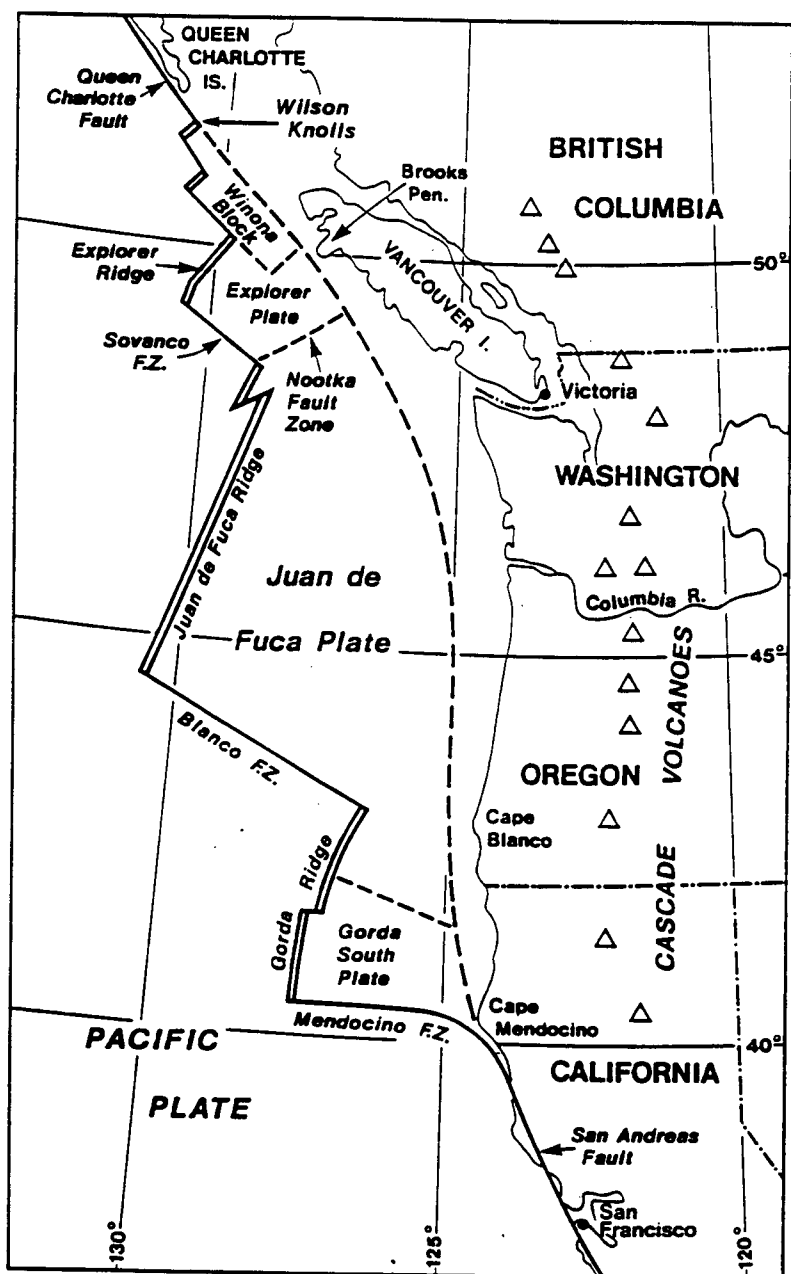
Figure 4.1. Cascadia Subduction Zone (from Rogers, 1988).

Adams (1989) ├──────────────┼──┼────┼─┼┤
Atwater (1987)   ├┼─┼────┼──┼─┤
Hull (1987)   ├─┼──┼┼┼───┼────────┤

├──────┼┼───────────┼┼┼────┼──────────┼──┼──────┤

HOPE 1 └─┘   └─┘ KATZ   *   * HOPE 2
       LOTW   CHEAM

┌────┬─────┬─────┬─────┬─────┬─────┐
10000 8000   6000   4000   2000   0
Radiocarbon Years Before Present
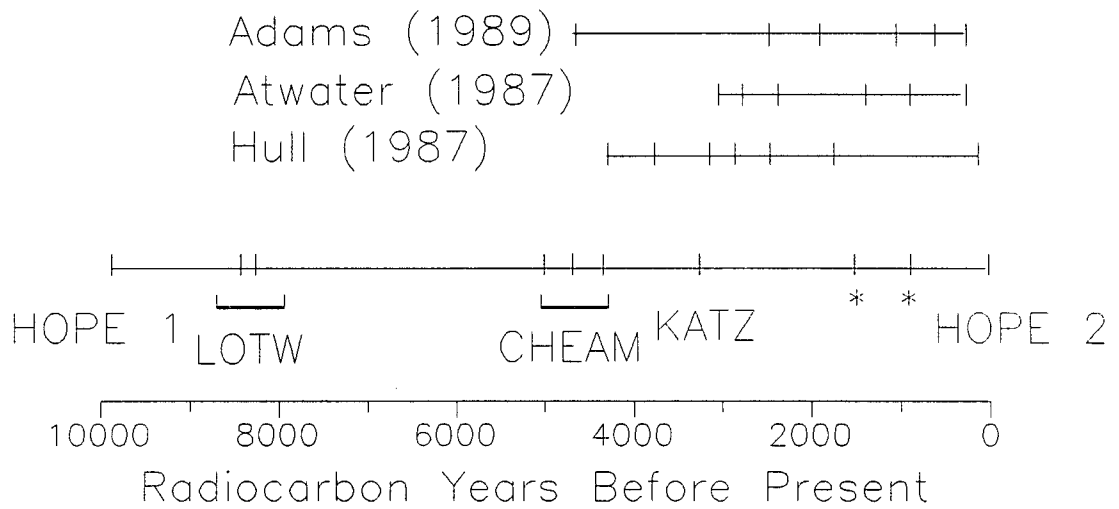
* Lake Washington landslides

Figure 4.2. Chronological comparison of established paleoseismicity and large rock avalanches in southwestern British Columbia and northwestern Washington.

CHAPTER 5

INTRODUCTION
TO STABILITY ANALYSIS

5.1 Introduction

The preceding chapters were concerned with the geology and geomorphology of

the Katz, Lake-of-the-Woods and Cheam slides with emphasis placed on Cheam Slide.

It was determined that Cheam Slide was a wedge failure with a volume of

approximately 150×10^6 m^3. The southwest failure plane is believed to have been

controlled by a predominant thrust fault and the northeast failure plane by an

extensive joint set (Sec. 3.4.4 and 3.4.5). The orientations of the two failure planes

have been determined (Sec. 3.4.2) and their accuracy confirmed through centre of mass

comparisons (Sec. 3.6.1).

Little information is known regarding the conditions of Cheam Slide when

catastrophic failure occurred. Specifically the trigger for the event and the nature of

possible progressive deformations that could have systematically decreased the factor

of safety, are unknown. There is a growing awareness of a relationship between

seismicity and catastrophic landslide events (Wetmiller and Evans, 1989; Evans, 1989;

Evans *et al.*, 1987; Keefer, 1984; and others). Although available data precludes a definitive stability analysis of Cheam Slide, an evaluation of the relative significance of pore pressure related verses seismic triggers is possible and represents an important contribution to a more comprehensive hazard risk assessment in the strategic Fraser Corridor.

5.2 Introduction to Stability Modelling

Slopes, governed by the laws of nature, strive to decrease their gravitational potential energy. Mass movements in various forms provide the mechanism. The most dramatic of the mass movements are large scale rock avalanches, which can be devastating in highly populated or frequently travelled areas. Effective ways to assess risks associated with large rock avalanches are of utmost importance.

To assess the risk of slope failure, or to determine the controls of a failed slope, a slope stability model is used frequently. Generally, the model is solved by computer technique. Computers can offer high computational speeds allowing very complex analysis processes to be used. However, complex programs often require very detailed input which is not always available. If data is limited a simpler process of analysis is often used.

The simple modelling technique is useful for determining the failure conditions of pre-historic slides. In these situations, rarely are parameters known with accuracy and therefore, complex analysis, is generally not warranted or possible. For this

reason, a simple modelling technique will be used for the stability modelling of Cheam Slide.

5.3 Triggering Instability

5.3.1 General

The initiation of a slope failure is the result of a disruptive change of the equilibrium forces within a slope. Stated simply, when the driving forces in the slope are less then the resisting forces the slope will be stable. If the driving forces overcome the resisting forces movement will occur.

The stability of slope is often expressed as a Factor of Safety (FOS) which is defined as:

$$\text{FOS} = \frac{\text{Sum of Resisting Forces}}{\text{Sum of Driving Forces}} \qquad [7.1]$$

A FOS >1 indicates a stable slope and conversely a FOS <1 indicates an unstable slope.

The driving and resisting forces within a slope can be altered in a number of ways. The removal of toe support, by either natural processes or the activities of man, lowers the resisting force. High pore pressures within a slope decrease the effective force between potential failure surfaces, thereby reducing their strength. Earthquakes cause momentary loading of the slope increasing the driving forces.

The failure of a slope is a time dependent phenomena. For example, if the resisting force is temporarily overcome by an applied load, movement will occur and the strength conditions will almost certainly change. The changed conditions may result in the acceleration of slope movement or, if the effect of the movement was minimal, the slope once again becomes stable.

5.3.2 Pore Water Pressures

One of the major causes of slope instability is the presence of higher than normal pore pressures at the potential failure surface. Increases in pore pressure can be attributed to: high rainfall, a quick spring snow melt resulting from higher than normal temperatures perhaps combined with heavy precipitation, the freezing of a saturated groundwater discharge zone at the toe of the slope, or the submergence of the toe of a slope.

A classic example of the effect of pore pressures on the stability of a slope is the 1963 Vaiont Slide in Northern Italy. 169×10^6 m^3 of rock failed catastrophically into the Vaiont Dam reservoir resulting in a wave that overtopped the dam by more than 160 m. The water rushed down the valley flooding towns and killing 1925 people. The major cause of the failure of Vaiont Slide was the increase in slope pore pressures resulting from the combined effect of raising the reservoir level and heavy rainfall (Hendron and Patton, 1985).

5.3.3 Seismic Loading

Earthquakes have long been recognized as a major cause of landslides. In 1970, a Richter Local Magnitude (M_L) 7.7 earthquake triggered a 50-100 x 10^6 m^3 rock avalanche from Nevados Huascaran, the highest peak in the Peruvian Andes causing an estimated 18 000 casualties (Plafker and Ericksen, 1978). The 1964, M_L 8.4 Alaskan earthquake is believed to have triggered the 10 x 10^6 m^3 Sherman Glacier Rock Avalanche, as well as approximately 80 other major rock avalanches (McSaveney, 1978). In Montana, the 1959 M_L 7.1 Hebgen Lake earthquake triggered the 20 x 10^6 m^3 Madison Canyon Rockslide (Hadley, 1964 and 1978). The rockslide blocked Madison River resulting in a lake 10 km long and about 60 m deep. In the summer of 1946 a M_L 7.3 earthquake shook central Vancouver Island. Mathews (1979) reported that as many rockfalls occurred in one minute as might be expected to occur in several decades in the absence of an earthquake. The largest of the landslides is believed to have occurred from the slope of Mt. Colonel Foster which plunged into a small lake resulting in a large wave (Evans, 1989). Two small earthquakes of M_L 3.2 and M_L 3.1 were associated with the 1965 Hope Slide. Wetmiller and Evans (1989) stated that although the validity of a seismic trigger cannot be demonstrated unequivocally, either of the two small earthquakes were capable of triggering the initial slope movement, provided it was located within a few kilometres of the slide site.

Keefer (1984) carried out a survey of earthquake induced landslides. He investigated the effect of 40 historic earthquakes[5] on the stability of slopes to determine the characteristics, geological environments, and hazards of landslides caused by seismic events. The landslides from the study were classified and the relative abundance of each type is shown in Table I (the values must be considered "order of magnitude" approximations). The most abundant landslides were rock falls, disrupted soil slides, and rock slides. Their abundance indicated that they were susceptible to initiation by seismic loading and that the geological conditions that produce them were widespread in the seismic regions.

5.4 Stability Analysis Methodology

The ability of a landslide to fail catastrophically is dependent on the relationship between the driving stress from the weight of the incipient slide mass and the residual strength of the failure surface. Figure 5.1 shows a typical elastic-plastic stress-strain curve and three zones of static driving stress. Zone (1) includes all static stress levels higher than peak strength. Zone (2) includes all values from residual to peak strength and zone (3) includes all values lower than residual strength.

A zone (1) static stress level would result in immediate catastrophic failure. A zone (2) static stress level would result in a metastable slope condition requiring an external force to surpass peak strength. Once peak strength has been exceeded there

---

5 Keefer's data is based on an incomplete data set. Many recognized areas of earthquake induced land sliding were not included in the study (Schuster, 1990).

would be sufficient static stress to allow continued acceleration of the slope resulting in catastrophic failure. The static stress levels of zone (3) would not result in catastrophic failure even if peak strength was surpassed, since there is insufficient static driving stress for continued acceleration.

Incorporating the above ideas, two stability constraints can be used for the modelling of Cheam Slide. The first constraint is: the slide was a catastrophic failure. Therefore, at the time of failure, the residual strength of the failure surface was lower than the static stress imposed by the incipient slide mass (zone (2)). The second constraint is: the peak strength must have been surpassed before the slide obtained residual strength. To determine if the criteria of zone (2) are met, the slope was modelled using residual strengths. To determine what conditions were necessary to surpass peak strength the slope was modelled using peak strength parameters[6].

---

[6] Peak Strength usage here refers to the highest available strength on pre-existing discontinuities, some of which have experienced considerable shear-displacement.

TABLE I. Relative abundance of earthquake-induced landslides. Numbers are order of magnitude estimates (after Keefer, 1984).

Landslide type,
listed in order of
decreasing total numbers

Very abundant: >100,000 in the 40 historical earthquakes

Rock falls
Disrupted soil slides
Rock slides

Abundant: 10,000 to 100,000 in the 40 historic earthquakes

Soil lateral spreads
Soils slumps
Soil block slides
Soil avalanches

Moderately common: 1,000 to 10,000 in the 40 historical earthquakes

Soils falls
Rapid soil falls
Rock slumps

Uncommon: 100 to 1,000 in the 40 historical earthquakes

Subaqueous landslides
Slow earth flows
Rock block slides
Rock avalanches

83
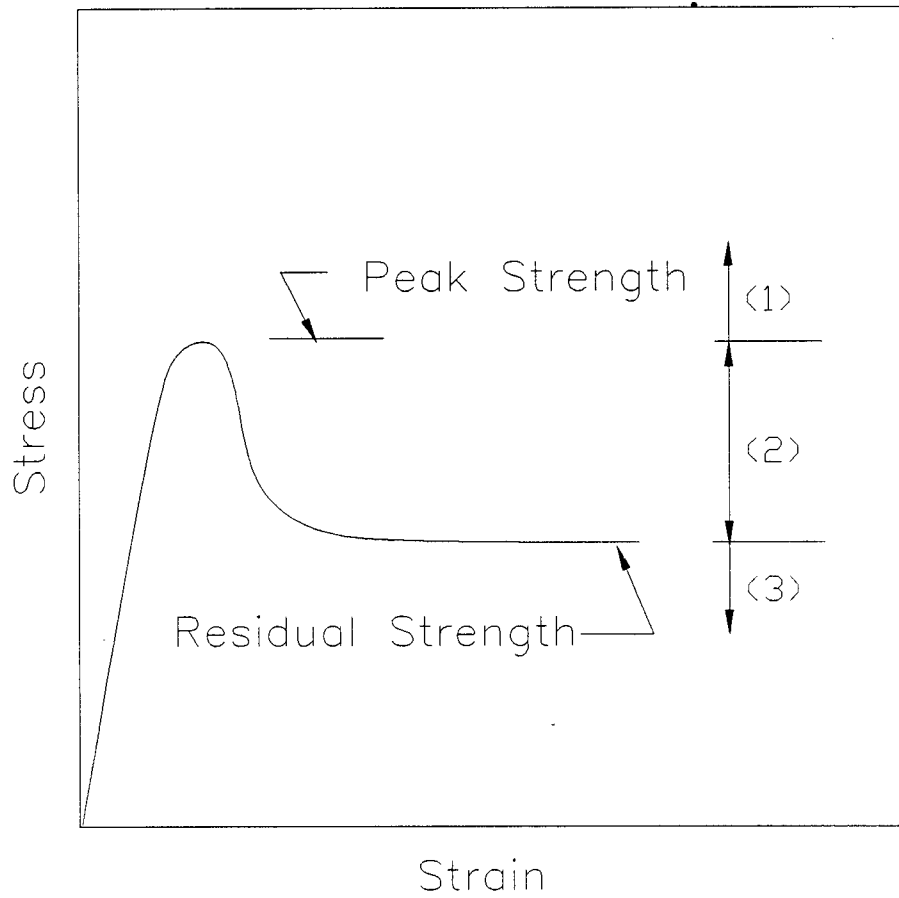
Figure 5.1. Static stress considerations for determining catastrophic failure.

CHAPTER 6

MODELLING PARAMETERS

6.1 Plane Orientations

Cheam Slide has an asymmetrical wedge geometry which can be represented in simplified form by five planar surfaces as shown in Figure 6.1. To confirm the accuracy of the simplified model, five down slope cross sections of the reconstructed slope were compared to five plane wedge geometry cross sections. All five sections compared favourably. Two of the sections are shown in Figure 6.2 as examples of the comparisons.

6.2 Southwest Failure Plane

6.2.1 Strength Considerations

The southwest failure plane of Cheam Slide is considered to have been controlled by a gouge filled thrust fault as discussed in Section 3.4.4. Rock discontinuities of this type represent one of the greatest problems in rock engineering

(Barton and Bakhtar, 1987). The strength is controlled by both the nature of the wall rock and the filling material. If the thickness of filling is less than the amplitude of the asperities of the wall rock, there will be rock-to-rock contact after some shearing. If the filling is thicker, then the strength of the rock is mostly controlled by the infilling material. When the filling is about 2 to 3 times thicker than the amplitude of the asperities, the wall rock effect is eliminated (Goodman, 1970).

6.2.2 Residual Strength

Under continued shearing all soils will eventually reach a condition where the shear strength and water content are functions of only the soil composition and applied stresses. At this point the soil is at its residual strength. When Cheam Slide failed catastrophically, it can be envisioned that one of the discrete shear zones within the thrust fault experienced sufficient movement to bring the strength to residual.

To obtain true residual strength the plates of the clay minerals in the gouge must be co-planar. The presence of granular particles hampers this formation. As the proportion of granular particles increases it becomes increasingly difficult to align the clay minerals, resulting in higher residual strengths (Skempton, 1985).

The residual friction angle of a clay rich soil is usually determined by shearing a soil sample under drained conditions at very low shearing rates over a large displacement (often >500 mm). A suite of these tests are undertaken to determine, with confidence, the residual friction angle. Unfortunately, such extensive testing was not possible within the time frame of this study.

Skempton (1985) described an empirical relationship between residual angle, clay fraction (CL) and activity (PI/CL ; PI=Plastic Index). The relationship was based on extensive residual field and laboratory direct shear testing and is shown in Figure 6.3.

The fault gouge was determined to have an activity of 0.4 and a clay content of 25%. From these values a residual friction angle of 26° was obtained using Skempton's relationship . This friction angle should be considered a maximum since the sample was almost certainly contaminated by sand and silt foreign to the shear zone. The sand and silt likely was introduced because of the difficulty in sampling only the thin shear zone without including some surrounding material.

A minimum residual strength can be determined from the clay mineralogy. Kenny (1967) performed extensive drained direct shear testing to determine the effect of mineralogy on the residual friction angle. He found that illite had a residual friction angle of between 17° and 24°. Using the results of Kenny (1967) as minimum and the results using Skempton's relationship as maximum, a residual value of between 17° and 26° was considered to be appropriate for residual strength stability testing of Cheam Slide.

6.2.3 Peak Strength

The thrust fault could have exhibited peak strength behaviour as a result of two factors. First: if the relief of wall rock asperities was larger than the thickness of the infilling, then some dilation related increase in shear strength parameters would have occurred. Second: if the thrust fault had not experienced enough movement for the

alignment of clay particles, or if the direction of tectonic displacement was different from that of gravity displacement, then the full residual strength would not have developed.

The possible effect of the thrust fault wall asperities on the peak strength could not be determined because of the lack of fault exposure. It is suspected that because the thrust fault separates two previously conformable units, the ramp angle of the major asperities would be quite small, likely less than 4°.

Slickensides were found in the clay gouge but were not aligned with the direction of slide movement. It is suspected that these slickensides were the result of fault movement. The fault has probably not undergone tectonic displacement since the emplacement resulting in some healing of the shear zone. The healing would result in the development of some increased strength but it is probable that the residual strength would only require minimal movement to be regained.

Incorporating the low ramp angle and the healing on the shear zone, peak friction angles 6° larger than the corresponding residual angles were considered maximum for stability testing, giving a peak strength range of 23 to 32°.

6.3 Northeast Failure Plane

6.3.1 Strength Considerations

The northeast failure plane of Cheam Slide is believed to have been controlled by an extensive rock joint set. The joints were not filled and likely had variable roughness depending on the grainsize of the rock. At the deepest location within the

incipient slide mass the normal pressure on the rock joints would not have exceed 6 MPa.

The peak strength of rock joints with roughness subject to low confining stresses (<10 MPa) is controlled dominantly by the angle and height of the asperities of the wall rock. As the joint begins to slip the rock will attempt to dilate. The more the rock must dilate to overrun the asperities, the higher the strength will be. If the asperities are steep, a higher shearing stress will be required to overrun the asperities resulting in higher joint strength.

When the rock dilates sufficiently to overrun the asperities the joint surfaces will no longer match and the residual strength will have been reached. From extensive testing it was determined that the residual strength of a rock joint is approximately equal to the friction angle between smooth surfaces (Barton and Bakhtar, 1987).

The peak strength failure envelope of a rock joint is rarely linear. Hassani and Scoble (1985) performed extensive shear testing on natural joints and saw cut surfaces (Figure 6.4). Rock joints have no true cohesion, thus, at zero normal stress the shear strength of the rock discontinuities is zero. With increasing normal stresses, frictional strength increases rapidly giving a curved strength envelope. The curve levels out at higher normal stresses into a linear relationship. The curvature of the failure envelope is pronounced most in rock joints of high roughness.

Typically, a near linear shear strength envelope is defined by the Mohr-Coulomb strength criterion which is given as:

$$T = C + \sigma_n \tan \emptyset \qquad\qquad [6.1]$$

where:

$$T = \text{shear strength}$$
$$C = \text{cohesion}$$
$$\sigma_n = \text{normal stress}$$
$$\emptyset = \text{friction angle.}$$

This relationship would tend to overestimate the strength of the discontinuities at lower normal pressures which would produce non-conservative results.

Hoek and Brown (1981) proposed a non-linear strength model given as:

$$T = A \, U_C \, (\sigma_n/U_C - D)^B \qquad\qquad [6.2]$$

where:

$$U_C = \text{uniaxial compressive strength of the intact rock}$$
$$A,B,D = \text{empirical constants.}$$

This more rigorous relationship should be used if the curvature of data is large or if the critical nature of the investigation warrants it.

6.3.2 Residual Strength

Monger (1966) described the rock in the Cheam Slide area as a dominantly medium to course grained sandstone. Barton and Bakhtar (1987) give a range of basic (residual) friction angles for sandstone obtained from testing of sand-blasted, rough sawn and residual surfaces. The friction angle range is given as 31 to 35° for normal stresses of 0.1 to 7.3 MPa. This normal stress range corresponds well to the expected stress range from the 0 to 250 m of overburden at Cheam Slide. The strength values were arbitrarily expanded to a range of 30 to 36° for the stability analysis of Cheam Slide.

6.3.3 Peak Strength

Peak strengths for natural sandstone joints are given by Hassani and Scoble (1985) and are shown in Figure 6.5. The failure envelope is slightly curved but it was decided that the Mohr-Coulomb failure criterion would be used for simplicity . The effect of using a linear failure criterion on the accuracy of the stability modelling is considered minor in comparison to the uncertainty of the rock joint strength parameters.

Maximum and minimum linear bounds were drawn through the results of Hassani and Scoble (Fig. 6.5). The lower bound closely represents the strength envelope of a smooth joint and the upper bound defines the roughest possible joint. Three equally spaced lines were drawn through the data between the upper and lower

bound to represent intermediate strengths. The rock strengths obtained are shown in Table II and these were used for the stability modelling of Cheam Slide.

6.4 Unit weight

The medium and coarse grained sandstone that dominates the slide area is composed of mostly altered albite and oligoclase plagioclase feldspar (Monger, 1966). The specific gravity of pure albite plagioclase is 2.62 and the highest specific gravity for oligoclase is about 2.67 (Klein and Hurlbut, 1985). Typically a sandstone has a porosity of 5-30% (Freeze and Cherry, 1979). Since the sandstone is well cemented, has undergone plastic deformation and is not extensively jointed a porosity of 6% has been assumed resulting in a calculated unit weight of about 25 kN/m^3.

6.5 Water Conditions

6.5.1 General

The groundwater flow regime has pronounced effect on the stability of a slide. The presence of pore pressures reduces the effective normal stress on the potential

failure surface resulting in a lowering of frictional strength. Effective stress is defined as:

$$\sigma' = \sigma - u \qquad\qquad [6.3]$$

where:

σ' = effective stress
σ = total stress
u = pore pressure.

The groundwater flow pattern within an incipient slide mass can be determined with extensive detailed monitoring. Detailed monitoring is often not possible and rarely is of long enough duration to include extreme events. Thus, the response of the groundwater flow to extreme events must be predicted. Predicting groundwater flow patterns of pre-historic landslides presents further problems because climate conditions, the pre-slide configuration and pre-slide permeabilities are often unknown.

For simple geological settings, the groundwater flow pattern can be reasonably predicted using simple flow net construction. Computer models are available to assist in the determination of groundwater flow patterns for more complicated situations (Hodge and Freeze, 1977; Forster, 1987). Such programs are especially useful if they can be calibrated against known values. Once calibrated, extreme values can be input to determine "worst case" groundwater flow conditions.

6.5.2 Cheam Slide Groundwater Conditions

Cheam Slide occurred between approximately 4350 and 5000 years BP. It has been shown that the climate at the time of failure was similar to that of today (Sec. 2.2.3). The southwest failure plane is believed to have been controlled by a thrust fault containing a clay gouge which would act as an impermeable barrier. Frequently, the rock surrounding a fault is heavily fractured resulting in high hydraulic conductivity values. This was investigated at Cheam Slide but no extensive fracturing on either side of the fault was found in the limited exposure.

The relatively impermeable thrust fault would have had a pronounced effect on the groundwater flow pattern. Two down slope cross sections taken at the intersection of the two failure planes is shown in Figure 6.6. The upper cross-section shows a probable location of the water table if there were no impermeable layer and the lower cross-section shows the water table location if an impermeable layer was present. The water table does not daylight on the slope that lacks an impermeable layer, resulting in much lower pore pressures on the failure plane leading to greater slope stability. The work of Hodge and Freeze (1977) supports this hypothesis.

In extreme conditions it may have been possible to approach complete saturation of the Cheam Slide slope. To determine the pore pressure level on the failure plane the flow conditions must be investigated. Figure 6.7 shows two groundwater flow

scenarios. CASE 1 assumes a no flow condition which corresponds to a failure plane pore pressure given as:

$$u = \gamma_w \cdot h_w \qquad\qquad [6.4]$$

where:

γ_w = unit weight of water
h_w = height of water table

CASE 2 shows groundwater flow directly parallel to the impermeable layer. For this situation the pore pressure is defined as:

$$u = \gamma_w \cdot h_w \cdot Cos^2\beta \qquad\qquad [6.5]$$

where:

β = slope inclination

It is unlikely that the groundwater flow conditions at Cheam Slide are either static (CASE 1) or parallel (CASE 2). It is anticipated that the groundwater flow field will be between these two extremes.

For stability modelling the maximum pore pressure was taken to be about medial to [6.4] and [6.5]. Water conditions ranging from dry to completely saturated were considered.

6.6 Seismic Conditions

6.6.1 National Building Code of Canada Design Earthquake

All new structures built in Canada are designed to resist seismic loading based on the maximum probable earthquake within the design life of the building. The maximum level of seismic load and the probability of occurrence for a given site is outlined in the National Building Code of Canada (NBCC).

The NBCC was upgraded in 1985 to include new probabilistic strong motion seismic ground motion maps. The new ground motion estimates are used to produce new peak acceleration and peak velocity zoning maps. The probability of exceedence has been changed from 40 percent in 50 years (0.01 per annum) on the 1970 maps to 10 percent in 50 years (0.0021 per annum) on the new maps.

The new zoning maps incorporate the Cornell-McGuire method (Cornell, 1968; McGuire, 1976). The Cornell-McGuire method requires that the seismicity of the region under consideration be divided into source zones. Canada has been divided into 32 source zones based on:

1. a description of historic and recent seismicity;
2. a map showing the geographical limits of the zone;
3. a discussion of the seismotectonics used to rationalize the distinct zone;
4. a magnitude recurrence relation derived by the method described by Weichert (1980) and a list of the earthquakes selected on the basis of a magnitude completeness test;
5. a discussion of the choice of upper-bound magnitude used to truncate the recurrence relation.

For each of the 32 source zones a magnitude recurrence relationship is determined. This is quite simply the number of occurrences of a given magnitude earthquake plotted against that magnitude. The magnitude recurrence relationships have upper bound magnitudes based on historical seismicity and geological factors.

Next the strength of the seismic force as a function of distance must be determined. For the 1985 NBCC the attenuation relationship of Hasegawa *et al.* (1981) was used. This relationship is given as:

$$A = 10 \; e^{1.3M} \; R^{-1.4}$$

where:

```
A = acceleration
M = Richter local magnitude of the event
R = hypocentral distance from the event.
```

Once the ground motion as a function of distance has been determined for various earthquake magnitudes, it is combined with the magnitude recurrence relationship to determine the number or rate of exceedence per annum of a given or chosen acceleration level for a specific site. A Poisson distribution is assumed when calculating the probability from the rate. An illustration of probabilistic ground motion methodology was given by Heidebrecht *et al.* (1983) and is shown in Figure 6.8.

The problem with the NBCC of 1970 was that the response spectrum of the earthquake was not included. This is not appropriate because different structures will behave differently under different excitation frequencies. To overcome this deficiency, the new NBCC incorporates both a velocity and an acceleration. The velocity is more appropriate for taller buildings that have a natural frequency of about 1 Hz. The acceleration value is used for structures of higher natural frequency. The dynamic analysis of natural slopes requires both acceleration and velocity values.

Currently, the possibility of a megathrust earthquake is not included in the NBCC, but because of the increasing awareness of such an event, it will likely be included in the next NBCC update expected in 1995. For a complete discussion of the seismic methodology used in the preparation of the 1985 NBCC seismic zoning maps of Canada, the reader is directed to Basham *et al.* (1982).

6.6.2 Cheam Slide Seismicity

The Pacific Geoscience Centre in Sidney, B.C will calculate the seismic hazard for sites in Canada based on the methodology used in the National Building Code of Canada. Available seismic hazard data for Wahleach was used for Cheam Slide because of their close proximity to one another. The results are shown in Figure 6.9 as a recurrence relationship (see also Appendix V).

The NBCC requires that structures be designed for a 475 year return period earthquake which corresponds to a 10% chance of exceedence in 50 years (0.0021 per annum). For this return period a maximum acceleration value of 0.15 g and velocity

of 0.14 m/s can be expected for the Cheam Slide area, based on the Wahleach data. For more critical structures a value double that of the 475 year earthquake should be used as a maximum credible earthquake (P. Byrne, 1990, personal communication). Doubling the 475 year earthquake values, resulted in an acceleration of 0.30 g and a velocity of 0.28 m/s which approximately corresponds to a 1800 year return earthquake (Fig. 6.9). To account for the proportionately larger velocities at larger return periods the velocity was raised to 0.30 m/s.

The current building code does not include the possible effects of a large subduction zone earthquake. Because of the lack of seismic loading information, it was difficult to predict expected seismic loading. Attenuation relationships currently exist, but are based on events smaller than M_L 7.5. The magnitude expected from a subduction zone earthquake is well beyond the ML 7.5 maximum of the attenuation relationships.

In an attempt to estimate the potential acceleration values from a megathrust earthquake, the strong motion record from the M_W 8.1 1985 Mexico earthquake was examined. The strong motion record was recorded at a station set in rock at a distance of 400 km from the earthquake source. The peak acceleration in the record was 0.035 g which is shown in Figure 6.10. For the purposes of analysis, it was assumed that a M_W 8.1 event would be close in size to a M_L 7.7 event. These values were used in conjunction with several attenuation relationships to determine the expected acceleration levels (Fig. 6.10).

Cheam Slide is located some 250 to 350 km from the probable source zone of a Cascadia Subduction Zone earthquake. Using the values in Figure 6.10, the M_W 8.1 Mexico earthquake would have produced accelerations of about 0.03 to 0.1 g at a distance of 250 km. It can be argued that even an earthquake as large as M_W 9.3, predicted for the failure of the entire Cascadia Subduction Zone, would not result in acceleration values significantly higher than 0.03 to 0.1 g. The MW 9.0 earthquake was calculated for the rupture of the entire subduction zone. An individual site would not feel the full effect of the whole rupture zone. At higher magnitudes the subsurface is no longer able to efficiently transmit energy as extreme deformation takes place.

In summary, the large distance of Cheam Slide from the probable megathrust earthquake hypocenter, makes it doubtful that the NBCC 1800 year earthquake acceleration values will be exceeded at Cheam Slide for the largest subduction zone earthquake. The greater travel distances from the outer reaches of the rupture would produce disproportionately higher velocities. These would likely not exceed the velocities of the 1800 year earthquake. For the design and maximum credible earthquakes , the following NBCC values were used for modelling:

```
A_M = 0.15 g , V_M = 0.14 m/s (   475 year return EQ)
A_M = 0.30 g , V_M = 0.30 m/s (≈1800 year return EQ)
```
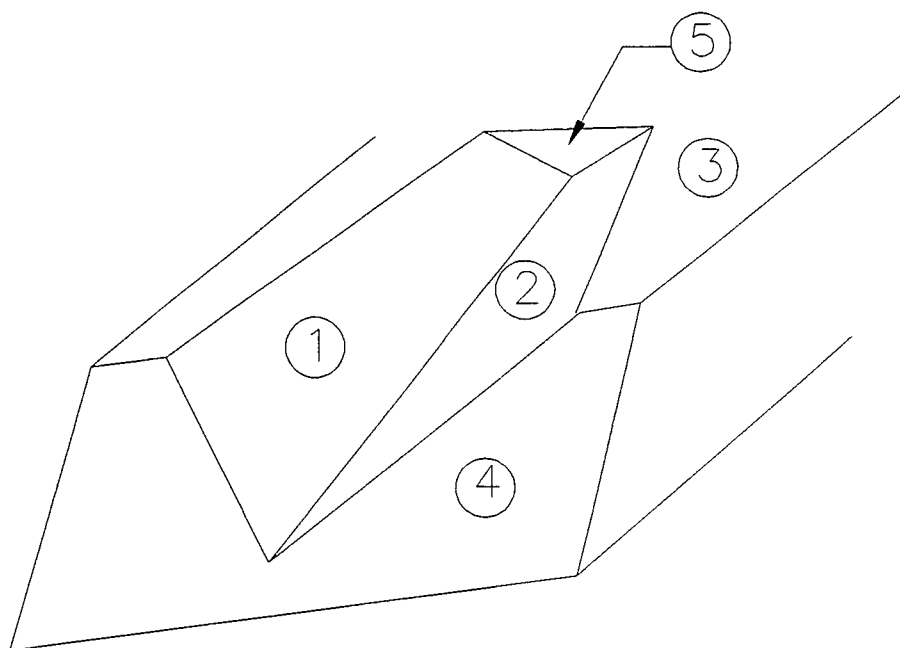
	Dip	Dip Direction
1.	38.7	265
2.	20.7	340
3.	11.0	308
4.	40.0	308
5.	85.0	295

Figure 6.1. The asymmetrical wedge geometry of Cheam Slide can be closely approximated by the five planar surfaces shown.

SOLID
=modelled geometry
DASHED
= *in situ* geometry
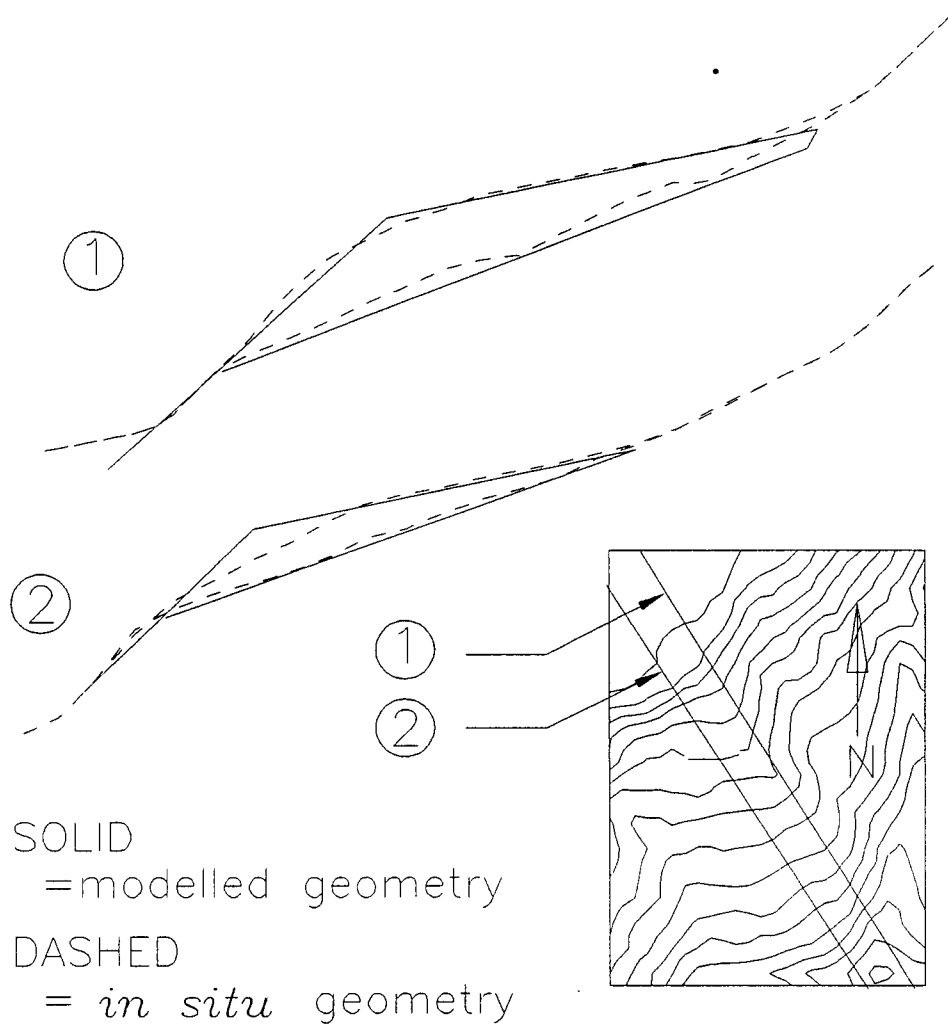
Figure 6.2. Comparison between cross-sections of the modelled Cheam Slide wedge geometry and the *in situ* wedge geometry.
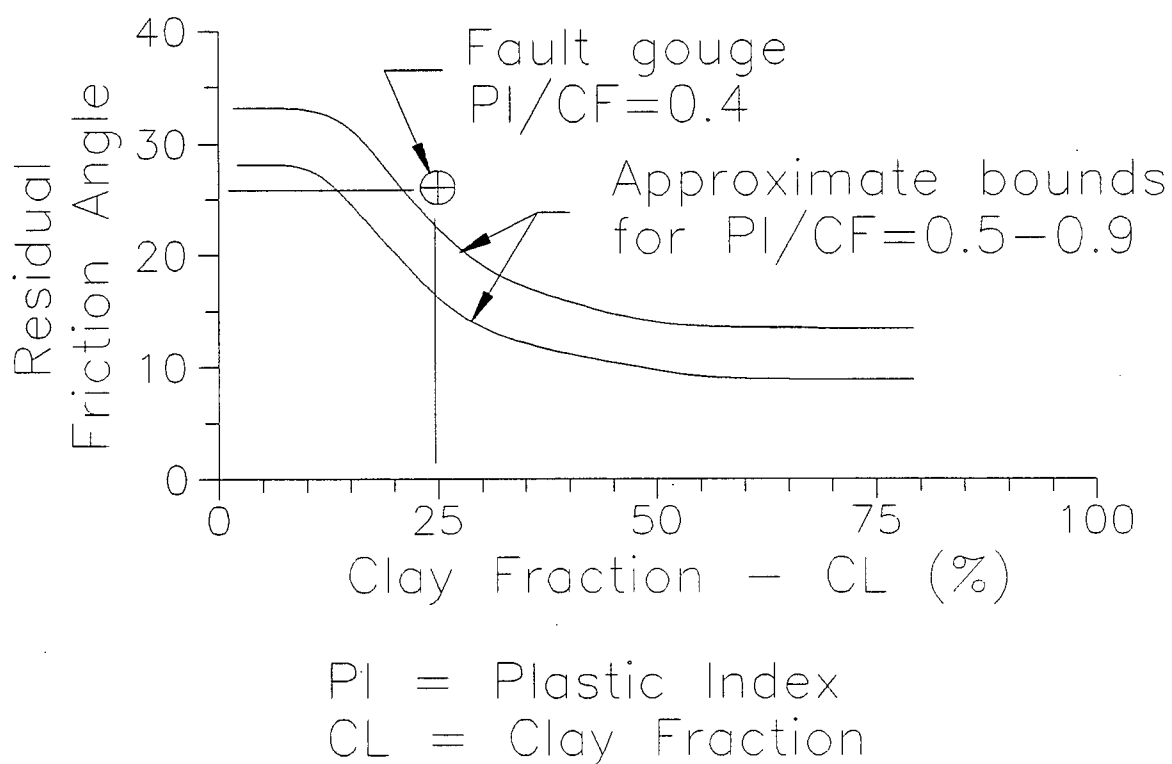
Figure 6.3. Relationship between residual friction angle, clay fraction and activity (after Skempton, 1985). The clay gouge from the thrust fault which is believed to have controlled the southwest failure plane is shown.
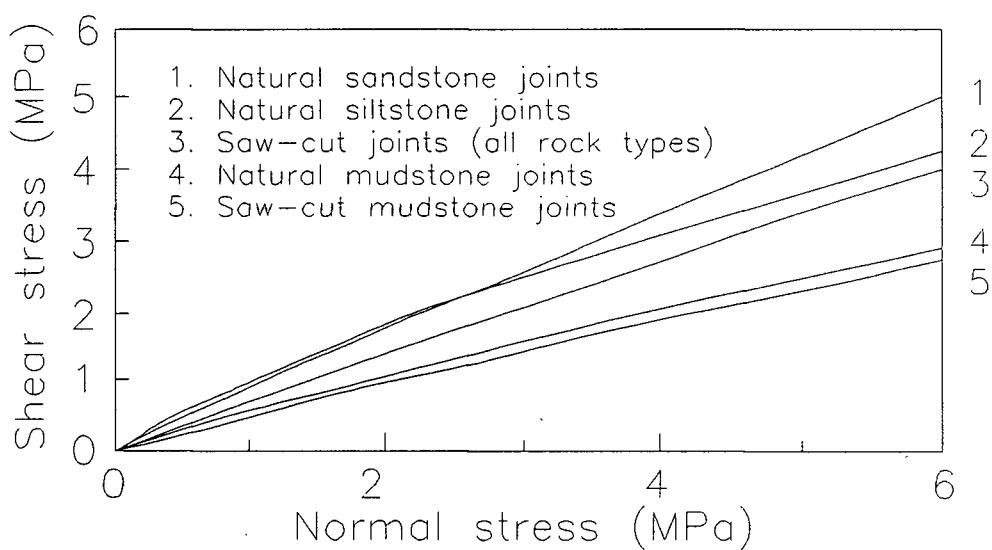
Figure 6.4. General peak shear strength failure envelopes for different rock discontinuities (after Hassani and Scoble, 1985).
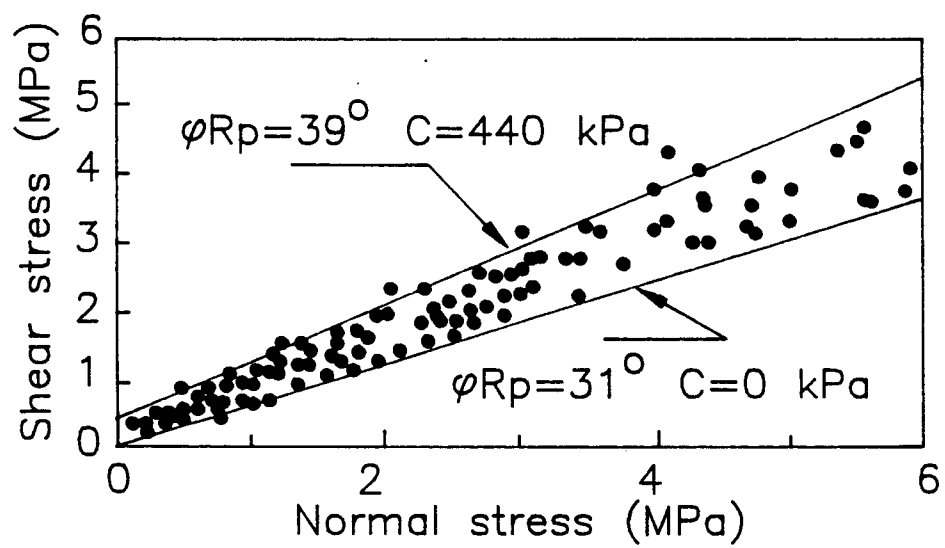
Figure 6.5. Peak shear strength of natural sandstone joints (after Hassani and

Scoble, 1985). Shown are the upper and lower bound peak strength envelopes

used for the stability modelling of Cheam Slide (see also Table II).

Table II. Peak rock joint strengths used in the stability modelling of Cheam Slide.

Rock Joint Peak Strengths	
Cohesion - C (kPa)	Friction Angle - øRp (degrees)
0	31
110	33
220	35
330	37
440	39
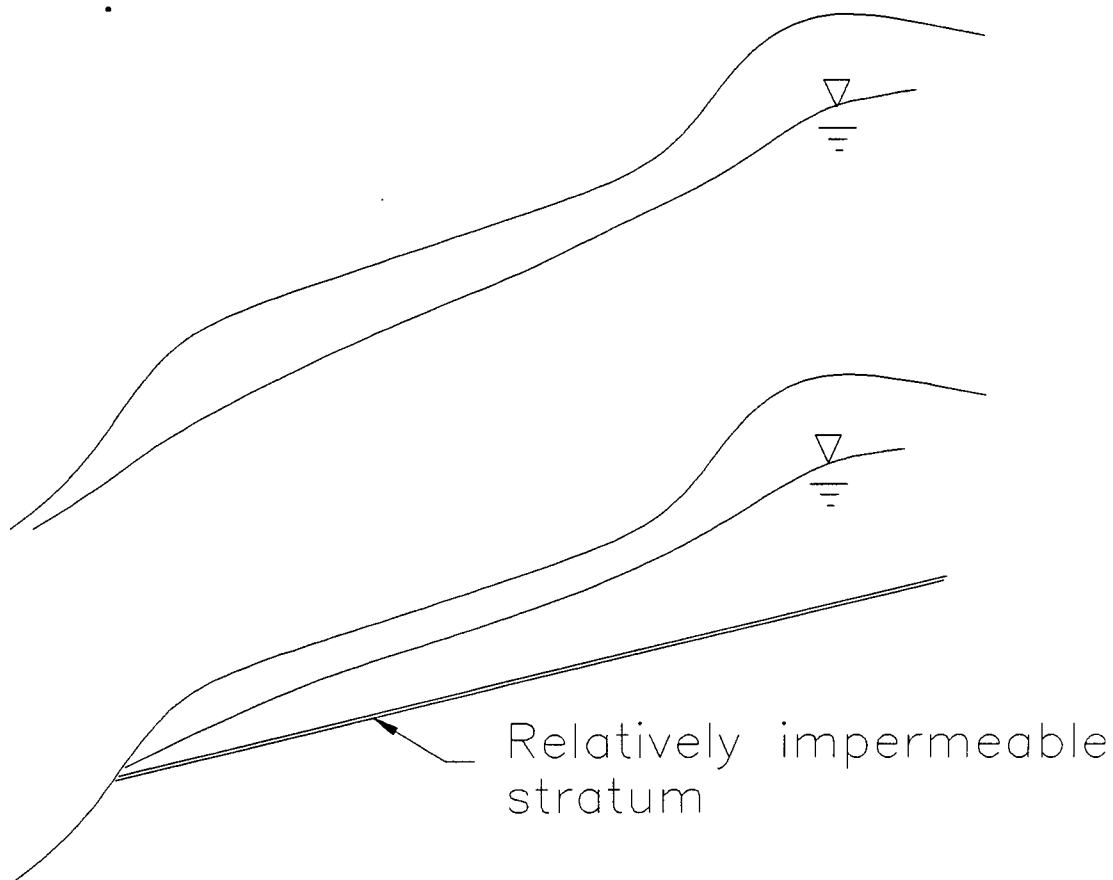
Figure 6.6. Effect of a relatively impermeable stratum at Cheam Slide on the location of the water table. The impermeable stratum results in higher pore pressures in the slope.
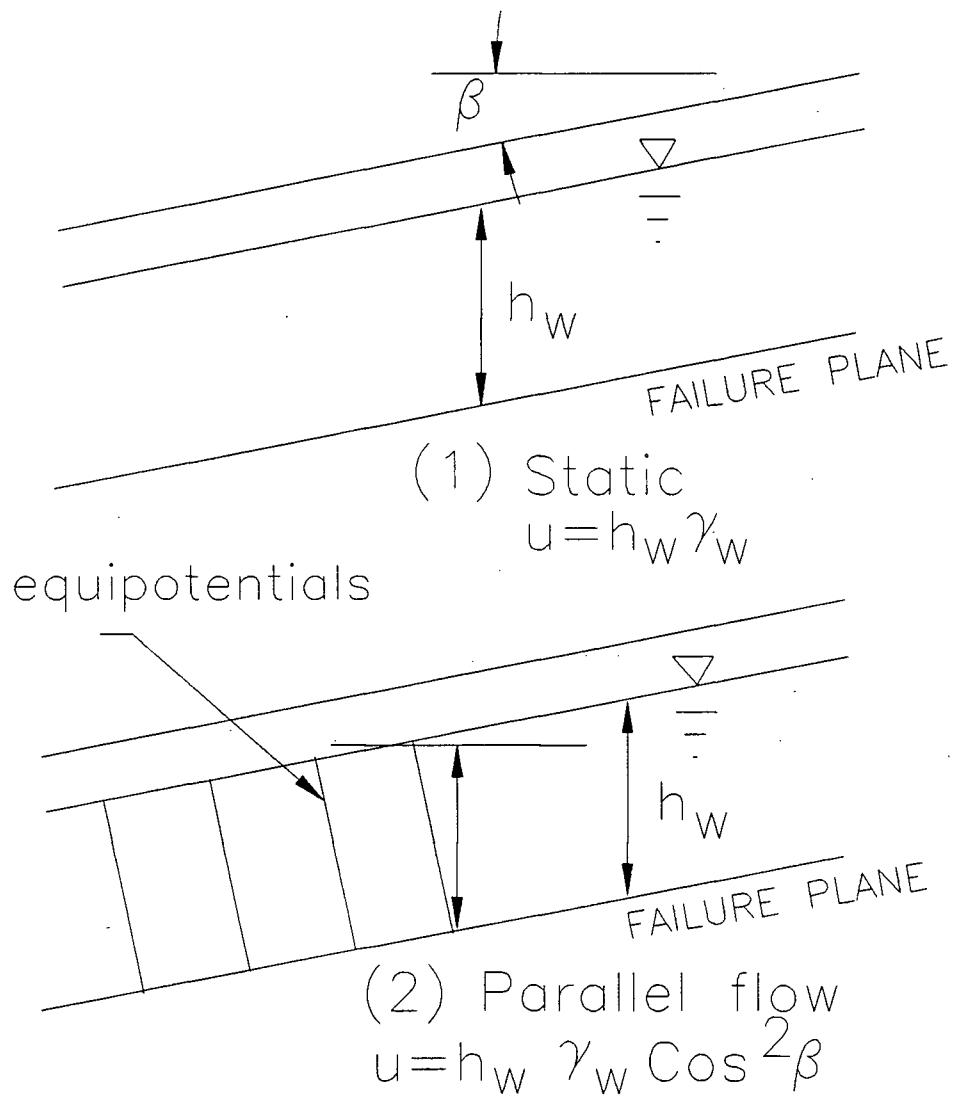
Figure 6.7. Failure plane piezometric pressure resulting from two groundwater flow conditions. CASE 1 shows the pore pressure resulting from a static water flow condition. CASE 2 shows the pore pressure resulting from a ground water flow parallel to the impermeable lower layer.
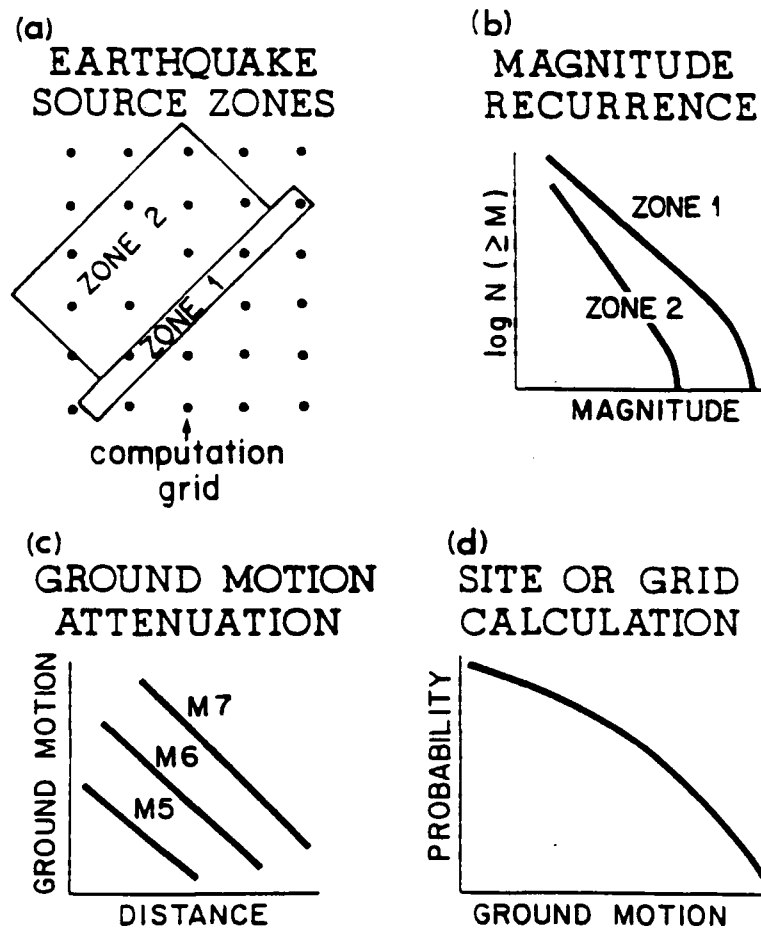
Figure 6.8. Schematic of probabilistic seismic ground motion methodology showing: (a) earthquake source zones and computational grid; (b) magnitude recurrence relations terminated at upper-bound magnitude; (c) ground-motion attenuation; and (d) probability distribution of ground motion parameter at a site of grid (from Heidebrecht *et al.*, 1983).
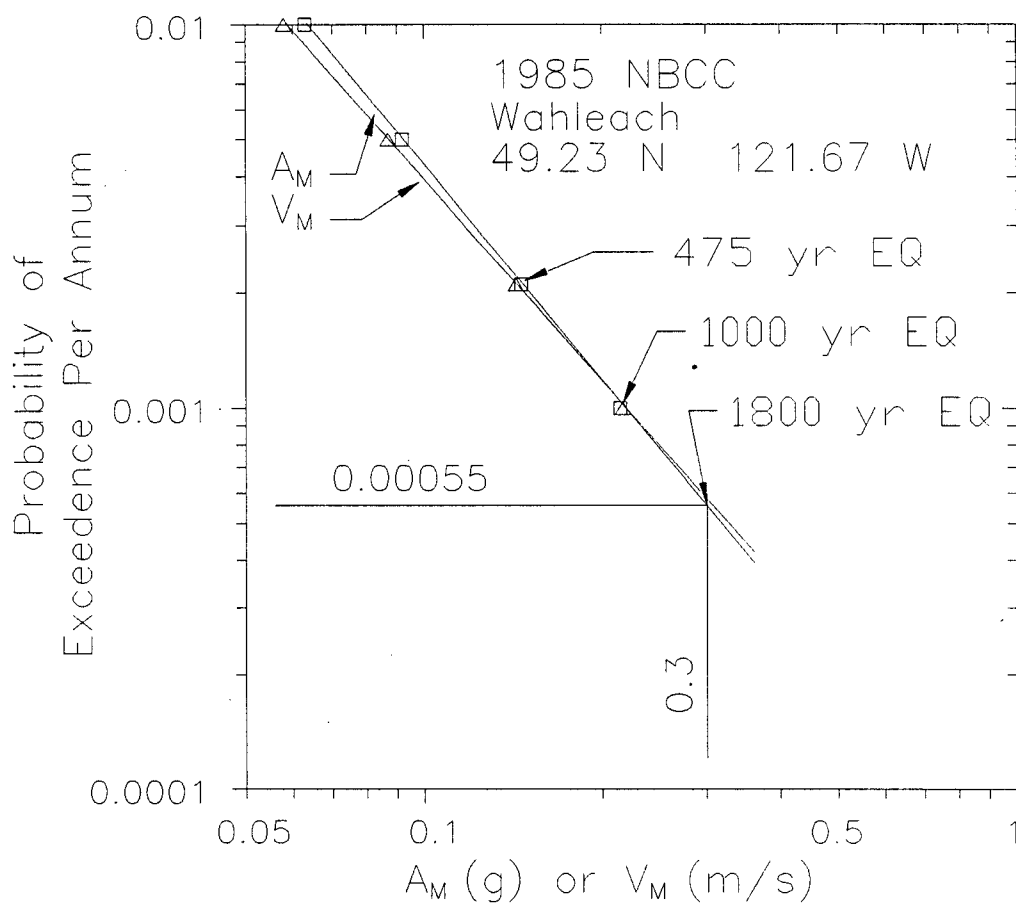
Figure 6.9.   National Building Code of Canada (NBCC) predicted maximum acceleration and velocity values for a given earthquake return period at Wahleach near Cheam Slide. Maximum credible earthquake is taken to be twice the acceleration expected from a 475 year return earthquake.
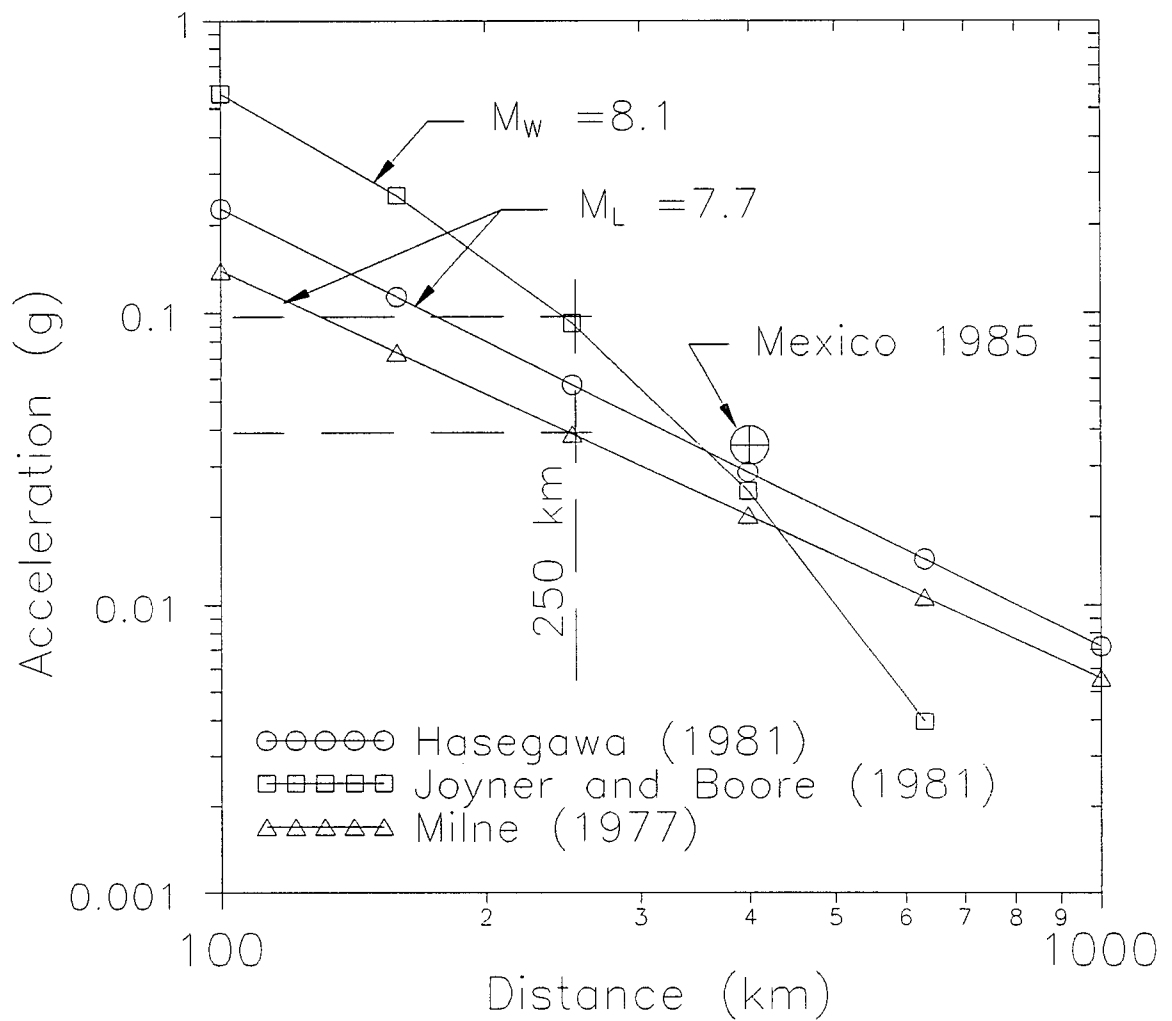
Figure 6.10. Expected acceleration levels verses distance for the Mexico 1985 earthquake. Cheam Slide is about 250 km from the anticipated Cascadia Subduction Zone earthquake epicentre.

CHAPTER 7

COMPUTER
MODELLING PROCEDURE

7.1 Modelling Considerations

When choosing a slope stability modelling procedure, the geometry of the problem, the amount of input data available (Sec. 5.2) and the expected accuracy of the outcome must be considered. Since Cheam Slide has a wedge geometry, the stability procedure must be capable of three dimensional modelling. The model input parameters will be limited in numbers and accuracy because the conditions at the time of failure are known inadequately. The outcome of any modelling procedure is only as good as its input, thus, with such limited input data, great care must be taken in interpreting the results. For these reasons, a simple three dimensional modelling procedure is best suited for the stability modelling of Cheam Slide.

Two methods are currently available for simple three dimensional modelling. Hoek and Bray (1977) presented a closed form solution for the stability of a rock block wedge and, recently, an interactive three dimensional, general stability program, CLARA, was developed by Dr. O. Hungr. CLARA incorporates the methods of

Bishop (1955) and Janbu (1957), which were modified by Hungr (1987a) for three dimensions.

7.2 Wedge Failure

A purely translational slide moves on a slide plane in the dip direction. A wedge is forced to move in the direction of the intersection of the two slide planes, creating lateral forces. Hoek and Bray (1977) discussed this "wedge effect" on the stability of a wedge block failure.

For the purposes of discussion, the wedge geometry is defined in Figure 7.1. The factor of safety of the wedge with zero cohesion and planes of equal strength, is defined as:

$$F_W = \frac{(R_A + R_B) \, \text{Tan} \, \phi}{W \cdot \text{Sin} \, \theta_i} \qquad [7.1]$$

where:

$$W = \text{weight of the wedge}$$
$$\theta_i = \text{dip of the line of intersection}$$
$$\phi = \text{friction angle}$$
$$R_A, R_B = \text{normal reactions provided by planes A and B.}$$

Rewriting [7.1]:

$$F_W = \frac{Sin(\beta)}{Sin(\frac{1}{2}\epsilon)} \frac{Tan(\phi)}{Tan(\theta_i)} \qquad [7.2]$$

where ß and ϵ are described in Figure 7.1.

For a translational plane failure in which the slope face is inclined at θ_{fi} and the

failure plane is inclined at θ_i, the factor of safety is given as:

$$F_P = \frac{Tan(\phi)}{Tan(\theta_i)} \qquad [7.3]$$

Thus:

$$F_W = K \cdot F_P \qquad [7.4]$$

where K is the wedge factor defined by:

$$K = \frac{Sin(\beta)}{Sin(\frac{1}{2}\epsilon)} \qquad (for \; \beta > \frac{1}{2}\epsilon) \qquad [7.5]$$

Notice that K will never be less than one indicating that a plane analysis is always

conservative.

The Cheam Slide failure planes correspond to $\frac{1}{2}\epsilon = 75.8^O$ and ß$=79.4^O$. Since

ß $> \frac{1}{2}\epsilon$ the failure would have behaved as a wedge. The calculated wedge factor K

using these values was 1.014 indicating an expected 1.4% error in the results if the

wedge was modelled as a translational slide. However, the wedge factor calculation

assumes equal frictional strength on both planes and no cohesion. Cheam Slide has

failure planes of different frictional strengths and cohesion, thus the wedge effect may have been significant.

7.3 Program CLARA

7.3.1 General

CLARA is a user friendly slope stability program for use with IBM compatible microcomputers. The program is licensed for use in the Department of Civil Engineering at The University of British Columbia.

The program is based on an extension of Bishop's Simplified Method of Slices (Bishop, 1955) to three dimensions (Hungr, 1987a). The present version includes modifications due to Fredlund and Krahn (1977). These modifications make the method applicable to non-rotational geometries within limitations. For a complete discussion of the stability methods the reader is directed to the above references and Hungr (1987b).

7.3.2 Water Conditions

CLARA incorporates three methods to specify the pore pressures acting on the sliding surface. They are as follows (see also Fig. 7.2):

1) A Pore Pressure Ratio can be associated with a material or a discontinuity. The pore pressure is calculated by multiplying the total vertical stress at the centre of each column by the Pore Pressure Ratio.

2) A piezometric surface of a given number can be associated with a material or a discontinuity. The pore pressure is calculated as the hydrostatic pressure corresponding to the elevation of the piezometric surface above the base of each column.

3) A "B" value can be entered for each material layer other than the upper most material. The piezometric pressures in the upper layer are increased by adding an excess pore pressure equal to "B" times the total weight of the layer.

7.3.3 Program Limitations

The three dimensional Bishop's method does not take into account vertical or transverse horizonal forces, thereby ignoring internal strength effects. Intuitively, the internal strength effect will depend on the depth of the sliding surface and the relative magnitude of the mobilized strength. Two index parameters were defined by Hungr *et al.* (1989) as:

$$I_D = \tan \left[\left(\alpha_b - \alpha_a \right) - \left(\phi_a - \phi_b \right) \right] \qquad [7.6]$$

where:

I_D = Modified Depth Factor

and the remaining parameters refer to angles as shown in Figure 7.3.

and:

$$I_S = \tan \phi_i / \tan \phi_{av} \qquad\qquad [7.7]$$

where:

I_S = Internal Strength Factor

ϕ_i = friction mobilized on the interslice surfaces

ϕ_{av} = weighted average friction angle for the entire sliding
surface.

As either or both of these parameters increase, the error in using Bishop's method increases. To limit the error to 10% the Internal Strength Factor should be less than 3 and the Modified Depth Factor should be less than 0.5 (Hungr *et al.*, 1989).

Transverse forces are ignored when using Bishop's method leading to errors. CLARA calculates the unbalanced forces allowing the user to determine when errors become excessive. The Lateral Imbalance index is given as:

$$I_L = (\tan \delta) * P_h / W_t \qquad\qquad [7.8]$$

where:

P_h = lateral imbalance force

W_t = total weight of the slide

δ = included angle as shown in Figure 7.4.

The most recent version of CLARA (version 2.3) can establish equilibrium of lateral forces by proportional weight distribution (O. Hungr, 1990, personal

communication). The effectiveness of this procedure, along with the effect of lateral imbalance on the accuracy of results, will be investigated in Section 7.5.

7.3.4 Cheam Slide Considerations

The calculated Modified Depth Factor and Internal Strength Factor for Cheam Slide were much larger than those necessary to limit the error to 10%. However, these factors ignore the size of the backscarp. The Cheam Slide backscarp area is only 0.02% of the total area of the failure surfaces, minimizing internal deformation and resulting in an accurate solution from the three dimensional Bishop's method. Also, the asymmetrical wedge geometry of Cheam Slide was a concern because it was suspected that the wedge effect would result in large unbalanced transverse forces, requiring compensation in the analysis.

7.4 Program WEDGE

7.4.1 General

Program WEDGE is a wedge stability program encoded by the writer specifically for this study and is based on the algorithm of Hoek and Bray (1977). The program was written in double precision quickBASIC 4.0 and is highly user interactive. Parameter changes can be rapidly made using on screen editing, making the program ideal for sensitivity analysis. For seismic analysis, program WEDGE can quickly determine the critical acceleration value of the slope. The water conditions of Hoek and Bray (1977) are included in the program, as is the Pore Pressure Ratio r_U.

7.4.2 Methodology

The algorithm presented by Hoek and Bray (1977) is based on the stability of a non-rotational rigid block wedge defined by five planes. The algorithm utilizes a vector analysis to determine wedge volume, failure plane surface areas, and force distributions. The total weight of the wedge is determined from the unit weight of the material and the wedge volume. The normal reactions on the two failure planes are determined from the weight of the wedge. The resistance to sliding is determined using a strength criteria. The driving force is taken as the component of the weight that is parallel to the direction of the intersection of the two lateral failure planes.

7.4.3 Water Conditions

The Hoek and Bray algorithm utilizes two water conditions. For both conditions it is assumed that the permeability of the rock itself is very low and, hence, most of the water in the slope is transmitted along the discontinuities such as the two failure planes and the tension crack. The conditions are based on rainfall extremes such that the fissures are completely full of water, with the water pressure varying from zero at the free face to a maximum value at some point on the line of intersection of the two failure planes.

The first water condition has no tension crack giving the relationship:

$$u_1 = u_2 = \gamma_w \cdot H_w/6 \qquad . \qquad [7.9]$$

where:

u_1, u_2 = total uplift pressures normal to planes 1 and 2
γ_w = unit weight of water
H_w = total height of the wedge.

This implies that the height of the piezometric surface at the backscarp is one half the total height of the wedge. For long, thin wedges with minimal backscarps this, groundwater condition gives very conservative results.

The second water condition includes a water filled tension crack which gives the relationship:

$$u_1 = u_2 = u_5 = \gamma_w \cdot H_{5w}/3 \qquad [7.10]$$

where:

u_1, u_2, u_5 = uplift pressures on planes 1, 2 and 5.
H_{5w} = depth of the bottom vertex of the tension crack below the ground surface.

This implies a piezometric surface that decreases linearly from the ground surface at the backscarp to the outcrop of the line of intersection of the two failure planes.

The groundwater conditions given by Hoek and Bray (1977) are well suited for conservative stability designs, but are not specific enough for determining conditions

at the time of slide failure. An alternate method was needed to define water conditions for Cheam Slide stability calculations.

An attempt was made to incorporate a user defined piezometric surface into the Hoek and Bray algorithm, but this proved to be an insurmountable task. The Pore Pressure Ratio is often used to define piezometric conditions for stability analyses and is defined as:

$$r_U = u/(\gamma \cdot h) \qquad\qquad [7.11]$$

where:

r_U = Pore Pressure Ratio
 u = pore pressure
 γ = total unit weight of overburden
 h = overburden height

The average total vertical force on each failure plane was determined using a slightly modified Hoek and Bray algorithm and this was incorporated into [7.11] to calculate pore pressures. Using the expected groundwater flow pattern (Sec. 6.5.2) and an overburden unit weight of 25 kN/m^3, it was determined that a Pore Pressure Ratio of 0.37 represented a completely saturated slope.

7.5 Comparison Testing

7.5.1 General

The accuracy and applicability of programs WEDGE and CLARA were determined as the first step in the modelling of Cheam Slide. Hoek and Bray (1977)

presented solutions to their wedge algorithm for several test cases and these solutions were accurately reproduced using WEDGE. To test the applicability of WEDGE and CLARA at determining wedge stability, the outcome of several test cases, that exploited the anticipated Cheam Slide modelling problems, were compared.

The most recent version of CLARA (hereafter referred to as CLARA 2.3) became available in the later stages of the Cheam Slide modelling. CLARA 2.3 was comparison tested against WEDGE and the earlier version of CLARA (hereafter simply referred to as CLARA). These results are presented in the next three sections.

7.5.2 Symmetrical Wedge - CASE 1

A symmetrical wedge was used for the first comparison test (CASE 1). The strength of the two failure planes was varied between 15 and 45° for plane 1, and from 2 to 30° for plane 2. The wedge was dry and cohesion was zero. The results from WEDGE and CLARA are given in Table III along with the orientations of the planes defining the geometry. Table III also includes the ratio of the transverse forces to the total weight of the wedge (P_h/w).

The results show that for a zero transverse force imbalance the results of CLARA match those of WEDGE. When there is a transverse force imbalance the results for CLARA become conservative. If the force balancing algorithm of CLARA 2.3 is invoked the CASE 1 results for WEDGE and CLARA match. The transverse imbalance resulted purely from a change in strengths, indicating that a geometrically symmetrical problem can become asymmetrical by varying strength parameters.

7.5.3 Asymmetrical Wedge - CASE 2,3,4

The dip and dip direction of failure planes 1 and 2 were altered in CASE 2 to give the wedge an asymmetrical geometry. The strength of both failure planes was varied from 5 to 45°. The wedge was dry and cohesion was zero. The test results and the orientation of the five planes are shown in Table IV. The results indicate that larger transverse force imbalances resulted in increasingly conservative unbalanced CLARA results. By invoking the lateral force balancing algorithm of CLARA 2.3, the results became equal to those of WEDGE.

To increase the geometrical asymmetry for CASE 3, the face of the wedge was skewed slightly and the dip of the shallow plane was further reduced. The strength of both failure planes was varied from 5 to 45°. The wedge was dry and cohesion was zero. The orientation of the five planes and the test results are shown in Table V. The extreme asymmetry of the problem lead to large transverse force imbalances causing unbalanced CLARA results to be non-conservative. The force balancing algorithm of CLARA 2.3 effectively balanced the transverse forces producing results equal to those of WEDGE.

CASE 4 used the geometry and parameters of CASE 3 but also included cohesion of up to 500 kPa to further unbalance the lateral forces. The result are shown in Table VI. The force balancing algorithm of CLARA 2.3 compensated for the imbalance resulting in only a few slightly conservative results.

7.5.4 Pore Pressure Ratio - CASE 5,6

Programs WEDGE and CLARA can utilize Pore Pressure Ratio to describe pore pressures on the failure planes. To ensure the accuracy of the WEDGE pore pressure calculations, stability results for a range of pore pressure levels were compared to CLARA for the symmetrical wedge and to CLARA 2.3 for the asymmetrical wedge. The results for the symmetrical wedge (CASE 5) and the asymmetrical wedge (CASE 6) are shown in Tables VII and VIII, respectively. The maximum difference between the stability results of the programs was 3.5%.

7.5.5 Discussion

The lateral imbalance algorithm in CLARA 2.3 was able to compensate for the transverse forces ignored in Bishop's method giving results equal to WEDGE. The Pore Pressure Ratio is well matched between programs proving program accuracy.

The bulk of the stability modelling of Cheam Slide was completed before CLARA 2.3 became available,and since the earlier version of CLARA was unable to accurately model Cheam Slide, program WEDGE was used for all Cheam Slide stability modelling.
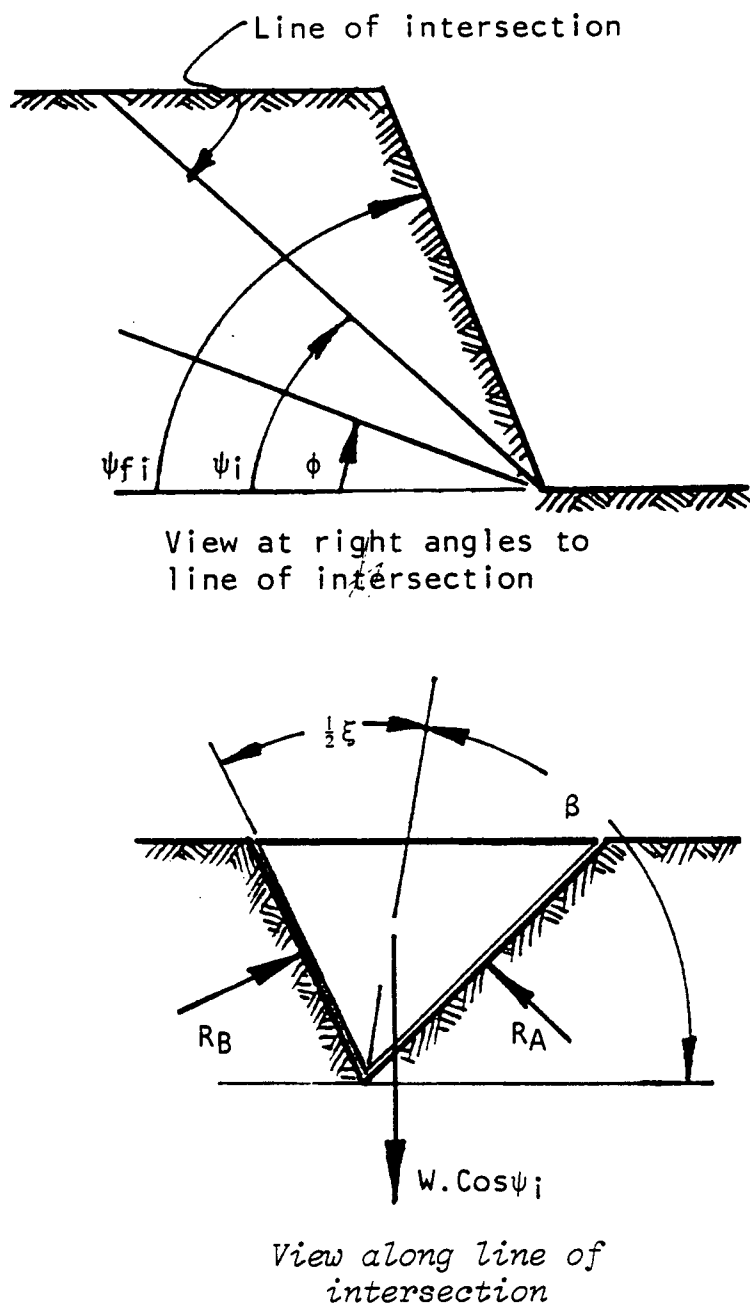
Figure 7.1. Parameters used for the determination of wedge effect (from Hoek and Bray, 1977).

$$u = \gamma \, h \; r_u \qquad\qquad u = \gamma_w \, h_w \qquad\qquad \text{see Eqn.(1)}$$
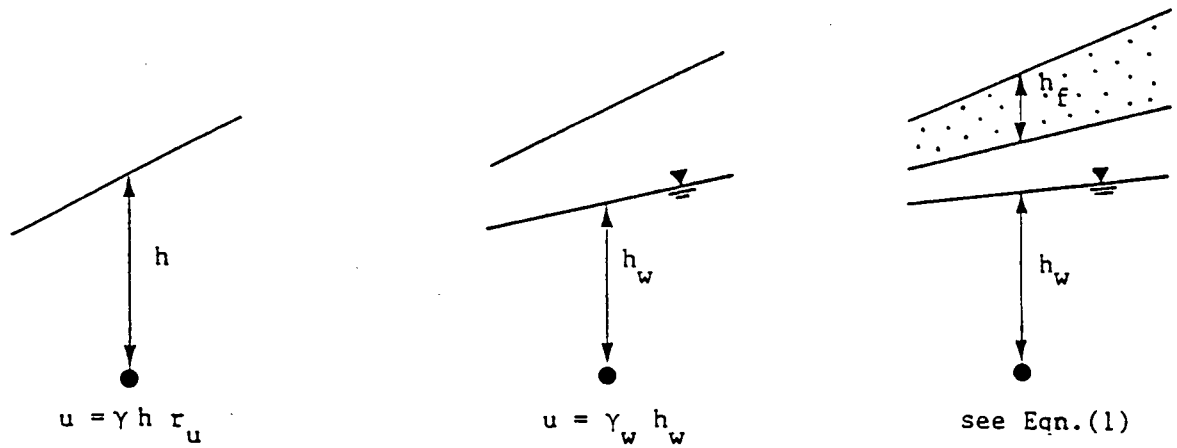
Figure 7.2. Three alternate methods of piezometric pressure specification in program CLARA (from Hungr, 1988).
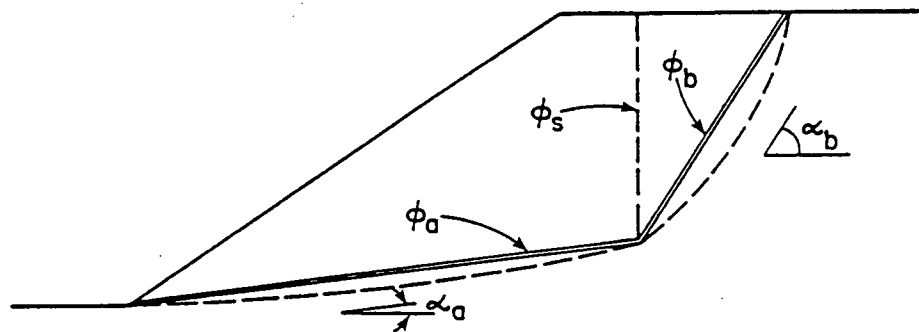
Figure 7.3. Bi-linear sliding surface used for calculation of the Modified depth factor (from Hungr *et al.*, 1989).
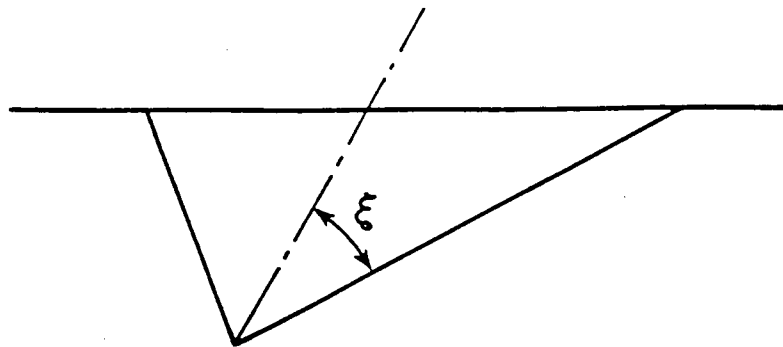
Figure 7.4. Wedge included angle used for Lateral Imbalance calculation (from Hungr *et al.*, 1989). View is along the line of intersection of the two lateral planes.

TABLE III. Comparison testing of programs CLARA and WEDGE using a dry symmetrical wedge.

CASE 1. SYMMETRICAL DRY		Dip	Dip Direction
	Plane 1	30.0	300
	Plane 2	30.0	060
	Plane 3	00.0	000
	Plane 4	45.0	000
	Plane 5	85.0	000

Plane 1 $\varnothing 1$	Plane 2 $\varnothing 2$	WEDGE FOS	CLARA FOS	Ph/w	CLARA 2.3 FOS
45	2	1.99	1.85	0.0354	1.99
40	10	1.95	1.89	0.0240	1.95
35	10	1.68	1.64	0.0218	1.68
35	15	1.86	1.83	0.0161	1.86
31	15	1.67	1.65	0.0138	1.67
31	20	1.85	1.85	0.0088	1.85
15	15	1.03	1.03	0.0000	--
20	20	1.40	1.40	0.0000	--

TABLE IV. Comparison testing of programs CLARA and WEDGE using a dry asymmetrical wedge. Asymmetry induced by altering dip and dip direction of failure planes 1 and 2.

CASE 2. ASYMMETRICAL DRY		Dip	Dip Direction
	Plane 1	40.0	300
	Plane 2	25.0	060
	Plane 3	00.0	000
	Plane 4	45.0	000
	Plane 5	85.0	000

Plane 1 $\varnothing1$	Plane 2 $\varnothing2$	WEDGE FOS	CLARA FOS	Ph/w	CLARA 2.3 FOS
45	5	0.78	0.57	0.0623	0.77
45	15	1.12	1.02	0.0342	1.12
45	30	1.71	1.68	0.0143	1.70
45	45	2.50	2.50	0.0016	2.50
30	30	1.45	1.45	0.0016	--
20	20	0.91	0.91	0.0016	--
30	45	2.25	2.24	-0.0089	2.25
15	45	2.06	2.02	-0.0194	2.06
5	45	1.95	1.87	-0.0274	1.95

TABLE V. Comparison testing of programs CLARA and WEDGE using a dry asymmetrical wedge. Further asymmetry induced (see Table IV) by skewing the face of the wedge (plane 4).

CASE 3. ASYMMETRICAL DRY		Dip	Dip Direction
	Plane 1	40.0	295
	Plane 2	20.0	015
	Plane 3	00.0	000
	Plane 4	45.0	330
	Plane 5	85.0	000

Plane 1 $\phi1$	Plane 2 $\phi2$	WEDGE FOS	CLARA FOS	Ph/w	CLARA 2.3 FOS
45	5	0.60	1.19	-0.1368	0.60
45	15	1.06	1.61	-0.1539	1.06
45	30	1.85	2.26	-0.1689	1.85
45	45	2.92	3.08	-0.1803	2.92
15	15	0.78	0.82	-0.1803	0.78
30	45	2.76	2.55	-0.1907	2.76
15	45	2.64	2.14	-0.2016	2.65
5	45	2.58	1.87	-0.2114	2.58

TABLE VI. Comparison testing of programs CLARA and WEDGE using a dry asymmetrical wedge. Further asymmetry induced (see Tables IV and V) by including cohesion.

CASE 4. ASYMMETRICAL DRY			Dip	Dip Direction	
	Plane 1		40.0	295	
	Plane 2		20.0	015	
	Plane 3		00.0	000	
	Plane 4		45.0	330	
	Plane 5		85.0	000	

| Plane 1 | | Plane 2 | | WEDGE | CLARA 2.3 |
c1	ø1	c2	ø2	FOS	FOS
500	45	00	5	0.91	0.89
500	45	00	15	1.37	1.35
250	30	00	30	1.83	1.83
00	15	500	45	3.08	3.07
00	5	500	45	3.01	3.00

TABLE VII.   Comparison testing of programs CLARA and WEDGE using a symmetrical wedge with water conditions defined by pore Pressure Ratio (r_U).

CASE 5. SYMMETRICAL		Dip	Dip Direction	ϕ
	Plane 1	30.0	300	20
	Plane 2	30.0	060	20
	Plane 3	00.0	000	--
	Plane 4	45.0	000	--
	Plane 5	85.0	000	--

r_U	WEDGE FOS	CLARA FOS	Difference
0.0	1.399	1.399	0.0 %
0.185	1.124	1.118	0.5 %
0.37	0.850	0.838	1.4 %

TABLE VIII.   Comparison testing of programs CLARA and WEDGE using an asymmetrical wedge with water conditions defined by pore Pressure Ratio (r_U).

CASE 6. ASYMMETRICAL		Dip	Dip Direction	$\emptyset$
	Plane 1	40.0	295	15
	Plane 2	20.0	015	30
	Plane 3	00.0	000	--
	Plane 4	45.0	330	--
	Plane 5	85.0	000	--

r_U	WEDGE FOS	CLARA 2.3 FOS	Difference
0.0	1.570	1.570	0.0 %
0.185	1.262	1.279	1.3 %
0.37	0.954	0.989	3.5 %

CHAPTER 8

STATIC BACK CALCULATION

8.1 General

At the initiation of failure the factor of safety of the slope will be equal to one. This constraint can be to determine the conditions of failure. This type of analysis is termed a "back analysis".

Many possible combinations of parameters provide a FOS = 1. If the parameters are not known, the problem will be indeterminate and must be solved by alternately assigning anticipated values to all except one unknown parameter, which is solved for. Often the solution is more sensitive to certain parameters, thus, the number of investigated parameters can be reduced. This type of parameter range back calculation is termed a "sensitivity analysis" and was used for the modelling of Cheam Slide.

8.2 Residual Strength Conditions

Catastrophic slope failure occurs only when the static driving force is greater than the residual strength, or in other words, when the residual FOS is less than 1

(Sec. 5.4). To determine the stability of Cheam Slide using residual strength

parameters a series of realizations was performed using the following range of

parameters:


```
Pore Pressure Ratio                   rU = 0.0 to 0.37
Thrust fault residual friction angle øTr = 10 to 35°   (C=0)
Rock joint residual friction angle    øRr = 30 to 35°   (C=0)
```

Figure 8.1 shows the combinations of thrust fault friction angle, rock joint friction

angle and Pore Pressure Ratio necessary to produce FOS =1. All three curves lie

above the lower bound thrust fault residual strength envelope, indicating that for the

lowest øTr, slope failure would occur for all values of r_U and øRr. The highest øTr

value resulted in failure with r_U values higher than about 0.26.

The results show the stability to be more sensitivity to changes in øTr than øRr.

A 1^O change in øTr produced the same effect as a 6° change in øRr. This result can

be expected since the thrust fault failure plane has more than twice the area of the

rock joint failure plane and a lower dip angle. Also evident from the results is the

large effect r_U has on the stability of the slide. A change in water conditions from

dry to fully saturated resulted in a 10° change in the øTr value required for failure.

The results of the static residual back calculation indicate that the residual

instability (FOS <1) necessary for catastrophic failure is easily attainable. Since this

correctly predicts the catastrophic failure of Cheam Slide, the modelling parameters

are considered to be representative.

8.3 Peak Strength Conditions

Before residual conditions were attained at Cheam Slide the peak strength was surpassed. Peak strength stability was determined for the following range of parameters:

```
Pore Pressure Ratio          rᵤ = 0.0 to 0.37
Thrust fault peak strength   øTp = 15 to 35°, c = 0 kPa
Rock joint peak strength     øRp = 31 to 39°, c = 0-440 kPa
```

The results are shown Figure 8.2. The higher thrust fault peak friction angle of $32°$ resulted in stability for all rock joint peak strengths and water conditions. The lower thrust fault peak friction angle of $23°$ resulted in an unstable slope for $r_U >0.19$ when combined with the lowest øRp, and for $r_U >0.37$ when combined with the highest øRp. To summarize, low øTp and øRp values in combination with high r_U values were required for slope failure.

Ideally, only extreme water conditions should result in slope failure. Since normal Cheam Slide slope conditions are most likely in the $r_U = 0.19\text{-}0.28$ range, the required higher pore pressures predicted for failure gives credibility to the range of input parameters used.
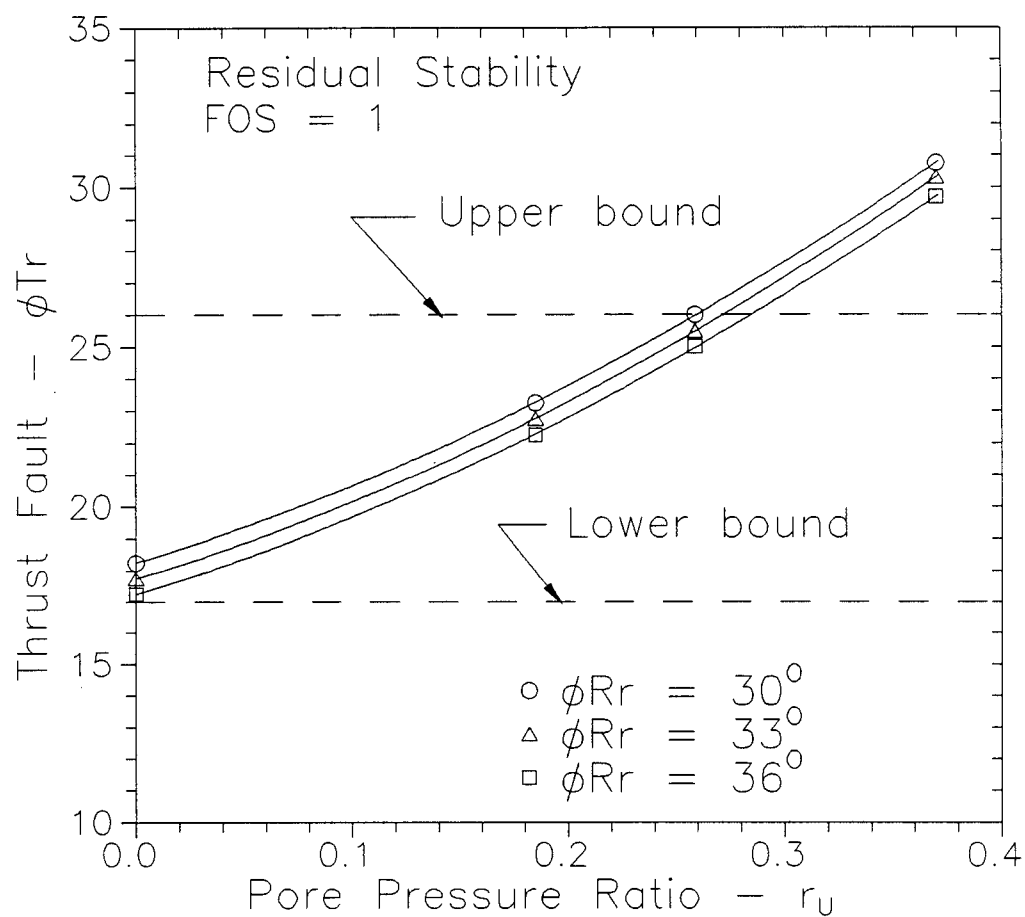
Figure 8.1. Sensitivity analysis of Cheam Slide using residual strength parameters. Curves represent parameter combinations that resulted in a safety factor of one.
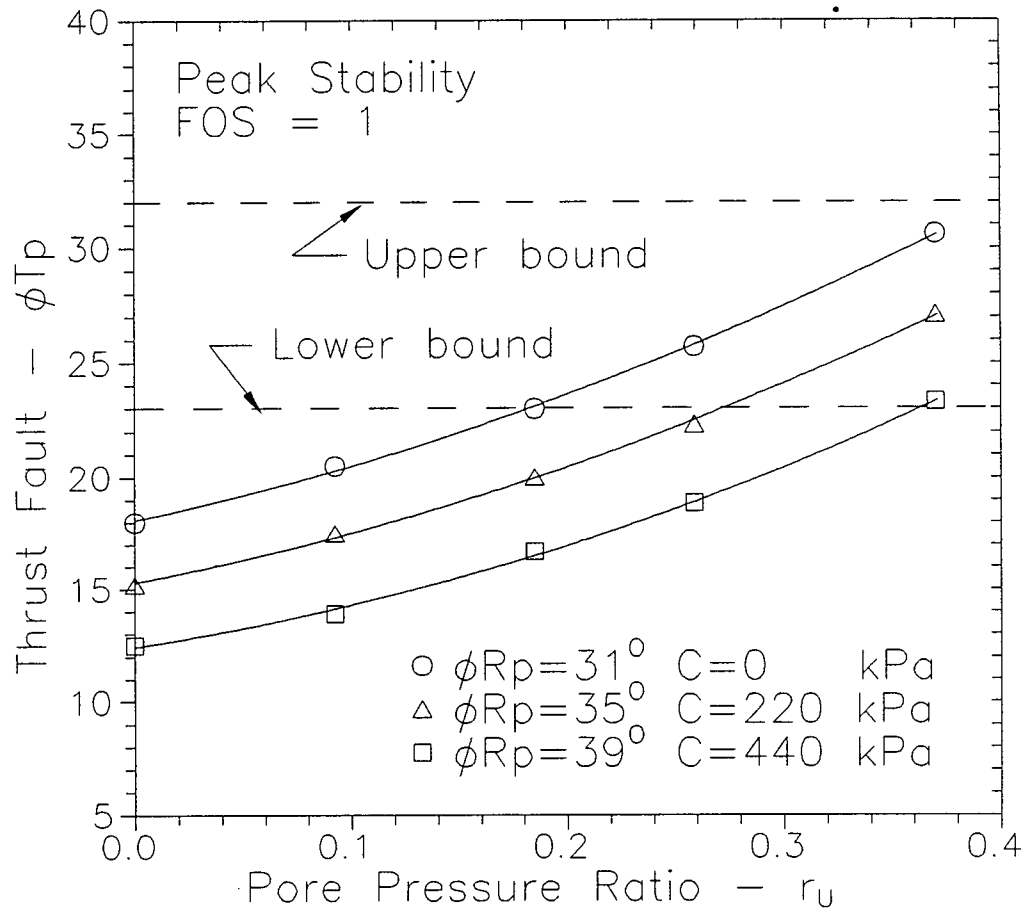
Figure 8.2. Sensitivity analysis of Cheam Slide using peak strength parameters. Curves represent parameter combinations that resulted in a safety factor of one.

CHAPTER 9

DYNAMIC
BACK CALCULATION

9.1 General

The results of the static back calculation showed that high pore pressures could have triggered the failure of Cheam Slide. The slide is located in a seismically active area shows possible correlation to paleoseismic evidence of great subduction earthquakes. To determine possible effects of a large earthquake in southwestern British Columbia, it is of benefit to quantitatively evaluate possible effects of seismic triggering of the slide. A dynamic stability analysis was performed using pseudostatic and critical displacement methods.

9.2 Pseudostatic Method

9.2.1 Methodology

The pseudostatic method incorporates a seismic force in the static equilibrium calculations. The seismic force is assumed static and is equal to the seismic

acceleration multiplied by the mass of the slide. Slope failure occurs if the addition of the seismic force results in a FOS of less than one.

9.2.2 Cheam Slide Pseudostatic

The pseudostatic method was used to determine the stability of Cheam Slide when subject to a NBCC, 475 year return period earthquake (A_M=0.15 g). The range of parameters used for the pseudostatic analysis was equal to those used for peak strength determinations. The results, which are shown in Figure 9.1, indicate that for the lower bound thrust fault peak strength, the slope was unstable for almost all water conditions and peak rock joint strengths. The upper bound thrust fault peak strength resulted in a slope that was unstable for water conditions higher than about $r_U = 0.19$.

9.2.3 Pseudostatic Stress-Strain Relationship

The pseudostatic results indicate that a small seismic load (A_M=0.15) would have an unrealistically large destabilizing effect on the stability of Cheam Slide. This effect was determined to be directly related to the method of calculation of pseudostatic stability. The method assumes that the seismic load is constant, which is unrealistic since seismic loads are not constant, but rather dynamic.

Indirectly, the pseudostatic method does not allow the slope to undergo displacement before failure. Figure 9.2a shows the stress-strain relationship representative of an analysis that does not allow for slope displacement. For comparison a "normal" strain softening elastic-plastic deformation curve is included in

the figure. Clearly, the zero displacement curve is unrealistic. Figure 9.2b shows a "normal" stain softening elastic-plastic deformation curve along with a curve that takes into account cumulative displacement prior to failure. Clearly, the method that defines failure by cumulative displacement would give more realistic results then a zero displacement method.

9.3 Newmark Analysis

9.3.1 Methodology

Newmark (1965) recognized that ground motions from earthquakes are transient events and that some permanent deformation of the slope generally precedes complete failure (Fig. 9.2b). It was recognised that during seismic loading, slope movement occurred only while FOS <1. These two ideas were incorporated into a slope stability analysis.

Newmark's analysis models the slope as a rigid block on an inclined slope. The block has a critical acceleration value A_C, which is defined as the level of acceleration necessary to begin movement of the block. A given strong motion record is applied to the block and when A_C is exceeded the block undergoes acceleration equal to the earthquake acceleration A(t) minus A_C. When A(t) drops below A_C the block continues to move but is decelerating. Once movement of the block stops it remains stationary until A_C is again exceeded. This type of Newmark analysis (hereafter called the "pure Newmark analysis") is presented in Figure 9.3.

Newmark utilized the algorithm in conjunction with series of California earthquakes and determined that the amount of cumulative movement of the block was a function of maximum earthquake acceleration (A_M), maximum earthquake velocity (V_M), and critical acceleration of the block. From his study, a set of empirical relationships defining the cumulative displacement of the block were determined and are given as follows (hereafter called the "empirical Newmark analysis"):

$$D = \frac{V_M^2}{2gA_C} \left(1 - \frac{A_C}{A_M}\right) \frac{A_M}{A_C} \quad ; \quad \text{for } \frac{A_C}{A_M} >= 0.5 \qquad [9.1]$$

$$D = \frac{V_M^2}{2gA_C} \frac{A_M}{A_C} \quad ; \quad \text{for } 0.13 < \frac{A_C}{A_M} < 0.5 \qquad [9.2]$$

$$D = \frac{6V_M^2}{2gA_C} \quad ; \quad \text{for } \frac{A_C}{A_M} <= 0.13 \qquad [9.3]$$

where D is displacement and the remaining parameters are defined in the preceding paragraphs.

The empirical Newmark analysis is an upper bound approximation of the cumulative motion a block would undergo for a given level of seismic loading and is, therefore, conservative (Newmark, 1965). For more rigorous applications, the pure Newmark analysis is used in conjunction with a suite of representative strong motion records to determine potential slope movements. The pure Newmark analysis has an

accuracy advantage because it directly includes the duration of the seismic loading while the empirical Newmark analysis assumes an average duration of seismic loading.

Wilson and Keefer (1985) used the pure Newmark analysis to determine cumulative block displacement for a range of critical accelerations for several strong motion records. From these result, the calculated displacements from the El-Centro and Parkfield strong motion records were chosen for comparison against the displacements predicted by the empirical Newmark analysis.

The two chosen strong motion records are shown in Figure 9.4 and represent two extremes of possible ground motions. The El-Centro record has many pulses of motion extending over many seconds while the Parkfield record has a single pulse lasting just a few seconds. The displacements determined from each method for a given A_C are shown in Figure 9.5. The pure Newmark analysis resulted in equal displacements for both records. However, the empirical Newmark analysis over predicted displacements for the Parkfield earthquake because the method ignores earthquake duration.

Typically, west coast strong motion records are more like the El-Centro record than the Parkfield record and thus the empirical Newmark analysis should give comparable results in most cases. In anticipation of a typical earthquake, the Cheam Slide was modelled using the empirical Newmark Analysis. A possible exception to typical earthquake loading would be that from a subduction zone thrust earthquake.

9.3.2 Critical Displacement

The failure criterion of a slope modelled with the Newmark analysis is a specified cumulative displacement necessary for slope failure. Wilson and Keefer (1985) stated that the actual value of critical displacement may vary widely depending on the mechanism of slope failure, the lithology, the slope geometry, and the previous history of slope movement. For regional application in California, a critical displacement value of 100 mm was chosen by Wilson and Keefer (1985) based on two ideas:

1. In moving 100 mm, a landslide will probably have broken most of the cohesive bonds along the slip surface and across the scarp at the top of the landslide and will also have begun to override the toe of the bottom.

2. One hundred (100) mm is the estimated displacement that a typical house foundation could withstand before experiencing significant damage.

It was further stated that some failures, such as rock falls and most other disruptive landslides, have a more brittle mechanism, and therefore, lower critical displacements. An estimate of 20 mm was quoted.

The failure plane that is believed to have dominantly controlled the stability of Cheam Slide was a gouge filled thrust fault. Therefore, most of the slide would not have had a brittle mechanism. For this reason a critical displacement of 20 mm seems unreasonably small. The 100 mm critical displacement used by Wilson and Keefer (1985) is perhaps more representative, but with the typically large movements

preceding the failure of slides such as Cheam Slide, a higher critical displacement may be more appropriate. For the seismic back analysis of Cheam Slide, critical displacement values of 100 and 1000 mm were used.

9.3.3 Cheam Slide Newmark Analysis

9.3.3.1 General

The empirical Newmark analysis requires as input the acceleration necessary for pseudostatic failure of the slope (A_C). Program WEDGE was used in conjunction with the modelling parameters equal to those used in the determination of the peak strength stability (Sec. 8.3) to determine critical acceleration levels. Once the displacements for the range of parameters and critical acceleration values were determined by the empirical Newmark analysis the results were constrained by the chosen critical displacement values of 100 and 1000 mm.

9.3.3.2 Modelling

Cumulative displacements were determined using the following range of parameters:

```
Pore Pressure Ratio        r_U = 0.0 to 0.37
Thrust fault peak strength øTp = 15 to 35o, c = 0 kPa
Rock joint peak strength   øRp = 31 to 39°, c = 0 to 440 kPa
Seismic loading            475 & 1800 year EQ
```

The parameter combinations necessary for slope failure under the constraint of a critical displacement of 100 mm are shown in Figure 9.6. The 1800 year return earthquake resulted in an unstable slope for all but the lowest values of r_U. A 475 year earthquake resulted in an unstable slope for $r_U = 0.11$ to 0.28 depending on øRp value. These data indicate that, when compared to the pseudostatic method, the empirical Newmark analysis gives less conservative and more realistic results. The results also show the larger earthquake results in a less stable slope.

The parameter combinations necessary for failure of the slope when subject to the constraint of 1000 mm critical displacement are shown in Figure 9.7. The 475 year earthquake resulted in a slope that was unstable for $r_U = 0.17$ to 0.35 depending on the øRp value. The 1800 year earthquake resulted in an only slightly more unstable slope requiring an $r_U > 0.11$ to 0.30 for slope failure.

When comparing critical displacements, the results showed that for a critical displacement of 1000 mm, the stability of Cheam Slide was less sensitive to the magnitude of seismic loading. The results also showed that the higher critical displacement of 1000 mm predicted a much more stable slope. The sensitivity of the calculated stability to the critical displacement was substantial indicating the importance of choosing the correct critical displacement.

9.3.3.3 Effect of Critical Displacement

The results of the previous section showed the pronounced effect of the chosen critical displacement on the calculated stability of the slope. To further investigate this effect, the stability of Cheam Slide with an intermediate rock joint peak strength was determined for a 475 and 1800 year return earthquake. The results are shown in Figures 9.8 and 9.9, respectively. Zero critical displacement required the highest failure plane strength for slope stability while the lowest failure plane strength correlated to the static case. The strengths required for slope stability, incorporating critical displacements of 20 mm, 100 mm and 1000 mm, were intermediate to these results.

Figures 9.8 and 9.9 show similar strength requirements for the stability of the dynamically loaded slope with a critical displacement of 1000 mm and the static slope (FOS=1). This suggests that, for the 475 and 1800 year earthquakes, it would be very difficult for the slide to move 1000 mm over the duration of shaking from a single event.

The results of this section suggest that slides with very low critical displacements (brittle) are most likely to fail under conditions of seismic loading, while slides with higher critical displacements require much higher seismic loading levels .

9.3.3.4 Slope Stability Sensitivity to Critical Displacement

To further investigate the effects of different levels of seismic loading on the Cheam Slide, the slope was modelled using a range of seismic parameters. The stability results for critical displacements of 0 mm, 100 mm and 1000 mm are shown in Figure 9.10. For simplicity, it was assumed that the maximum acceleration (g) was numerically equal to maximum velocity (m/s) for a given earthquake.

A critical displacement of 0 mm resulted in the expected one to one linear relationship between critical acceleration and earthquake acceleration. Both the 100 and 1000 mm critical displacement curves are non-linear and steeply sloped near the origin, but level off at higher critical acceleration levels. The steep slope near the origin indicates that the stability of slopes with lower critical accelerations are proportionately less sensitive to increased levels of earthquake loading than those slopes with higher critical accelerations. This effect is greatest at higher critical displacements. It seems reasonable that if a slope were marginally stable it would require a disproportionately high level of seismic loading for failure. In this case other factors such as high pore pressure may be more effective in causing slope failure.

The levels of seismic loading and r_U values necessary for slope failure of the Cheam Slide model are shown in Figure 9.11. The curves are the reverse of the

critical acceleration curves of Figure 9.10 since the critical acceleration is directly related to pore pressures. To explain the effects of pore pressures changes verses critical acceleration an, r_U value of 0.3 is chosen for discussion. To produce failure with this pore pressure the slope required a seismic load of 0.07 g (0.07 m/s) for a critical displacement of 100 mm and a seismic load of 0.2 g (0.2 m/s) for a critical displacement of 1000 mm. Alternatively, failure could have been initiated by raising the pore pressures 10% to r_U =0.32. Thus, because such a small change in pore pressure, verses a large seismic load, was needed for a high critical displacement slope failure, it may be possible that a slope with a high critical displacement and a low critical acceleration would be more likely to fail under conditions of high pore pressure than of seismic loading. It must be realized, however, that this result would depend on other factors such as the frequency and level of seismic loading as well as the climate.

The preceding paragraphs suggested that the type of slope that will fail during dynamic loading depends on the size of the earthquake event relative to the initial static stability of the slope and its critical displacement. Small earthquakes may only cause failure in marginally stable slopes with low critical displacements. Larger earthquakes may be required for marginally stable slopes with higher critical displacements to fail. Slopes that are fairly stable and have large critical displacements will likely require very large seismic loads for failure.

Often, slopes that show significant previous movements have a high critical displacement. Unless they are very close to failure at the time of seismic loading, they

would require large levels of seismic loading for failure. This leads to the conclusion that, because of the greater probability of smaller earthquake events, it is the low critical displacement slopes that have not necessarily shown extensive previous movement that present the greatest risk.
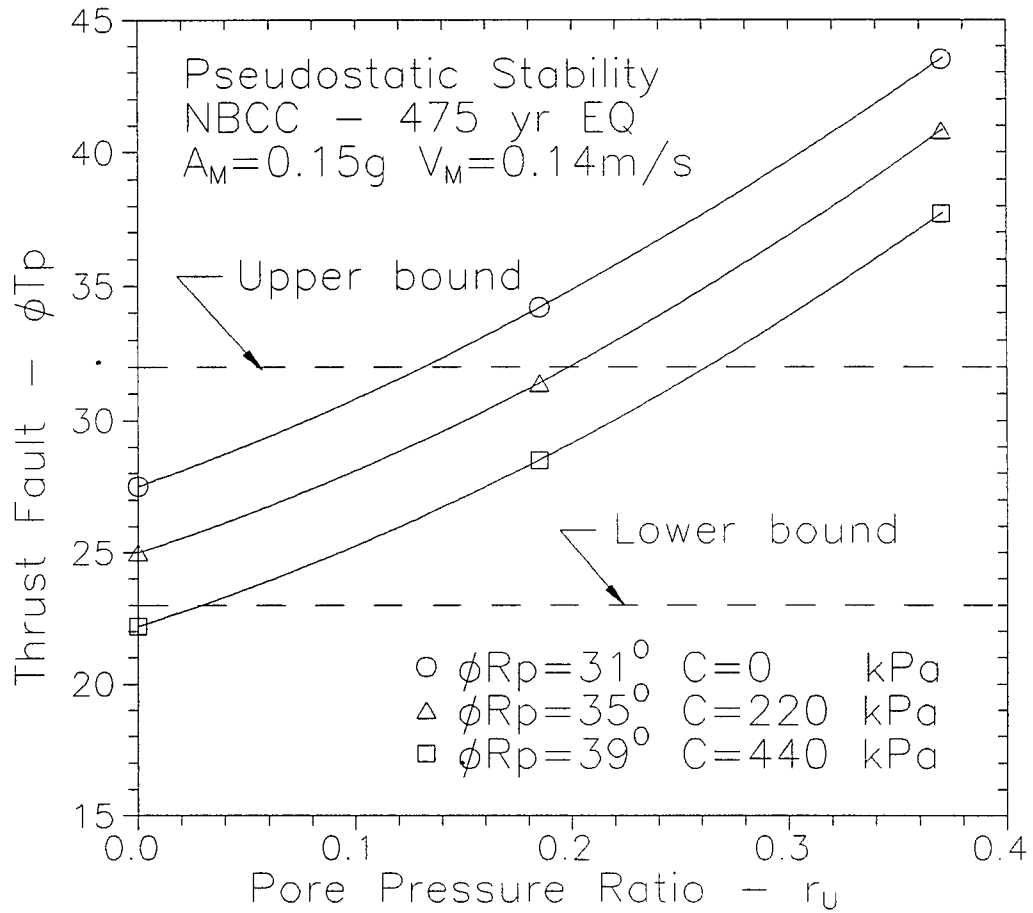
Figure 9.1. Pseudostatic stability analysis of Cheam Slide. Curves represent the parameter combinations that resulted in a safety factor of one when the slope was subject to a NBCC 475 year return period earthquake.
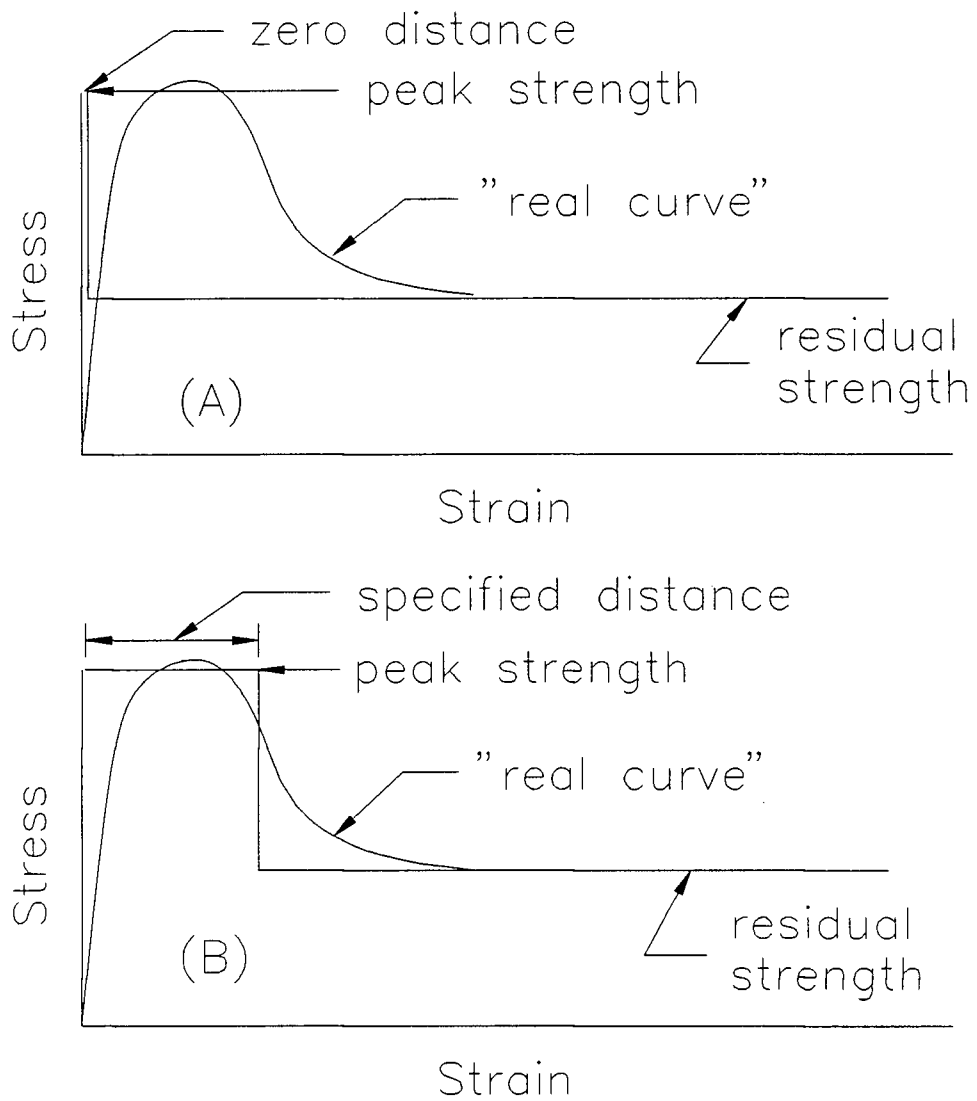
Figure 9.2. Comparison of methods of dynamic analysis. (A) is zero displacement method and (B) is the Newmark method in which a finite displacement necessary for failure is specified.
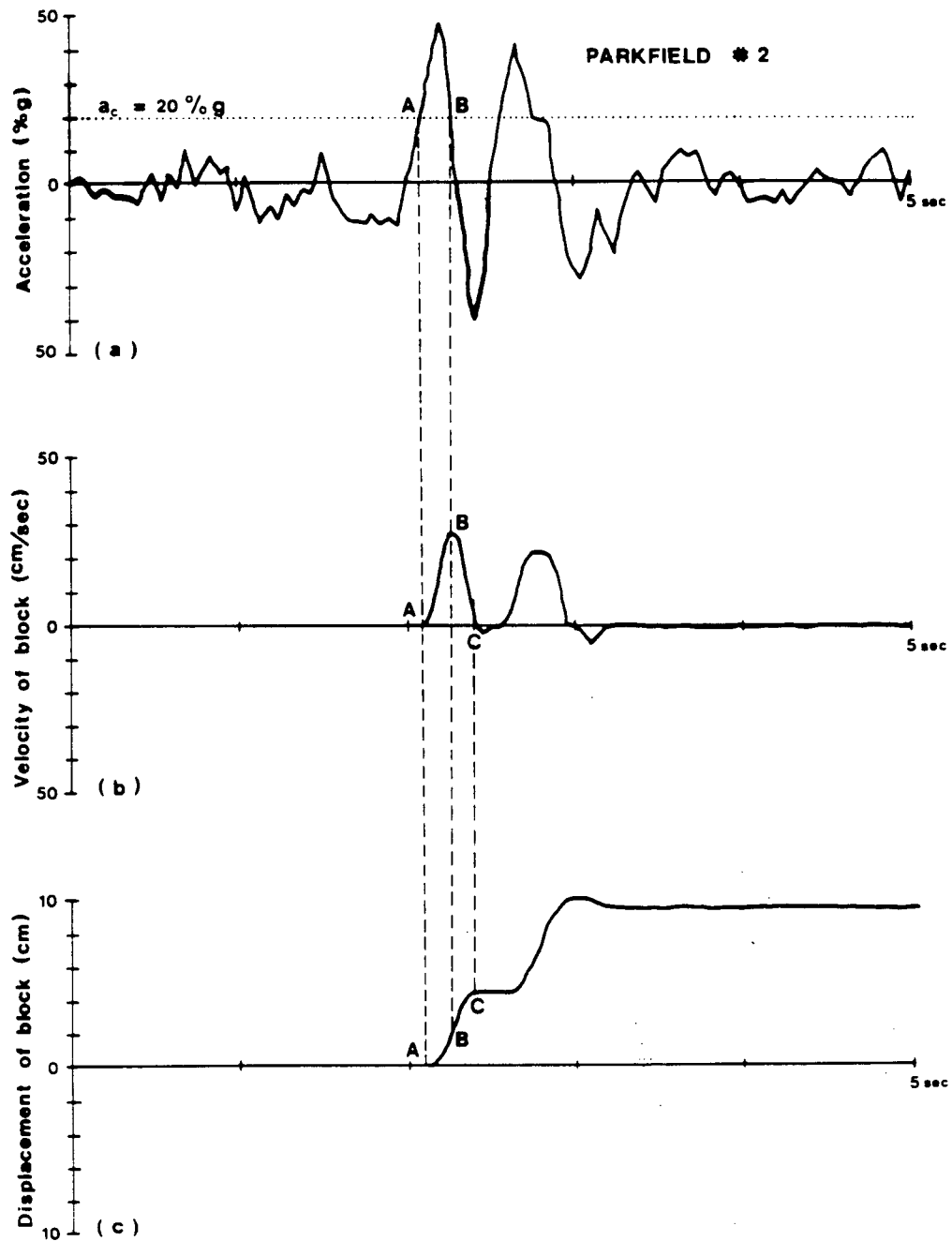
Figure 9.3. Example of the pure Newmark analysis algorithm: (a) strong-motion record with critical acceleration (dotted line) superimposed; (b) velocity of block verses time; and (c) displacement of block verses time (from Wilson and Keefer, 1983).
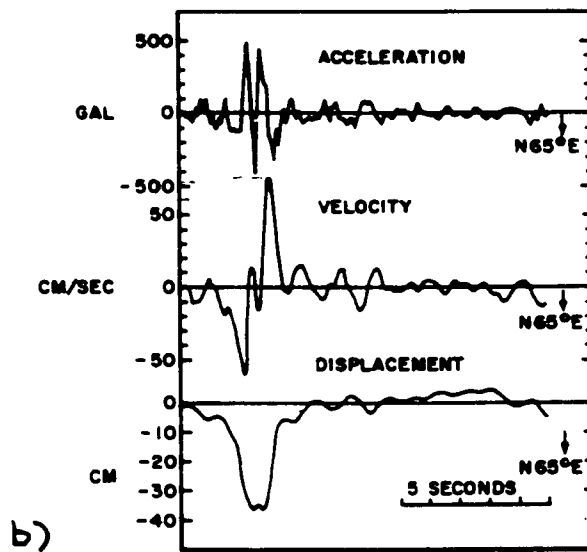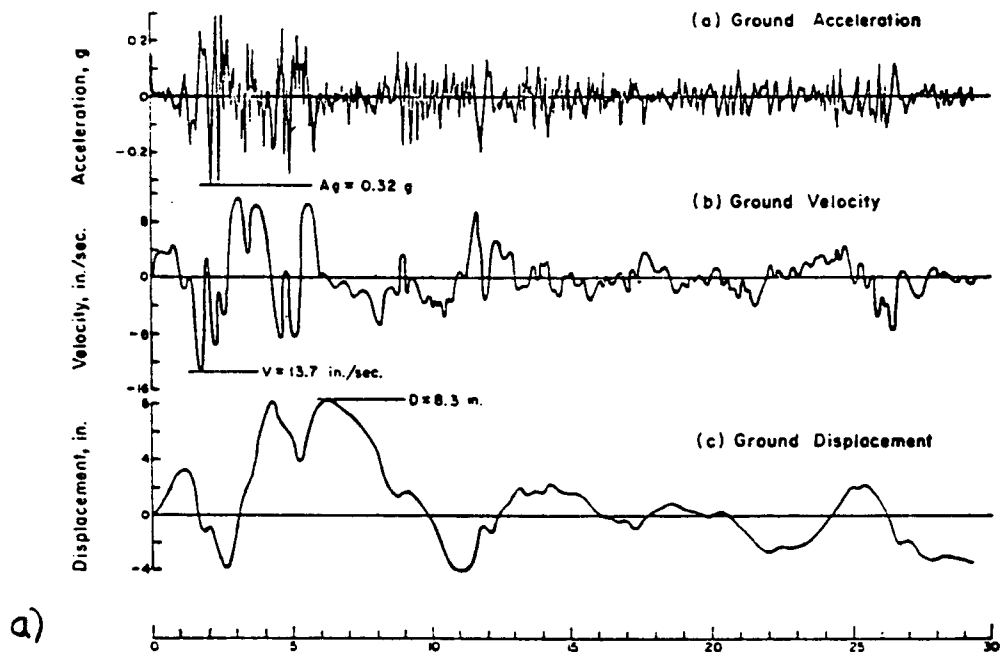
Figure 9.4. North-South component of the 1940 El Centro strong motion record (a) (from Newmark, 1965). Strong motion record from the Parkfield earthquake (b) (from Housner and Trifunac, 1967).
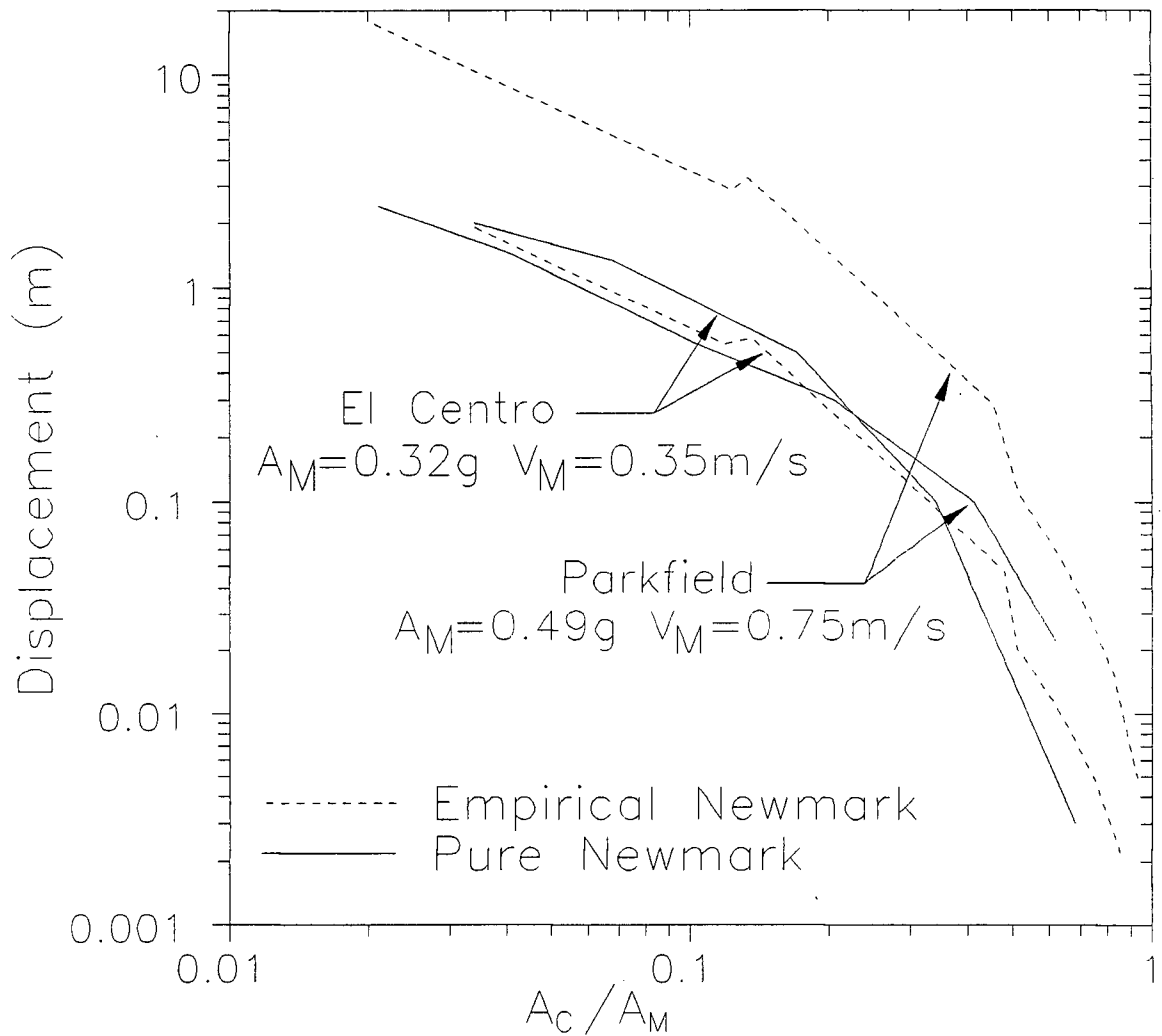
Figure 9.5. Comparison of the calculated cumulative displacements between the pure and empirical Newmark analyses. The El Centro strong motion record has many pulses while the Parkfield strong motion record has one large spike lasting a few seconds (see Fig. 9.4 for the strong motion records).
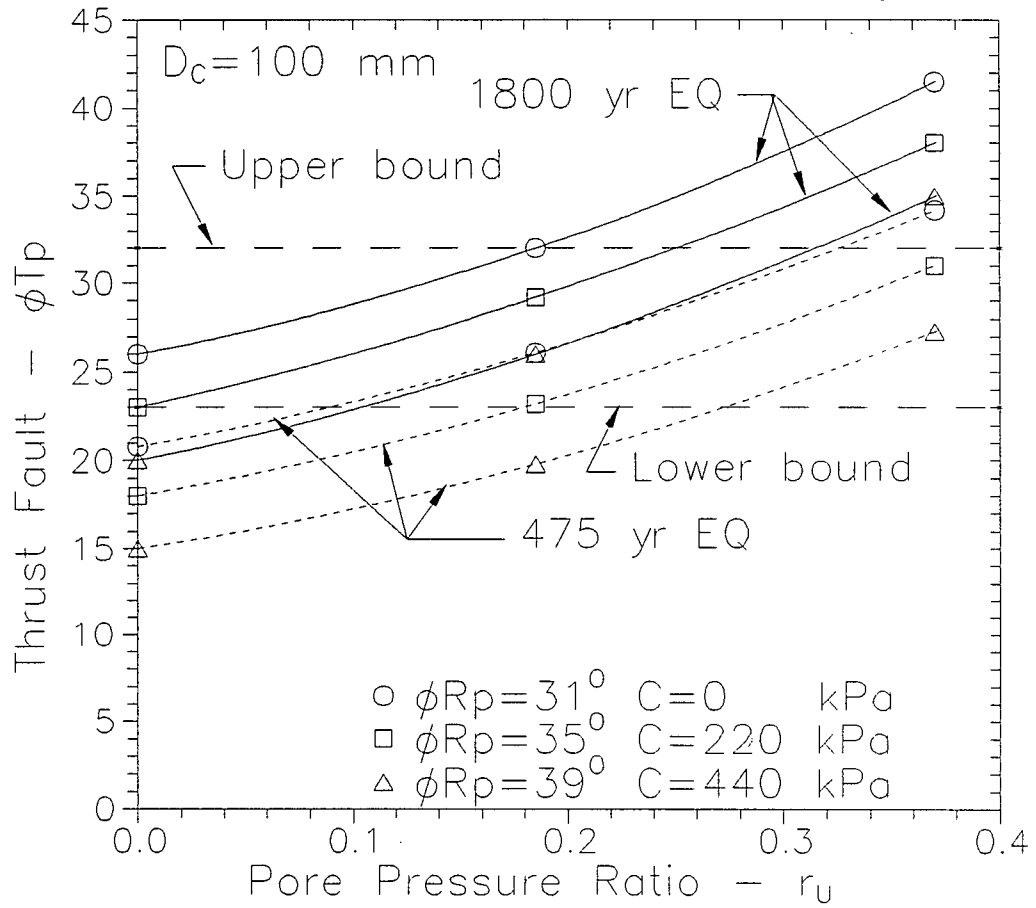
Figure 9.6. Dynamic stability analysis of Cheam Slide. Curves represent parameter combinations that resulted in slope failure under the constraint of a 100 mm critical displacement.
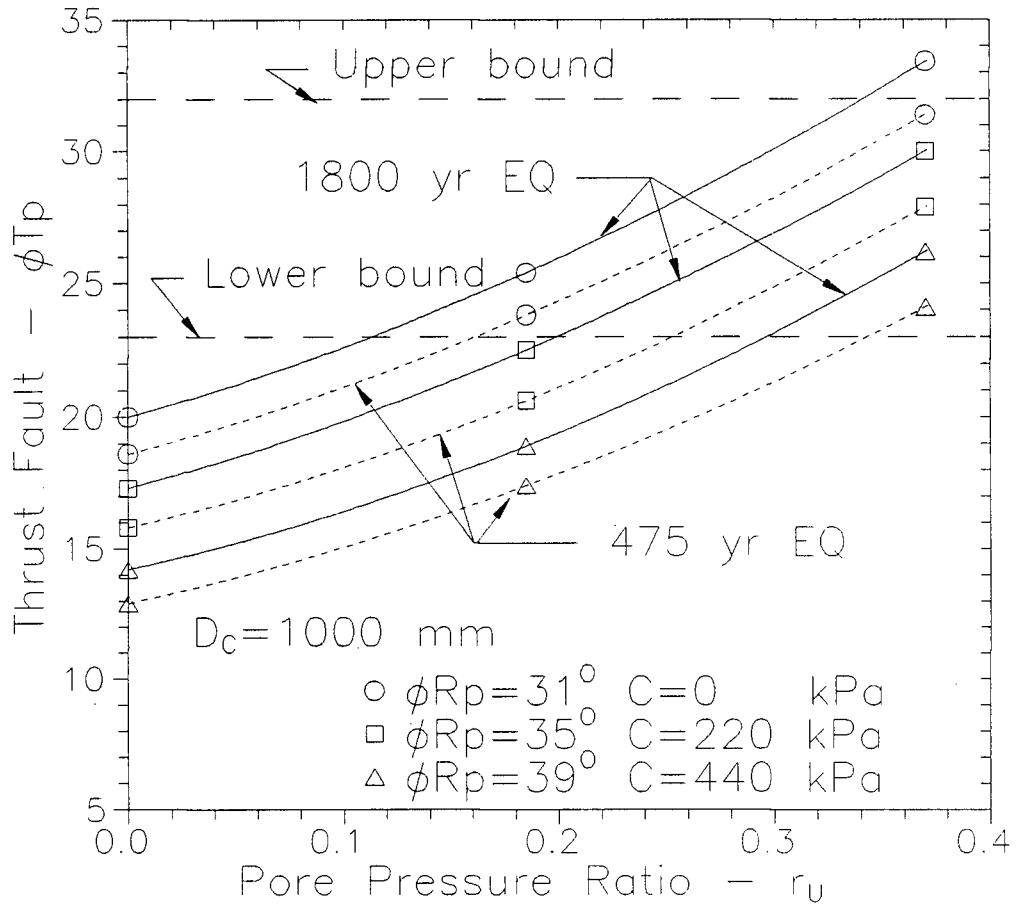
Figure 9.7. Dynamic stability analysis of Cheam Slide. Curves represent parameter combinations that resulted in slope failure under the constraint of a 1000 mm critical displacement.
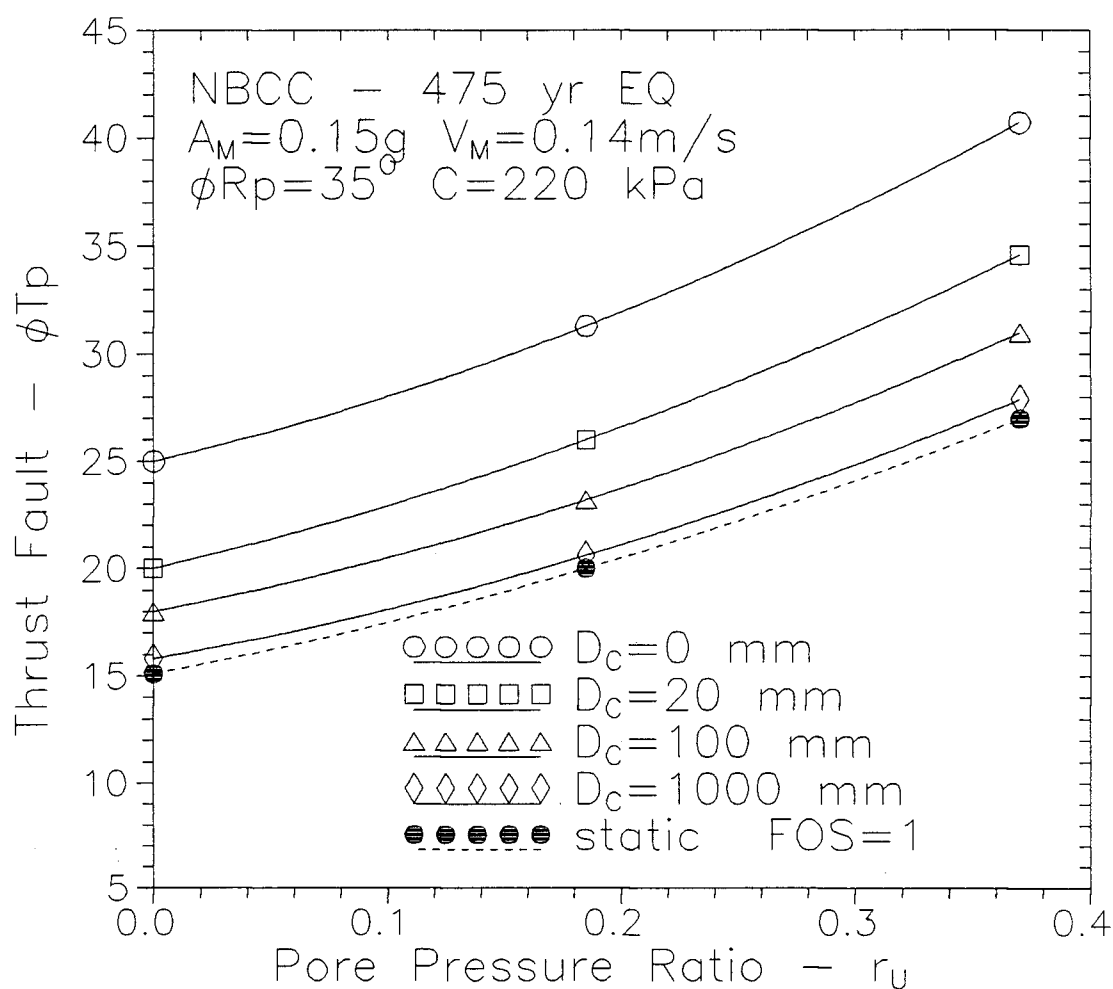
Figure 9.8. Dynamic stability of Cheam Slide when subject to a NBCC 475 year return period earthquake. Rock joint strength was held constant to investigate the effect of critical displacement on slope stability.
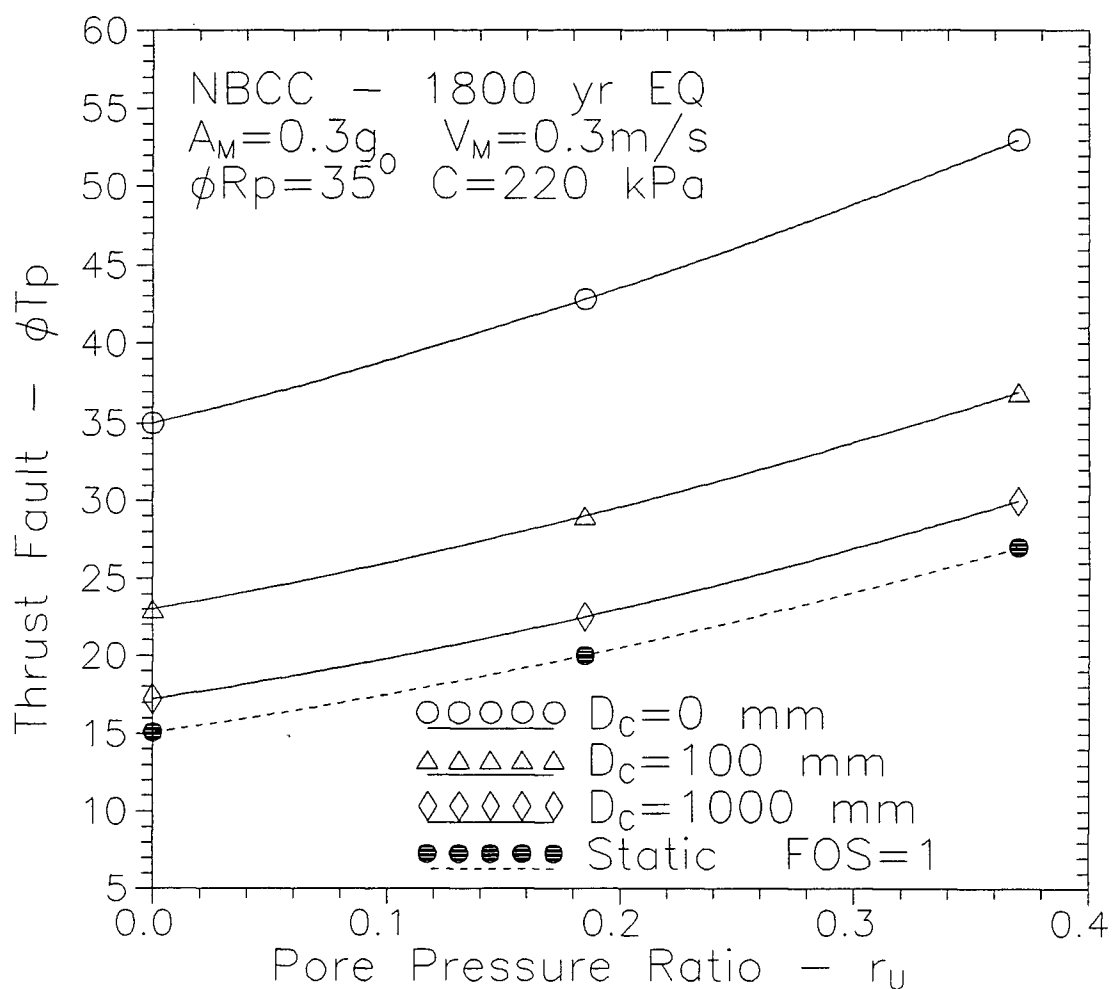
Figure 9.9. Dynamic stability of Cheam Slide subject to a NBCC 1800 year return period earthquake. Rock joint strength was held constant to investigate the effect of critical displacement on slope stability.
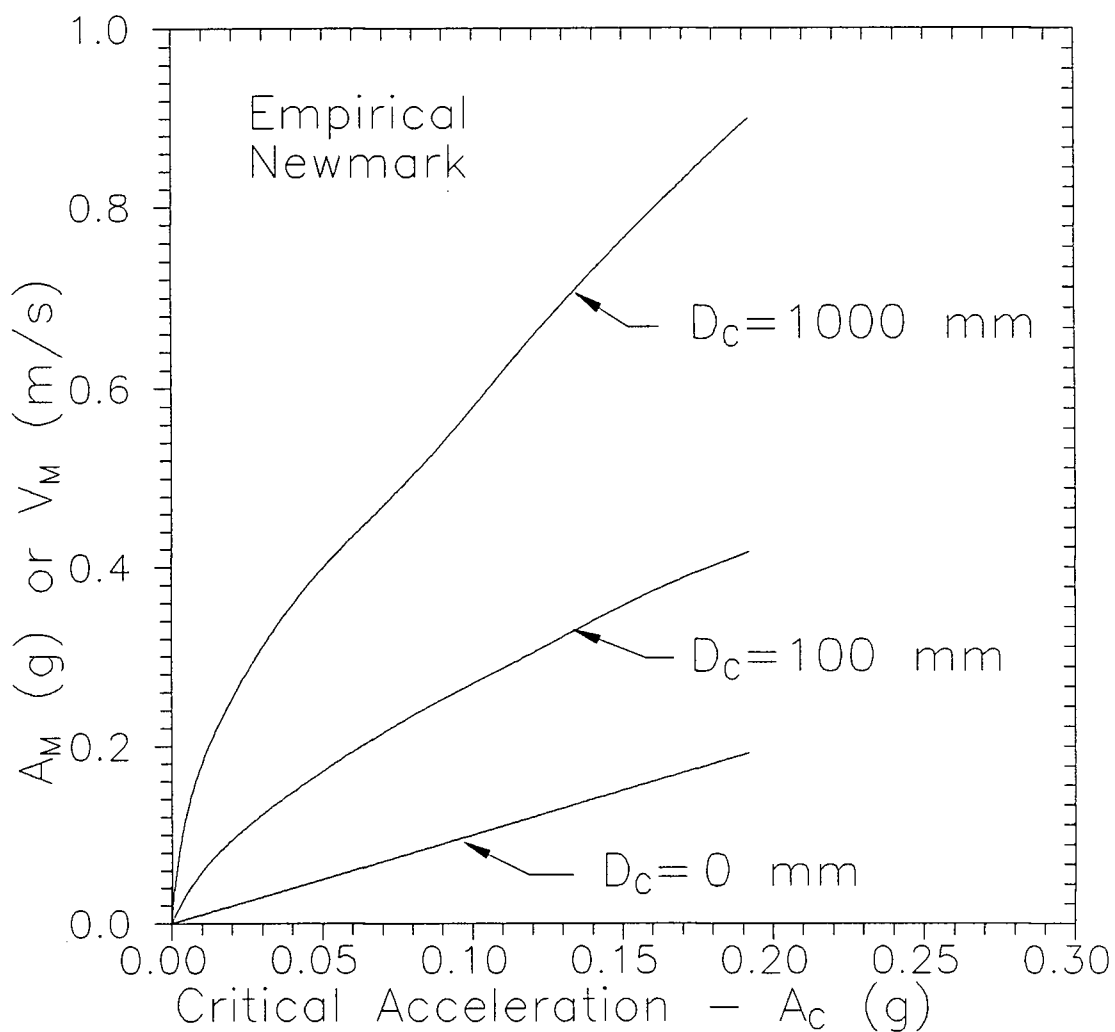
Figure 9.10. Seismic loading levels necessary for slope failure depending on critical acceleration and critical displacement. Displacements are calculated using the empirical Newmark analysis.
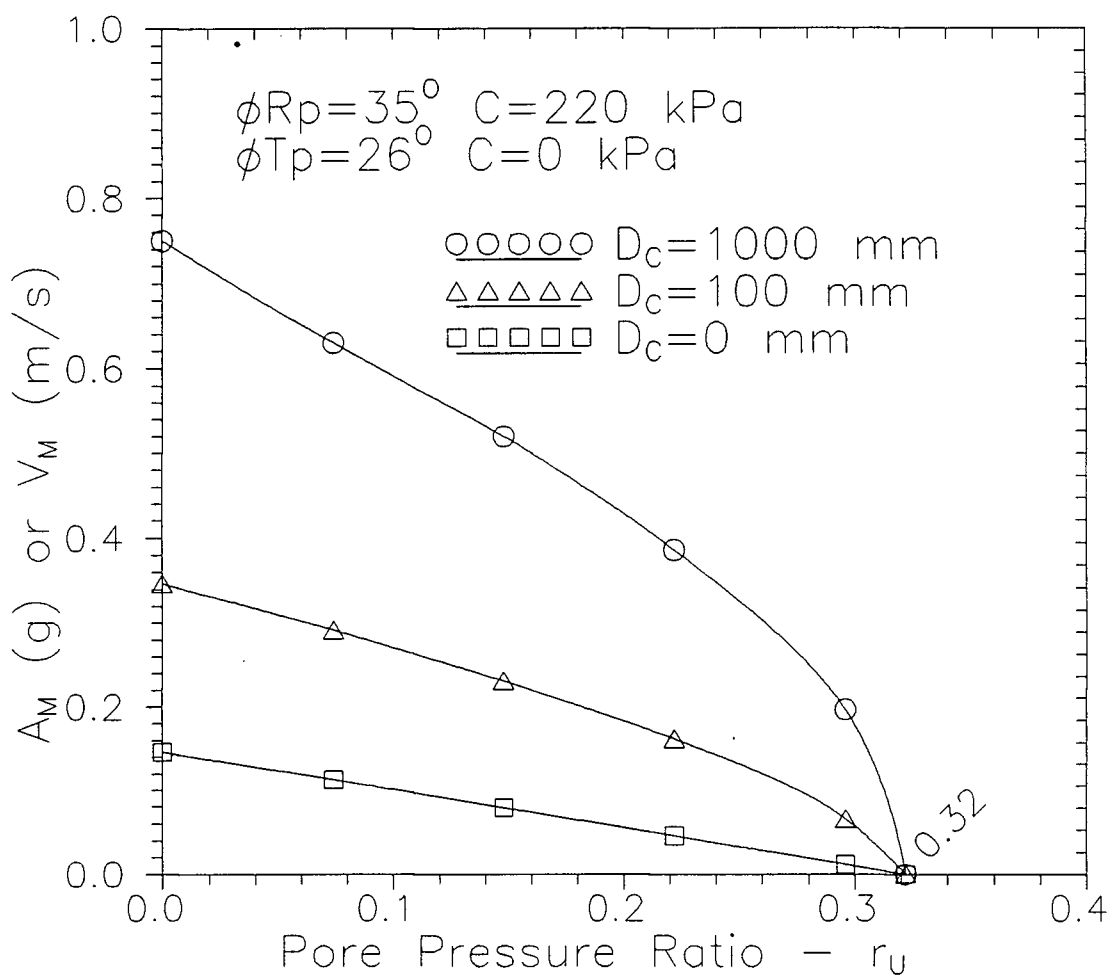
Figure 9.11. Dynamic stability of Cheam Slide subject to a range of seismic loading levels. Strength of thrust fault and rock joint failure planes were held constant to compare the relative effects of pore pressure and seismic loading on the stability of the slope.

CHAPTER 10

FAILURE MECHANISM

10.1 Rigid Block Failure

The stability modelling of Cheam Slide used a rigid block wedge analysis. A rigid wedge allows for immediate and complete transfer of forces to all locations of the block before movement takes place. For example, if circumstances resulted in the first failure plane having a FOS <1, then the extra driving force would be transferred to the second failure plane. If the extra driving force resulted in the second failure plane having a FOS <1, the block would fail. Because of the size of Cheam Slide and the different strength conditions on each failure plane, it is suspected that the wedge may have to undergo deformable rather than rigid behaviour. The deformable behaviour would have resulted in a gradual transfer of forces, perhaps allowing sections of the failure plane to approach or obtain residual strength, while other sections remained between peak and residual strength. The deformable behaviour also may have allowed for movement other than directly down the intersection of the two failure planes.

To investigate the potential for deformable behaviour of Cheam Slide, the stability of select sections of the slide was investigated. Figure 10.1 shows the factor of safety of a two dimension slice taken through the rock joint failure plane, a two dimensional slice taken through the thrust fault failure plane, and a three dimensional rigid wedge. The factor of safety of the 2-D section through the rock joint failure plane greatly exceeded that of the 2-D section through the thrust fault indicating that the portion of Cheam Slide set on the thrust fault had a greater potential for instability.

If deformation of Cheam Slide were allowed, the weaker thrust fault would have caused the southwest side of the wedge to move first. At some point the movement would have been held back by the strength of the rock joint failure plane resulting in two possible scenarios. In the first scenario, the stress applied to the rock joint failure plane would have caused shearing along the joints leading to failure (Fig. 10.2). In the second scenario, the wedge would have begun to rotate in a clockwise direction causing dilation along the upper region of the rock joint failure plane, resulting in decreased shear strength (Fig. 10.2).

If the mass failed in a purely non-rotational motion then the rigid block stability analysis would give representative results. However, if the motion involved rotation, the rigid block model would be inappropriate because motion other than directly down the line of intersection would not be included in the analysis resulting in over prediction of the stability of the slope. A 2-D translational stability analysis of the thrust fault failure plane would assume the rock joint failure plane provided no support

to the failing slope. This would give a conservative stability estimate for a rotational failure. It is suspected that, since there may have been some rotational component to motion and the rock joint failure plane would likely have provided support, the failure conditions at Cheam Slide would require an analysis intermediate to the 2-D translation and 3-D rigid methods.

10.2 Field Evidence

A spur located directly to the northeast of the slide scar has undergone extensive movement since glaciation, indicated by a series of large grabens (Fig. 3.1). Tension forces caused by the loading of the spur by the rotational failure of Cheam Slide may have caused these grabens (Fig. 10.3). However, the grabens may have been formed by relaxation of the oversteepened slope from glacial debutressing.

10.3 Failure Sequence

If one was to postulate a series of events leading to the failure of Cheam Slide, they would proceed as follows. Between about 4350 and 5000 years BP, initial motion of Cheam Slide was triggered perhaps by high pore pressures, earthquake loading, or a combination of the two. The high scarp at the rear of the wedge would have caused higher pore pressures in that location giving the mass at the headscarp lower stability. A down slope compressional force would result as the unstable upper section of the slide attempted to overrun the more stable lower zone. The compressional forces would normally have prevented large tension cracks from opening in the middle and

lower portions of the slope but because the northeast side of the slide was held back by the strength of the rock joint failure plane, tension cracks opened, mostly on the northeast side of the wedge. As movement continued, the rock joint failure plane could no longer hold back the slide and failure occurred.

10.4 Seismic Susceptibility

Dynamic stability modelling (Chapter 9) showed the importance of critical displacement to the dynamic stability of a slope. Cheam Slide likely underwent changes in critical displacements throughout movement to failure. At the start of deformation a high critical displacement gave the slope relative immunity to failure by seismic trigger. As deformation progressed the slide was held back on the brittle rock joint failure plane decreasing its critical displacement, thus increasing its susceptibility to earthquake triggering
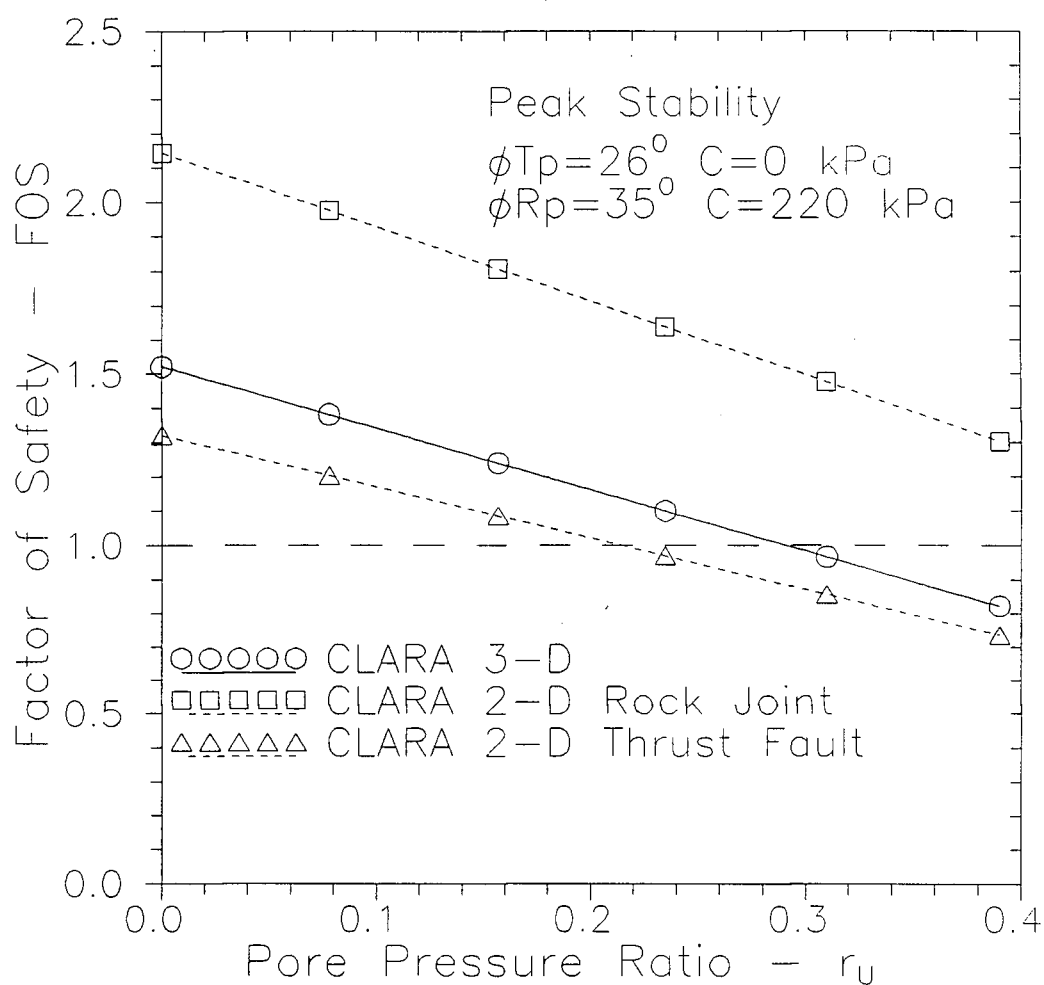
Figure 10.1. A Cheam Slide stability comparison between a three dimensional rigid wedge, a downslope cross-section through the thrust fault failure plane, and a downslope cross-section through the rock joint failure plane.
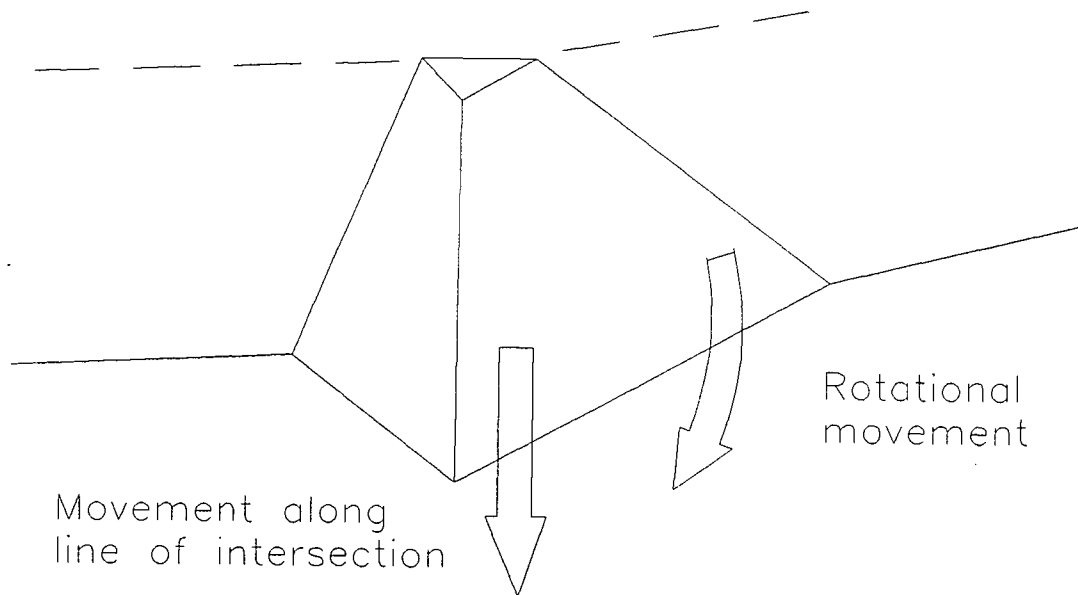
Figure 10.2. Schematic of Cheam Slide showing rotational motion and motion along

the line intersection of the failure planes.
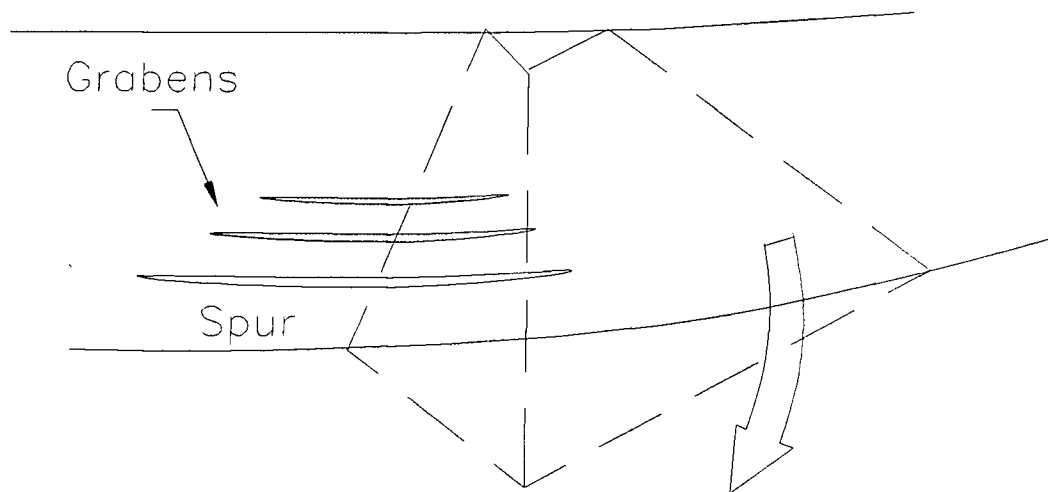
Figure 10.3. Schematic of Cheam Slide showing a possible mechanism for the formation of the graben features on the spur.

CHAPTER 11

RECOMMENDATIONS
FOR FURTHER STUDY

11.1 Slide Volume

The large discrepancy between the source reconstruction and colluvium volumes of Cheam Slide should be further investigated. This would be best accomplished by determining the vertical and areal extent of the slide colluvium since there are large inaccuracies involved in source reconstruction.

11.2 Dating

11.2.1 Katz Slide

Attempts should be made to determine the repeat times of Katz Slide by obtaining a date for the first post-glacial event. This would likely involve upstream drilling.

11.2.2 Cheam Slide

The two ^{14}C dates obtained as part of this study did not correlate well with each other or the previous ^{14}C date. These discrepancies should be investigated and more dating may be necessary to accurately determine the age of the slide.

11.3 Loading Structures

Future gravel workings in the slide debris are should be monitored to take advantage of new exposures where stratigraphy can be further interpreted.

11.4 Failure Plane Strength

11.4.1 Thrust Fault

The residual strength of the thrust fault gouge was determined through an empirical relationship developed by Skempton (1985) and from mineralogy (Kenny, 1967). Direct shear testing of the gouge material would give a more representative range of expected residual values. This type of testing would best be done using a ring shear device such as that described by Bosdet (1980). Direct shear testing could also be done using a standard reversing direct shear box.

The peak strength of the thrust fault also requires further investigation. The angle of the major asperities of the wall rock of the thrust fault should be determined so that the influence of the wall rock on the peak strength of the thrust fault can be assessed. Undisturbed gouge samples should be tested in a large direct box to determine peak strength.

11.4.2 Rock Joints

Peak and residual rock joint strengths were determined from published values. Direct shear testing of natural and saw-cut surfaces would give a more accurate indication of the range of expected peak and residual strengths.

11.5 Groundwater Conditions

11.5.1 Flow Regime

The expected groundwater flow conditions should be determined with greater accuracy. The presence of a relatively impermeable thrust fault, and the lack of knowledge about pre-failure conditions complicates the determination of the pre-failure ground water flow system.

11.5.2 Stability Modelling

Program WEDGE uses Pore Pressure Ratio to simplify groundwater flow conditions. Program CLARA 2.3 allows the user to define the piezometric surface on the failure planes, thus it is better able to accurately represent pore pressure conditions. For this reason, and because CLARA 2.3 is able to compensate for lateral force imbalances, CLARA 2.3 should be used for further modelling of Cheam Slide.

11.6 Design Earthquake

The maximum credible earthquake used for the dynamic analysis of Cheam Slide was based on NBCC maximum acceleration and velocity values for a 1800 year return period earthquake. The potential level of loading from a megathrust earthquake was briefly examined. It was determined that seismic levels from a megathrust earthquake would not exceed those of the 1800 year earthquake. As knowledge of the effects of a megathrust earthquake increases, further dynamic modelling may be necessary.

11.7 Newmark Analysis

The empirical Newmark method was used in this study to determine slope displacements resulting from dynamic loading. For more accurate determination of expected displacements, it would be beneficial to use a pure Newmark analysis incorporating both select local earthquakes and subduction zone earthquakes from around the world. The pure Newmark analysis would more accurately account for the expected higher velocity and longer duration of a subduction zone earthquake.

11.8 Failure Mechanism

The ability of glacial debutressing to produce the grabens on the spur should be investigated. Also, the effect of the postulated deformable-rotational failure of Cheam Slide on the formation of grabens should be determined. Both problems could be effectively addressed by discrete element computer modelling.

11.9 Critical Displacement

A better understanding of critical displacement is needed to determine the seismic susceptibility of slopes. To achieve this, cracks in strategic areas should be monitored for progressive deformation and coseismic movement. Also, the amount of progressive deformation of existing rock avalanches should be investigated.

CHAPTER 12

CONCLUSIONS

This thesis attempts to increase the understanding of the interaction of earthquakes and large rock avalanches. The ages of the Katz, Lake-of-the-Woods and Cheam slides were determined in an attempt to find a cluster or a link between paleoseismicity and Holocene rock avalanches. The ^{14}C dates of these slides, as well as dates for the Hope Slide and two northwestern Washington slides, were compared to established paleoseismicity but no conclusive correlation was found.

There are two possible explanations for the lack of correlation between paleoseismicity and the occurrence of the above mentioned rock avalanches. The first is that these rock avalanches may have been triggered by local seismic events and not by large subduction events. The second explanation is that these rock avalanches may not have been susceptible to earthquake triggering. Chronological evidence of large local events does not exist, so the investigation was directed towards determining the susceptibility of large rock avalanches to earthquake triggering. As a starting point Cheam Slide was chosen for a detailed stability investigation.

A geomorphological study was necessary before numerical study could begin. It was determined that the Cheam Slide was a wedge failure, believed to have been controlled on the northeast flank by an extensive rock joint set and on the southeast side by a pervasive thrust fault containing a zone of clay rich gouge. Source reconstruction produced a pre-slide volume of 150×10^6 m^3 which disagrees with previous volume calculations by Smith (1971). The relatively impermeable thrust fault may have acted to increase the pore pressures in the slope, possibly contributing to failure.

The slide was modelled first to determine if static residual conditions were low enough for catastrophic failure. This condition was meet. The modelling proceeded with peak static stability and it was determined that pore pressure could have resulted in the failure of Cheam Slide.

To determined the dynamic stability of Cheam Slide the empirical relationships of Newmark (1965) were used. It was discovered that the most important factor to the seismic stability of the Cheam Slide was the displacement necessary for failure. A large critical displacement resulted in a slope that was relatively immune to seismic triggering while a small critical displacement resulted in susceptibility to seismic triggering.

Failure of Cheam Slide likely began on the proportionately weaker thrust fault failure plane. As movement progressed, the slide was held back by the relatively stronger rock joint failure plane. The brittle nature of the rock joint failure plane would have made Cheam Slide susceptible to earthquake triggering. It would be

impossible to determine conclusively if an earthquake triggered the failure of Cheam Slide, but it does seem probable that if an earthquake occurred during a period of low critical displacement it could have provided the trigger.

The results from the modelling of Cheam Slide indicated that the susceptibility of large rock avalanches to seismic triggering may depend on the amount of displacement the slope must undergo before catastrophic failure can take place. If the slide has a large critical displacement, then it may not be susceptible to seismic triggering.

An interesting result of the dynamic analysis was the effect of smaller earthquakes on the stability of slopes. It appears that marginally stable slopes with high critical displacements require a disproportionately high seismic loading to produce failure and thus, may be far more likely to fail under conditions of elevated pore pressures than by a small seismic event. It may be stated that smaller earthquakes would only cause failure of brittle slopes, barely stable enough to withstand elevated pore pressures without failure. Since smaller earthquakes are far more frequent than larger events the greatest seismic slope hazard may well be from smaller brittle rock falls and rock avalanches.

REFERENCES

Adams, J. 1989. Turbidites off the Oregon-Washington margin record paleo-earthquakes on the Cascadia subduction zone. *In* Current Research, Part F, Geological Survey of Canada, Paper 89-1F, pp. 37-43.

Armstrong, J.E. 1980. Surficial geology, Chilliwack, British Columbia (West half). Geological Survey of Canada, Map 1487A, Scale 1:50 000.

Armstrong, J.E. 1981. Post-Vashon Wisconsin glaciation, Fraser River Lowland, British Columbia. Geological Survey of Canada, Bulletin 322, 32 p.

Armstrong, J.E. 1984. Environmental and engineering applications of the surficial geology of the Fraser Lowland, British Columbia. Geological Survey of Canada, Paper 83-23, 54 p.

Atwater, B.F. 1987. Aperiodic Holocene recurrence of widespread, probably coseismic subsidence in southwestern washington. Seismic Potential of Cascadia Subduction Zone, *Abstracts*, American Geophysical Union Fall Meeting, San Francisco, T22C-09.

Bacon, C.R. 1983. Eruptive history of Mount Mazama and Crater Lake Caldera, Cascade Range, U.S.A. Journal of Volcanology and Geothermal Research, 18:57-115.

Barton, N. and Bakhtar, K. 1987. Description and modelling of rock joints for the hydrothermal design of nuclear waste vaults. Atomic Energy of Canada Limited, Whiteshell Nuclear Research Establishment, Technical Record TR-418, 319 p.

Basham, P.W., Weichert, D.H., Anglin, F.M., and Berry, M.J. 1982. New probabilistic strong seismic ground-motion maps of Canada: A compilation of earthquake source zones, methods, and results. Earth Physics Branch, Energy, Mines and Resources Canada, Ottawa, Canada, Open Files Report 82-33, 205 p.

Beck, A.C. 1968. Gravity faulting as a mechanism of topographic adjustment. New Zealand Journal of Geology and Geophysics, 11:191-199.

Bishop, A. W. 1955. The use of the slip circle in the stability analysis of slopes. Geotechnique, 5:7-17.

Bosdet, B.W. 1980. The UBC ring shear device. Unpublished M.A.Sc. thesis, Department of Civil Engineering, The University of British Columbia. 110 p.

British Columbia Department of Agriculture, 1916-1976. Climate of British Columbia; British Columbia Department of Agriculture, Victoria, Annual Reports.

Cornell, C.A. 1968. Engineering seismic risk analysis. Bulletin of the Seismological Society of America. 58:1583-1606.

Environment Canada, 1951-1980. Climatic Atlas of Canada. Atmospheric Environment Service, Canadian Government Publications, Ottawa, Canada.

Evans, S.G. 1989. The 1946 Mount Colonel Foster rock avalanche and displacement wave, Vancouver, British Columbia. Canadian Geotechnical Journal, 26:447-452.

Evans, S.G., Aitken, J.D., Wetmiller, R.J., and Horner, R.B. 1987. A rock avalanche triggered by the October 1985 North Nahanni earthquake, District of Mackenzie, N.W.T. Canadian Journal of Earth Sciences, 24:176-184.

Evans, S.G., Clauge, J.J., Woodsworth, G.J. and Hungr, O. 1989. The Pandemonium Creek rock avalanche, British Columbia. Canadian Geotechnical Journal, 26:427-446.

Forster, C.B. 1987. Interaction of groundwater flow systems and the thermal regions in mountainous terrain: A numerical study. Unpublished Ph.D. thesis, Department of Geological Sciences, The University of British Columbia, 217 p.

Fredlund, D.G. and Krahn, J. 1977. Comparison of slope stability methods of analysis. Canadian Geotechnical Journal 14:429-439.

Freeze, R.A. and Cherry, J.A. 1979. Groundwater. Prentice-Hall, Inc., Englewood Cliffs, N.J.

Golder Associates Ltd. 1984. Report to Fraser Cheam Regional District on preliminary assessment of geotechnical hazards, Bridal Falls, British Columbia (File No. 832-1200, dated January, 1984).

Goodmann, R.E. 1970. Deformability of Joints. *In* Symposium on the determination of the *In Situ* modulus of deformation of Rock. American Society for Testing Materials, S.P.T. 477, pp. 174-196.

Griggs, G.B., Carey, A.G., and Kulm, L.D. 1969. Deep-sea sedimentation-fauna interaction in Cascadia Channel and on Cascadia Abyssal Plain. Deep-Sea Research, 16:157-170.

Hadley, J.B. 1964. Landslides and related phenomena accompanying the Hebgen Lake earthquake of August 17, 1959. United States Geological Survey Professional Paper 435; pp. 107-138.

Hadley, J.B. 1978. Madison Canyon rockslide, Montana, U.S.A. *In* Rockslides and avalanches, 1. *Edited by* B. Voight. Elsevier, New York, NY, pp. 167-180.

Hasegawa, H.S., P.W. Basham, and M.J. Berry 1981. Attenuation relations for strong seismic ground motion in Canada. Bulletin of the Seismological Society of America, 71:1953-1962.

Hassani, F.P. and Scoble, M.J. 1985. Frictional mechanisms and properties of rock discontinuities. Proceedings of the International Symposium on the Fundamentals of Rock Joints, Bjorkliden, 15-20 September, pp. 185-196.

Heaton, T.H. 1990. Cascadia Subduction Zone: The calm before the storm. Nature, 343(6258):511-512.

Heidebrecht, A.C., Basham, P.W., Rainer, J.H., and Berry, M.J. 1983. Engineering applications of new probabilistic seismic ground-motion maps of Canada. Canadian Journal of Civil Engineering, 10:670-680.

Hendron, A.J. and Patton, F.D. 1985. The Vaiont Slide, A geotechnical Analysis based on new geological observations of the failure surface. U.S. Army Engineer Waterways Experiment Station, Vicksburg, Miss. Technical Report GL-85-5, Vol. 1, main text 104 pp., plus 3 tables, 43 figures, 52 photos; Vol. 2 - Appendices A through G.

Herget, G. 1977. Pit slope manual, Chapter 2 - Structural geology; CANMET (Canada Centre for Mineral and Energy Technology), CANMET Report 77-41; 123 p.

Hodge, A.L., and Freeze, R.A. 1977. Groundwater flow systems and slope stability. Canadian Geotechnical Journal, 14:466-476.

Hoek, E. and Bray, J. 1977. Rock Slope Engineering. Revised Second Edition. Institution of Mining and Metallurgy, London, 402 p.

Hoek, E. and Brown, E.T. 1981, Rock engineering for underground openings.Institution of Mining and Metallurgy, London, 374 p.

Housner, G.W. and Trifunac, M.D. 1967. Analysis of accelerograms - Parkfield earthquakes. Bulletin of the Seismological Society of America, 57(6):1193-1220.

Hull, A.G. 1987. Buried lowland soils from Willapa Bay, southwest Washington: Further evidence for recurrence of large earthquakes during the last 5000 years. Seismic Potential of Cascadia Subduction Zone, *Abstracts*, American Geophysical Union Fall Meeting, San Francisco, T22C-09.

Hungr, O., 1987a. An extension of Bishop's Simplified Method of slope stability analysis to three dimensions. Geotechnique, 37:113-117

Hungr, O., 1987b. Three-dimensional slope stability analysis by method of columns, using a microcomputer. Proceedings of the 1st Canadian Symposium on Microcomputer Applications in Geotechnique, Regina, Saskatchewan, pp. 203-212.

Hungr, O., 1988. CLARA user's manual: slope stability analysis in two or three dimensions for IBM compatible microcomputers. O. Hungr Geotechnical Research, Vancouver, British Columbia, 76 p.

Hungr, 0., Salgado, F.M., and Byrne, P.M. 1989. Evaluation of a three-dimensional method of slope stability analysis. Canadian Geotechnical Journal, 26:679-686.

Janbu, N. 1957. Stability of slopes with dimensionless parameters. Harvard University Soil Mechanics Series, No. 46, 78 p.

Joyner, W.B. and Boore, D.M. 1981. Peak horizontal acceleration and velocity from strong-motion records including records from the 1979 Imperial Valley, California, earthquake. Bulletin of the Seismological Society of America, 71:2011-2038.

Keefer, D.K. 1984. Landslides caused by earthquakes. Geological Society of America Bulletin, 95:406-421.

Kenny, T.C. 1967. The influence of mineral composition on the residual strength of natural soils. Proceedings, Geotechnical Conference, Oslo, 1:123-129.

Klein, D.D. and Hurlbut, S.J. 1985. Manual Of Mineralogy. John Wiley & Sons, New York, NY., 20th ed. 596 p.

Lambe, T.W. 1951. Soil Testing For Engineers. John Wiley & Sons, New York, NY. 165 p.

Mathewes, R.W. and Heusser, L.E. 1980. A 12 000 year palynological record of temperature and precipitation trends in southwestern British Columbia. Canadian Journal of Botany. 59:707-710.

Mathews, W.H. 1979. Landslides of central Vancouver Island and the earthquake. Bulletin of the Seismological Society of America, 69:445-450.

Mathews, W.H., and McTaggart, K.C. 1978. Hope rockslides, British Columbia, Canada. *In* Rockslides and avalanches, 1. *Edited by* B. Voight. Elsevier, New York, NY, pp. 259-275.

McGuire, R.K. 1976. FORTRAN computer program for seismic risk analysis. United states Geological Survey Open-File Report 76-67, 90 p.

McSaveney, M.J. 1978. Sherman Glacier rock avalanche, Alaska, U.S.A. *In* Rockslides and Avalanches, 1. *Edited by* B. Voight. Elsevier, Amsterdam, The Netherlands, pp. 197-258.

Milne, W.G. 1977. Seismic risk maps of Canada. Proceedings of the Sixth World Conference on Earthquake Engineering, New Delhi, p.930.

Milne, W.G., Rogers, G.C., Riddihough, G.A., McMechan, G.A., and Hyndman, R.D. 1978. Seismicity of western Canada. Canadian Journal of Earth Sciences, 15:1170-1193.

Monger, J.W. 1966. The stratigraphy of the type-area of the Chilliwack Group, southwestern British Columbia. Unpublished Ph.D. thesis, The University of British Columbia, 173 p.

Monger, J.W. 1989. Geology, Hope, British Columbia. Geological Survey of Canada, Map 1691A, Scale 1:250 000.

Nasmith, H., Mathews, W.H., and Rouse, G.E. 1967. Bridge River ash and some other recent ash beds in British Columbia. Canadian Journal of Earth Sciences, 4:163-170.

National Building Code of Canada (NBCC) 1985, Supplement. National Research Council of Canada, No. 23178.

Newmark, N.M. 1965. Effects of earthquakes on dams and embankments. Geotechnique 25: 139-160.

Piteau, D.R. 1977. Regional slope-stability controls and engineering geology of the Fraser Canyon, British Columbia. Geological Society of America Reviews in Engineering Geology. 3:85-111.

Plafker, G. and Ericksen, G.E. 1978. Nevados Huascaran avalanches, Peru. *In* Rockslides and Avalanches, 1. *Edited by* B. Voight. Elsevier, Amsterdam, The Netherlands, pp. 269-279.

Rogers, G.C. 1988. An assessment of the megathrust earthquake potential of the Cascadia subduction zone. Canadian Journal of Earth Sciences. 25:844-852.

Ryder, J.M., Bovis, M.J. and Church, M. 1990. Rock avalanches at Texas Creek, British Columbia. *Submitted* to the Canadian Journal of Earth Sciences.

Savigny, K.W. 1990a. Engineering geology of large landslides in the Lower Fraser River Valley area, southwestern Canadian Cordillera. *Abstract*, Annual meeting of the Geological Association of Canada (GAC) and the Mineralogical Association of Canada (MAC), 1990.

Savigny, K.W. 1990b. Engineering geology of large landslides in the Lower Fraser River Valley area, southwestern Canadian Cordillera. Landslide Hazard in the Canadian Cordillera, First meeting, Vancouver, B.C. Special Paper.

Scheidegger, A.E. 1973. On the prediction of the reach and velocity of catastrophic landslides. Rock Mechanics, 5:231-236.

Schuster, R.L. 1990. Earthquake induced landslides: a worldwide geological hazard. *Presented at* Geotechnical Aspects of Earthquake Engineering; A Seminar. The University of Washington, Seattle Washington.

Skempton, A.W. 1985. Residual strength of clays in landslides, folded strata and the Laboratory. Geotechnique 35:3-18.

Smith, R.H. 1971. A study of a prehistoric landslide surface at Cheam Lake, east of Chilliwack, British Columbia. Unpublished B.A.Sc. thesis, The University of British Columbia, 24 p.

Steen-McIntyre, V.C. 1977. Collection, preparation, petrological description and approximate dating of tephra (volcanic ash). Unpublished Ph.D. thesis, The University of Idaho, Moscow, Idaho.

Thurber Consultants Ltd. 1984a. Landslide debris in the vicinity of the Popkum interchange (File 17-604-23, dated October 24, 1984).

Thurber Consultants Ltd. 1984b. Letter to B.A. Lambert, Deputy Municipal engineer on the Popkum Quarry operations (File 14-51-3, dated June 15, 1984).

Thurber Consultants Ltd. 1988a. Report to the Seventh Day Adventist Church on the Chawuthen area subdivision (File No. 19-567-1, dated September 6, 1988).

Thurber Consultants Ltd. 1988b. Report to the Regional District of Fraser-Cheam an a geotechnical hazard investigation, Ross Road/Lake-of-the-Woods area, Electoral Area B (File No. 14-50-6, dated October 11.1988).

Weichert, D.H. 1980. Estimation of the earthquake recurrence parameters for unequal observation periods for different magnitudes. Bulletin of the Seismological Society of America. 70:1337-1346.

Wetmiller, R.J. and Evans, S.G. 1989. Analysis of the earthquakes associated with the 1965 Hope landslide and their effects on slope stability at the site. Canadian Geotechnical Journal, 26:484-490.

Williams, H., Turner, F.J., and Gilbert, M.G. 1982. Petrography: An introduction to the study of rocks in thin section. Second Edition, W.H. Freeman and Company, San Francisco.

Wilson, M.J. 1987. A Handbook Of Determinative Methods In Clay Mineralogy. Chapman and Hall, New York, NY, 247 p.

Wilson, R.C. and Keefer, D.K. 1983. Dynamic analysis of a slope failure from the 6 August 1979 Coyote Lake, California, earthquake. Bulletin of the Seismological Society of America, 73:863-877.

Blank

Blank

APPENDICES

APPENDIX I

Stratigraphic Unit Description of:
Katz Slide - Section 2
Cheam Slide - CNR Gravel Pit

APPENDIX II

Radio Carbon Dating - Simon Fraser University
Radio Carbon Dating - The University of Toronto

APPENDIX III

Colluvium X-Ray Diffraction Results
Fault Gouge X-Ray Diffraction Results

Detailed Interpretation of Fault Gouge X-Ray
Diffraction Results

APPENDIX IV

Petrographic Study of Cheam Slide Tephra Deposit

APPENDIX V

Pacific Geosciences NBCC seismic
hazard calculations

APPENDIX I

Stratigraphic Unit Description of:

Katz Slide - Section 2
Cheam Slide - CNR Gravel Pit

KATZ SLIDE - STREAM CHANNEL CUTOFF SECTION
(Core #: KATZ-3)

1 SAND   Fine, dark grey in colour. Intermixed twigs and peat.

2 SILT   Interbedded clay and silty clay; colour is grey to very dark grey with decreasing clay content; believed to be overbank deposit.

3 SILT   Interbedded sand and silty sand; some organic layers; colour is a very dark grey; organics are black; believed to be an overbank deposit.

4 ORGANICS   Maturing downward from a flowing black ooze to a brownish peat; some rootlets from overlying organic matt.

5 ORGANICS   Organic mat, horse tails most common vegetation.

CHEAM SLIDE - CNR GRAVEL PIT SECTION

1 GRAVEL Poorly graded, sandy, with less than 2% fines (GP); generally light tan in colour; brown interbedded coarse sands are common; believed to be glacialfluvial.

2 SAND Uniform, medium, with trace fines (SP); shows slight fining upward trend; massive; light brown in colour; believed to be glacialfluvial.

3 SILT Clayey, occasional fine sand; light tan in colour but darkens to a dark bluish grey with increasing clay content; zones of rust coloured weathering commonly surround sand layers; believed to be fluvial (vertical accretion facies).

4 CLAY Grading upward from silty sandy clay to dominantly clay; subrounded intraclasts are common in the bottom 5 cm; believed to be fluvial (vertical accretion facies).

5 Soil Horizon Discontinuous organic soil layer; typically no thicker than 2 cm.

6 Mazama Ash Discontinuous, very light tan coloured volcanic ash; occurs in pockets; believed to have been disturbed by slide event.

7 SAND Silty, clayey, with gravel (SM-SC); proportions are typically 35% gravel, 55% sand and 10% fines; coarse fraction typically no larger than 25-30 cm, composed of comminuted rock from the Chilliwack Formation, subangular, matrix supported; colour is a distinct blue grey; organics in the form of logs and branches are common; prehistoric slide debris.

8 SAND Same characteristics as (7) except tan in colour; tan colouring believed to be a result of weathering.

APPENDIX II

Radio Carbon Dating - Simon Fraser University
Katz Slide
Cheam Slide

Radio Carbon Dating - The University of Toronto
Lake-of-the Woods

CARBON-14 DATING INDEX

<u>Katz Slide:</u>

- Simon Fraser University Radiocarbon Laboratory
- Sample# : W-02
   - branch and peat from bottom of paleochannel (Fig. 2.7)

<u>Lake-of-the-Woods Slide:</u>

- Isotrace Laboratory, University of Toronto
- Sample# : LW-PS1A and LW-PS3A
   - Gyttja from bottom of lake sediments (Fig. 2.9)

<u>Cheam Slide:</u>

- Simon Fraser University Radiocarbon Laboratory
- Sample# : W-03
   - Rootlet from CNR Gravel pit (Fig. 3.4)
- Sample# : W-04
   - Section of log from CNR Gravel pit (Fig. 3.4)

APPENDIX III

Colluvium X-Ray Diffraction Results

Fault Gouge X-Ray Diffraction Results

Detailed Interpretation of Fault Gouge X-Ray
Diffraction Results

XRD

Chlorite + Illite + Feldspar (Na)

BLUE-GREY COLLUVIUM

3.21
3.34
3.55

4.74
5.01

7.13

10.10

14.41

XRD

Chlorite + Illite + Feldspar (K) + Quartz

TAN COLLUVIUM

2.83

3.20

3.33

3.55

4.03

4.25

4.70

4.98

7.08

10.02

14.06

XRD
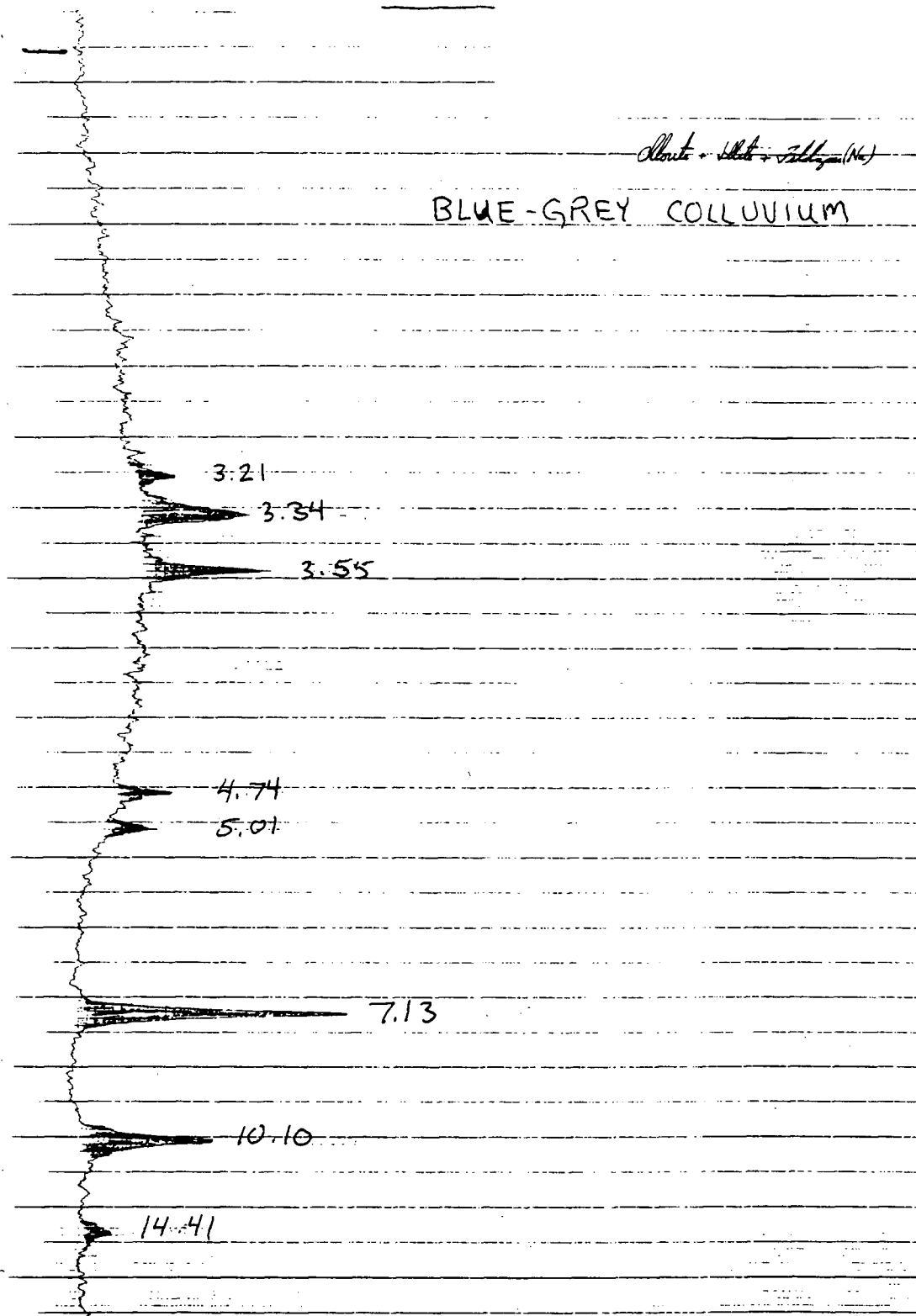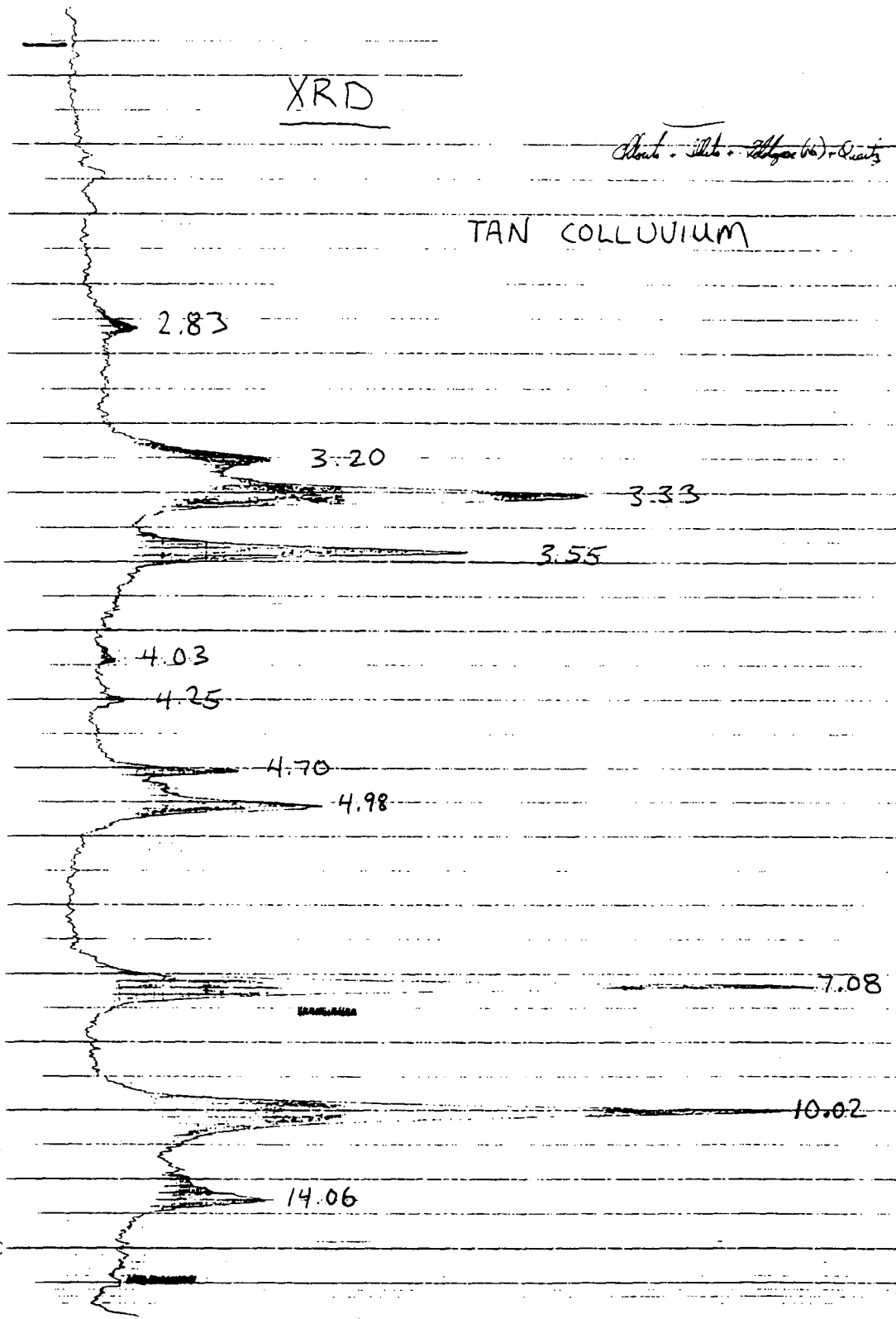
Chlorite + Illite + Quartz (Trace)

THRUST FAULT GOUGE

2.50

2.83

3.32

3.54

4.25

4.73

4.99

7.11

10.06

14.14

Detailed Interpretation of Fault Gouge X-Ray
Diffraction Results

The mineralization of the fault gouge is dominantly illite with minor chlorite, as seen from the extremely high illite peaks in comparison to the peaks of the other minerals. Swelling clays are often interstratified with other clays, the most common types being illite-smectite and chlorite-smectite. Also, illite rarely occurs without the presence of at least some smectite (Wilson, 1987).

Illite yields a strong reflection at about 10 Å and chlorite reflects at about 14.2-14.4 Å. The reflection of smectite varies greatly depending on exchangeable cation, relative humidity, association with certain organic molecules, and heat treatment. All smectites lose interstitial water at between 100 and 200°C resulting in basal spacing of 10 Å. The gouge was dried at about 105°C for several days so a smectite peak could possibly correspond with that of the illite peak. Treating the collapsed structure with ethylene glycol increases the basal spacing of most smectites to around 17 Å. This treatment resulted in very slight level increases in 17 Å range indicating the presence of some smectite.

The level of smectite in interlayered complexes of illite-smectite and chlorite-smectite can be approximated. Only illite-smectite interlayering will be dealt with here because the gouge material is dominantly illite. Interstratified illite-smectite will show

a peak at about 17 Å when treated with glycol. This peak will decrease with increasing proportions of illite. The peak will still be discernable up to about 60% illite, although the peak is weak, broad, and asymmetrical. There appears to be such a peak in the gouge XRD results so a first estimate of smectite content of the gouge is less than 40% smectite.

Wilson (1987) states that long range ordering in a illite-smectite system may be possible. This would be in the form of a IIS (illite-illite-smectite) order clay or a IIIS order clay. The IIIS-ordered clays correspond to a higher illite contents (>80%), and yield XRD patterns characterized by a strong peak at about 9.8 Å, with a subsidiary peak or shoulder at about 11 Å. This type of pattern describes results from gouge XRD very well. This would indicate a smectite content of less than 20%.

From the above arguments the smectite content of the clay gouge can be considered to be 10 to 40% smectite.

APPENDIX IV

Petrographic Study of Cheam Slide Tephra Deposit

_____

Petrographic Study of Cheam Slide Tephra Deposit

_____

The optical characteristics of the four most recent ashes in southern and middle British Columbia are given by Nasmith *et al.* (1967). Against this data, a petrographic study was done on the tephra collected from Cheam Slide

A sample of the tephra was prepared for petrographic study by sieving an oven dried sample and retaining the size reaction between the #100 and #200 mesh screens. (procedure modified from Steen-McIntyre, 1977). The sample had a high content of volcanic glass indicating a volcanic origin. The glass was a distinct buff colour. Zoned plagioclase was common and clinopyroxene was not found. Two minerals of high relief were found. Both were pleochroic. One was a pale yellowish-brown turning to pale green upon stage rotation and the other was dark green turning dark olive brown, indicating that these minerals were, respectively, orthopyroxene and hornblende.

The volcanic glass in the collected sample is buff coloured and therefore the ash is not Mt. St. Helens W ash, which is always white in colour. Additionally the St. Helens W ash has never been found north of the 49th parallel and it is much younger (600 years. B.P.) than the expected age of the Cheam slide event. All recent ashes contain zoned plagioclase, as did the collected sample, so this property is not diagnostic. Orthopyroxene was found in the ash from Cheam Slide. Orthopyroxene

is absent in the Mt. St. Helens Y ash and thus the choices are narrowed down to either Bridge River ash or Mazama ash. Since clinopyroxene was not found in the study ash and it is listed as abundant in the Bridge River ash it appears that the study ash is that of Mount Mazama which has only sparse clinopyroxene. Also, Bridge river ash should not be found this far south, thus, further supporting the Mazama ash diagnosis.

APPENDIX V

Pacific Geosciences NBCC seismic
hazard calculations

ENERGY, MINES AND
RESOURCES CANADA
GEOLOGICAL SURVEY OF CANADA

ENERGIE, MINES ET
RESSOURCES CANADA
COMMISSION GEOLOGIQUE DU CANADA

SEISMIC RISK CALCULATION *

CALCUL DE RISQUE SEISMIQUE *

REQUESTED BY/ DEMANDE PAR

Dr. K. W. Savigny / U. B. C.   mjg

SITE

Wahleach, B. C. Hydro

LOCATED AT/ SITUE AU

49. 23 NORTH/NORD   121. 67 WEST/OUEST

PROBABILITY OF EXCEEDENCE PER ANNUM/ PROBABILITE DE DEPASSEMENT PAR ANNEE	0. 010	0. 005	0. 0021	0. 001
PROBABILITY OF EXCEEDENCE IN 50 YEARS/ PROBABILITE DE DEPASSEMENT EN 50 ANS	40 %	22 %	10 %	5 %
PEAK HORIZONTAL GROUND ACCELERATION (G) / ACCELERATION HORIZONTALE MAXIMALE DU SOL (G)	0. 063	0. 092	0. 146	0. 215
PEAK HORIZONTAL GROUND VELOCITY (M/SEC) / VITESSE HORIZONTALE MAXIMALE DU SOL (M/SEC)	0. 058	0. 087	0. 143	0. 217

+ REFERENCES

1. NEW PROBABILISTIC STRONG SEISMIC GROUND MOTION MAPS
OF CANADA: A COMPILATION OF EARTHQUAKE SOURCE ZONES, METHODS AND RESULTS.
P. W. BASHAM, D. H. WEICHERT, F. M. ANGLIN, AND M. J. BERRY
EARTH PHYSICS BRANCH OPEN FILE NUMBER 82-33, OTTAWA, CANADA 1982.

2. ENGINEERING APPLICATIONS OF NEW PROBABILISTIC
SEISMIC GROUND-MOTION MAPS OF CANADA.
A. C. HEIDEBRECHT, P. W. BASHAM, J. H. RAINER, AND M. J. BERRY
CANADIAN JOURNAL OF CIVIL ENGINEERING, VOL. 10, NO. 4, P. 670-680, 1983.

3. NEW PROBABILISTIC STRONG GROUND MOTION MAPS OF CANADA.
P. W. BASHAM, D. H. WEICHERT, F. M. ANGLIN, AND M. J. BERRY, BULLETIN OF
THE SEISMOLOGICAL SOCIETY OF AMERICA, VOL. 75, NO. 2, P. 563-595, 1985.

4A. SUPPLEMENT TO THE NATIONAL BUILDING CODE OF CANADA 1985, NRCC NO. 23178.
CHAPTER 1: CLIMATIC INFORMATION FOR BUILDING DESIGN IN CANADA.
CHAPTER 4: COMMENTARY J: EFFECTS OF EARTHQUAKES.

4B. SUPPLEMENT DU CODE NATIONAL DU BATIMENT DU CANADA 1985, CNRC NO 23178F.
CHAPITRE 1: DONNEES CLIMATIQUES POUR LE CALCUL DES BATIMENTS AU CANADA.
CHAPITRE 4: COMMENTAIRE J: EFFETS DES SEISMES.

16-JUN-89 16: 51: 40

(2)

SITE   Wahleach, B.C. Hydro

ZONING FOR ABOVE SITE/ ZONAGE DU SITE CI-DESSUS

1985 NBCC/CNBC: ZA = 3,   ZV = 3,   V = 0.15 M/S

ACCELERATION ZONE/ ZONE D'ACCELERATION   ZA=3
ZONAL ACCELERATION/ ACCELERATION ZONALE   0.15 G

VELOCITY ZONE/ ZONE DE VITESSE   ZV=3
ZONAL VELOCITY/ VITESSE ZONALE   0.15 M/S

1985 NBCC/CNBC **
SEISMIC ZONING MAPS/ CARTES DU ZONAGE SEISMIQUE

PROBABILITY LEVEL: 10% IN 50 YEARS
NIVEAU DE PROBABILITE: 10% EN 50 ANNEES

G OR M/S	ZONE	ZONAL VALUE/ VALEUR ZONALE
0.00		
	0	0.00
0.04		
	1	0.05
0.08		
	2	0.10
0.11		
	3	0.15
0.16		
	4	0.20
0.23		
	5	0.30
0.32		
	6*	0.40

* ZONE 6:   NOMINAL VALUE/ VALEUR NOMINALE 0.40,
   SITE-SPECIFIC STUDIES SUGGESTED FOR IMPORTANT PROJECTS/
   ETUDES COMPLEMENTAIRES SUGGEREES POUR DES PROJETS D'IMPORTANCE.

** FOR NBCC APPLICATIONS, CALCULATED ZONE VALUES AT A SITE SHOULD BE
   REPLACED BY EFFECTIVE ZONE VALUES [ZA(EFF) OR ZV(EFF)] AS SHOWN BELOW/
   POUR APPLICATIONS SELON LE CNBC, ON DOIT REMPLACER LES VALEURS ZONALES
   CALCULEES POUR UN SITE PAR LES VALEURS EFFECTIVES [ZA(EFF) OU ZV(EFF)]
   COMME MONTRE CI-DESSOUS:

   1.   IF/SI (ZA - ZV) > 1,   ===>   ZA(EFF) = ZV + 1.
OR/OU
   2.   IF/SI (ZA - ZV) < 1,   ===>   ZA(EFF) = ZV - 1.
OR/OU
   3.   IF/SI ZV=0 AND/ET ZA > 0, ===>   ZV(EFF) = 1.

      (SEE REFERENCE 2 CITED ABOVE, PAGE 677)
      (VOIR PAGE 677 DE LA REFERENCE 2 CI-DESSUS)
                                              16-JUN-89 16:51:40